Phase Analysis of Low Frequency Hemodynamic Oscillations in Near Infrared Spectroscopy

A dissertation submitted by

Feng Zheng

In partial fulfillment of the requirements

for the degree of

Master of Science

in

BIOMEDICAL ENGINEERING

TUFTS UNIVERSITY

Februray 2011

ADVISER:

Sergio Fantini, Ph.D., Department of Biomedical Engineering, Tufts University

Committee Members:

Fiorenzo Omenetto, Ph.D., Department of Biomedical Engineering, Tufts University

Robert Jacob, Ph.D., Department of Computer Science, Tufts University

ABSTRACT

To study low frequency oscillations (around 0.1 Hz) of tissue, oxy-hemoglobin and deoxy-hemoglobin concentrations measured by near-infrared spectroscopy, we proposed two phase analysis methods: one is a cross-correlation phasor method, and another is a phase synchronization analysis method. Both methods yield similar results and provide a straightforward visualization of the phase relationships between deoxy- and oxy-hemoglobin concentrations with the help of circular statistics. We argued that measured oscillations of deoxy- and oxy-hemoglobin with an intermediate phase difference which is neither 0 nor π may results from the interplay of different physiological processes that are out-of-phase with respect to each other. We observed that in most cases under the Watson-Williams statistical test, there is a change in the phase difference between deoxy- and oxy-hemoglobin from rest conditions to mental workloads. The change in standard deviation of the phase distribution may be connected with the change in regulation of physiological processes in human cerebral cortex. The analytical tools we developed from phasor concepts, such as phase-sector (to display the phase distribution) and TARGET map (to display the temporal evolution of the phase), can be powerful tools for dynamic monitoring and physiological assessment. The phase methods in this thesis would provide novel opportunities for understanding cerebral autoregulation, functional connectivity networks and physiological processes underlying the measured near-infrared signals.

ACKNOWLEDGEMENTS

I would like to thank my advisor Prof. Sergio Fantini, for constant encouragements, guidance, insights, and advice, and for keeping me on track by your kindness and enthusiasm. I've learned a great deal from you over the years at Tufts.

I would like to thank Dr. Angelo Sassaroli, for sharing your expertise in theory and experimentation. You always explain difficult and complicate concepts in a patient and humor way. Without your help, I would not achieve so much.

I would like to thank all current and past members in Diffuse Optical Imaging Group of Biomedical Engineering Department at Tufts for all the wonderful collaboration and friendship throughout the years when I was at Tufts:

To Dr. Yunjie Tong and Dr. Debbie Chen Cockrell, for your help, support and great collaborative efforts over the years before and after your graduation from our group;

To Yang Yu, for all helpful discussions and understanding of my ideas; To Michele Pierro, for all great ideas we shared and the fantastic work we have done together; To Bertan Hallacoglu, for your support and useful feedback on my work; To Michael Coutts, for designing the top one helmet and teaching me how to make new helmets; To Chia-Hui Chen, and Xiao Da, for the time we worked together in the lab to pursue truths;

I would also like to thank the researchers that I have worked with in the HCI lab of Computer Science Department at Tufts: Prof. Robert Jacob, Dr. Leanne Millers Hirshfield, Dr. Audrey Girouard, and Erin Solovey, for your collaboration and sharing your knowledge about machine learning;

Special thanks to my wife Yue Zhang

For all your love, support, kindness, sacrifice and all the happiness and joy you bring to my life.

Special thanks to my dad Jixin Zheng and my mom Xiaomei Wan

For your endless love and ultimate support from distant China.

Table of Contents

1. Motivation and thesis outlook

Phase is a measure of the fraction of a complete oscillation cycle with respect to a specified point at a reference time. We can sense the phase and phase change everywhere: in alternating current used in our home, in traffic light switching in the street, in telephone, in audio waves in theatre, in 3-D movies, and even in moon shape and stars in the sky. In our research, the phase in hemodynamic oscillations has special meaning in brain autoregulation, functional connectivity and physiological processes. By investigating the phase and the phase difference between oxy- and deoxy-hemoglobin which are uniquely measured by near-infrared spectroscopy, we have a chance to understand the dynamic of physiologic parameters like blood volume, blood flow and oxygen consumption, which are widely studied nowadays. In this thesis, we will first explain why we chose the phase difference of hemodynamic oscillations as our experimental parameter and its physiological meaning. Then we will introduce near-infrared spectroscopy and the physiological models that underlie the changes in the detected signals. Afterwards we will discuss the details the phase analysis methods that we proposed: the cross-correlation phasor method and the phase synchronization analysis. We would also like to introduce some analytical tools based on phasors which would help us in the future to better monitor and characterize cerebral hemodynamics. Finally, we will present two sets of experimental data collected during two protocols of brain activation: a) a protocol involving the use of working memory; b) a protocol for the activation of the motor cortex.

2. Phase Relationship between Hemoglobin Species

"Phase", in this thesis unless stated otherwise, is defined as the phase relationship between oscillations of deoxy-hemoglobin and oxy-hemoglobin concentrations changes with respect to baseline values ($[Hb]$ and $[HbO]$ respectively) at frequencies in the range (0.06, 0.1) Hz. In this chapter, we will first introduce the low frequency oscillations (LFO) and their importance to understand the physiological mechanisms in human brain, and explain why we chose this frequency band rather than others, such as those centered on the heart or respiratory rate. Then we will use three sections to discuss the motivation of selecting phase as our research topic: 1) phase is the fundamental indicator related to brain auto-regulation; 2) phase is the important in functional connectivity studies; and 3) phase is the key to understand the basic underlying the physiological processes.

2.1 Spontaneous Low Frequency Oscillations

It is well known that spontaneous low frequency hemodynamic oscillations (LFOs) around 0.1 Hz happen in cerebral hemodynamics and metabolisms and they have been widely studied by different techniques and in different species (Obrig et al., 2000; Katura et al., 2006; Cordes et al., 2001; Chance et al., 1993; Golanov et al., 1994; Livera et al., 1992). Besides in cerebrum, LFOs had also been observed in the arterial blood pressure and heart rate of human adults and infants (Guyton et al., 2000; Siebenthal et al., 1999), these researchers called spontaneous oscillation around 0.1 Hz as "Mayer wave" (Mayer, 1876), "Vasomotion", "V-Signal" etc.

Generally, the amplitude of LFO is at least one order of magnitude greater than that of the response signal elicited by some cerebral task, and its period is comparable to the duration of the response signals (Mayhew et al., 1998; Spitzer et al., 2001). LFOs are characterized by their spontaneity, and they can be distinguished from other oscillatory phenomena such as the heart beat (0.6 to 1.2 Hz) and respiratory frequency (0.1 to 0.5 Hz) and can be influenced by pharmacological interventions with inhibitor of the NO synthase and by pathological conditions, e.g. ischemia, large and small artery disease (Obrig et al., 2000). Diehl's group (Diehl et al., 1995) investigated the phase relationship between the oscillation in blood flow and in arterial pressure. They have revealed that the oscillations may be used to explain autoregulatory mechanisms of the brain vasculature. Biswal's group (Biswal et al., 1995) has studied the synchronous oscillations in cerebro-cortical capillary blood velocity after nitric oxide synthase inhibition, and concluded that some temporal synchrony low frequency fluctuations send messages across corpus callosum and possibly carries messages synchronizing the activity between the bilateral, symmetric functional regions.

LFOs are helpful to uncover meaningful physiological mechanisms, lots of scientists put great efforts on LFOs' research. However, the origins of LFOs are still controversial: Fagrell et al stated that the fluctuations result from changes in arteriole diameter (Fagrell et al. 1980). Golanov et al presented evidence for a neurogenic origin (Golanov et al. 1994). Cooley and colleagues (Cooley et al., 1998) looked at the relationship between the arterial pressure and RR-interval which is the time elapsing between two consecutive R waves in the electrocardiogram, and thought that these oscillations originate from a central oscillator. Some studies believed that LFOs signals result from the oscillations in the arterial supply (Tomita et al., 1981; Colantuoni et al., 1994). Hudetz's group analyzed the mysterious origin of LFOs and proposed that this kind of

spontaneous oscillations in cerebral hemodynamics may represent autoregulatory processes of cerebral blood flow (Hudetz et al, 1998). Another recent research from Katura's group argued that although "Mayer waves" in arterial pressure and heart rate have similar spectral features of cerebrovascular LFOs, it is difficult to tell the causal relations between them only with spectral characteristics because of their nonlinear interrelations. And the origin of LFOs in cerebral hemodynamics may lie in the regulation of regional cerebral blood flow change and energetic metabolism rather than due to the systemic regulation of the cardiovascular system (Katura et al., 2006).

Because LFOs have the characteristics to reveal the autoregulatory mechanisms in the human brain, in this thesis, LFO around 0.1 Hz is the major frequency components of the hemodynamic signals we investigate.

2.2 Cerebral Autoregulation

In healthy adults, Cerebral Autoregulation (or brain autoregulation) refers to a homeostatic process whereby cerebral blood flow (CBF) remains constant between a mean arterial blood pressure (MAP) of 60 mm Hg and 160 mm Hg or between a cerebral perfusion pressure (CPF) of 50 mm Hg and 150 mm Hg (Paulson et al. 1990).

By observing the pial artery reaction to manipulation of MAP through a cranial window, Fog (Fog. 1937) introduced the cerebral autoregulation for the first time. CBF in humans was measured by Kety and Schmidt in 1948 (Kety and Schmidt, 1948) and Finnerty et al used Kety's method to determine cerebral hemodynamics of the ischemic brain after an acute reduction in MAP in attempt to define what now would be considered the lower limit of cerebral

autoregulation (Finnerty et al., 1954). Later, Lassen refined the concept of cerebral autoregulation and illustrated the relative stability of CBF over a wide range of blood pressure. He also identified the lower and upper limits of cerebral autoregulation by a decrease in CBF at a low MAP and an increase in CBF when MAP remains at a high level (Lassen, 1974). In 1989, Aaslid et al invented the transcranial Doppler method to determine mean flow velocity in basal cerebral arteries (Aaslid et al, 1989). Because transcranial Doppler reports a continuous mean flow velocity, cerebral perfusion could be followed during the drop in MAP that follows release of thigh cuffs. Transcranial Doppler ultrasound and non-invasive beat to beat blood pressure monitors allowed the dynamic relation between cerebral blood flow velocity and mean arterial pressure to be quantified giving a measure of so-called dynamic cerebral autoregulation which was referred as the acute response of cerebral perfusion to a change in MAP. The static cerebral autoregulation was assessed using steady state blood pressure changes and assessing the alteration in CBF without taking into account the speed at which the CBF recovers following a change in blood pressure. Dynamic cerebral autoregulation was believed to have different underlying pathophysiological control mechanisms than those in static cerebral autoregulation (Tiecks et al, 1995). Moreover, dynamic cerebral autoregulation has been shown to be influenced differently from static cerebral autoregulation in disease states such as stroke (Dawson et al, 2000).

Because the cerebrum is encompassed in the skull, the cerebral autoregulation is vital for 1) preventing cerebral edema and hemorrhage; 2) counteracting the effect on CBF of a reduction in MAP in response to hemorrhage or a change in body position. For example, when rising from a supine position, sometimes one may experience blurred vision or dizziness which are the symptoms of a reduced CBF. Nevertheless, with the help of dynamic cerebral autoregulation,

healthy adults would recover in seconds. Nowadays, the assessment of cerebral autoregulation has been widely used in clinical diagnosis and pathophysiologic researches (Rangel-Castilla et al, 2008; Urbano et al, 2008; Brady et al, 2008).

In previous observations in cerebral autoregulation, cerebral perfusion, even at rest, is not a constant but permanently oscillates at different frequencies. One of the most important frequencies is the spontaneous low frequency oscillations (LFOs) around 0.1 Hz. Diehl et al have shown that LFO of cerebral blood flow velocity (CBFV) in the large basal arteries do not occur simultaneous to those of arterial blood pressure (ABP) but with a phase shift, that is CBFV leads ABP (Diehl et al, 1998). Kuo et al explained this phase shift as the result of fast and steady effort of the cerebral autoregulatory system to counter-regulate the repetitive oscillations of cerebral blood flow during oscillating ABP (Kuo et al, 2003). The most appealing part is that this phase shift would be reduced in various acute and chronic cerebrovascular diseases. In LFO frequency band, Reinhard's group studied the phase relationship between oscillations of blood pressure, NIRS signal and CBFV in the middle of cerebral artery in 38 healthy adults and 28 patients with unilateral severe obstructive carotid disease. Their results in Fig. 2.1 and Fig. 2.2 clearly showed that 1) blood pressure induced cortical microvascular oscillations follow those of macrovascular oscillations with a 80 to 90 degree phase difference; 2) oscillations of oxy- and deoxy-hemoglobin are around 180 degree i.e. out-of-phase; 3) hemodynamic compromise in carotid obstruction leads to delayed microvascular oscillations in comparison to ABP due to disturbed autoregulation and an abrogation of the oxy- and deoxy-hemoglobin out-of-phase (Reinhard et al, 2006).

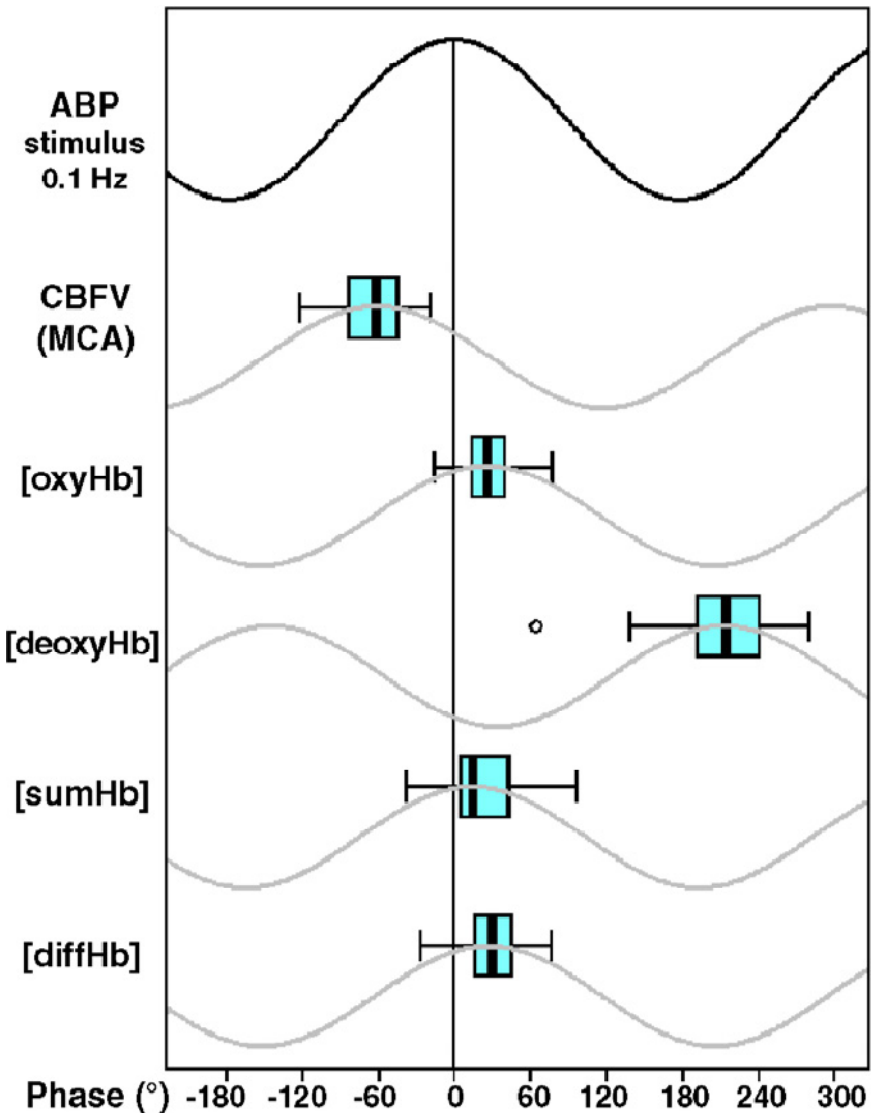

Fig. 2.1 (Reinhard et al, 2006) schematic illustration of phase relationship, **in control subjects**, between oscillations in arterial blood pressure and different cerebral hemodynamic parameters.

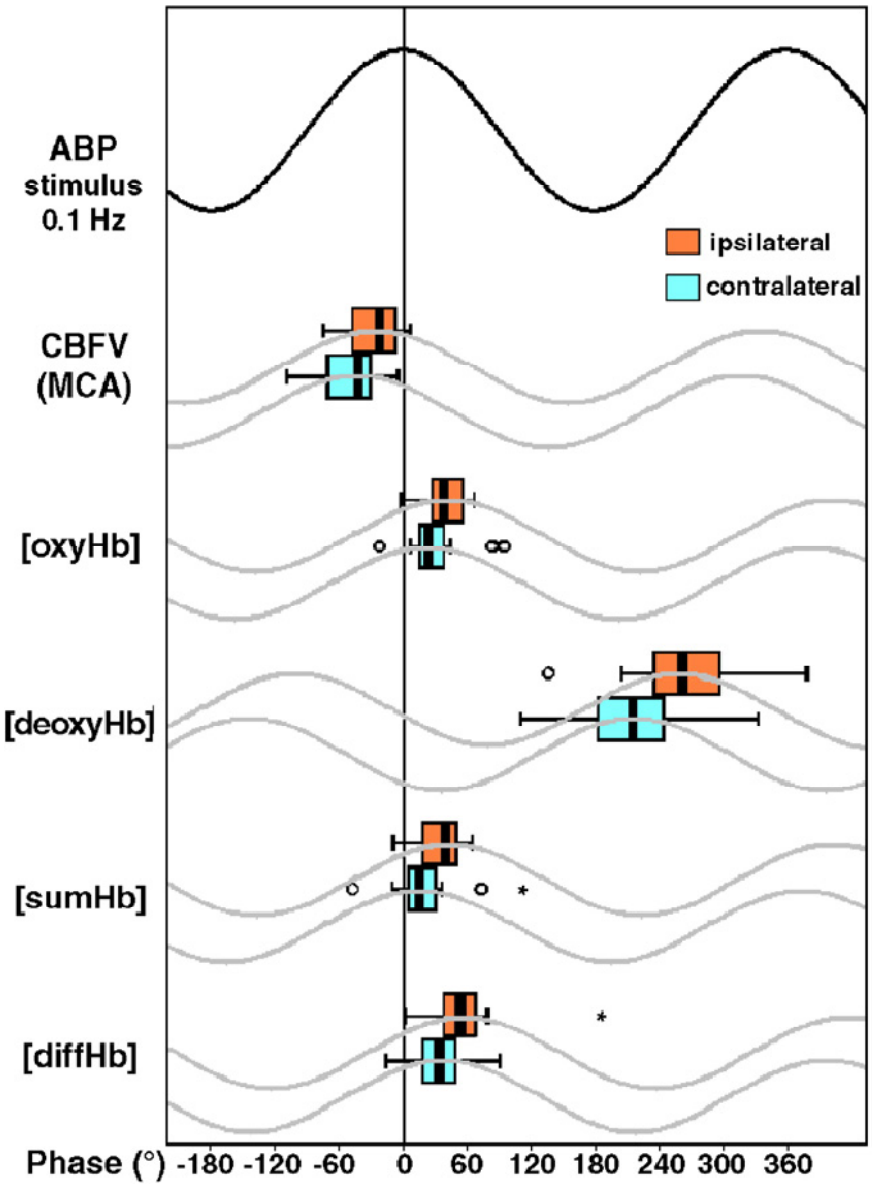

Fig. 2.2 (Reinhard et al, 2006) schematic illustration of phase relationship, **in patients with unilateral carotid obstruction**, between oscillations in arterial blood pressure and different cerebral hemodynamic parameters. “ipsilateral” refers to the injured side of the brain.

They argued that, due to cerebral autoregulatory action and circulatory transit time, specific phase relationships exist when cortical microvascular hemodynamic responds to blood oscillations. In case of unilateral carotid obstruction or impaired hemodynamics, these phase shifts are significantly changed reflecting disturbed autoregulation (Reinhard et al, 2006). Therefore, by measuring and comparing the phases in hemodynamic oscillations, we can understand the cerebral autoregulation.

Recently, using near-infrared spectroscopy, Steiner et al studied the correlation between a dynamic index of cerebral autoregulation assessed with blood flow velocity and tissue oxygenation index. They suggested that near-infrared spectroscopy would show promise for the continuous assessment of cerebral autoregulations (Steiner et al, 2008). So, in this thesis, we will use near-infrared spectroscopy to study the phase shift and development in hemodynamics, which would in the future provide a noninvasive, low cost and high temporal resolution methodology for cerebral autoregulation assessment.

2.3 Functional Connectivity

In human brain, all communication between nerve cells, with a few notable exceptions such as diffusible messengers, is carried out along physical connections, often linking cells that are separated by large distances. Signals within these connections consist of series of action potentials of unit magnitude and duration. The arrival of an action potential at a synaptic junction triggers numerous biochemical and biophysical processes and further cause the transmission of electrical signals to the postsynaptic cell or so-called receiving cell, which may in turn generate an output spike transmitted along the neuron's axon. Neurons in the cerebral cortex maintain

thousands of input and output connections with other neurons, forming a dense network of connectivity spanning the entire thalamocortical system. The human cerebral cortex approximately contains 8.3 billion neurons and 67 trillion connections. If one straightens all of connections within one human brain, the length would be from 100,000 km (equivalent to 10 times the diameter of the Earth) to 10,000,000 km (equivalent to 10 round-trip Earth to Moon). Despite this massive connectivity, cortical networks are exceedingly sparse, with an overall connectivity factor of around 10^{-6}, which is defined as the number of connections present out of all possible. Nevertheless, due to predominant feature of brain networks, local connectivity ratios can be significantly higher than those suggested by random topology. The brain is neither random nor still. Many brain networks remain plastic throughout the lifetime of the organism, exhibiting specific modifications of synaptic efficacy at multiple time scales, as well as continuous morphological change. As a result, the detailed structure and morphology of brain networks is the result of continuous interaction between neural substrate, ongoing neuronal activity and embodied action of an individual organism within an environment, thus will somehow reflect the history of development and experiences of the individual organism.

Neural connectivity and neural activity are so close in relationship that they support some specific patterns of functional interactions. The connectivity can be defined into two categories:

1) **Anatomical Connectivity**

   Anatomical connectivity refers to the set of physical or structural connections linking neuronal units in spatial levels at a given time. At the local circuit level, it would focus on the pattern of synaptic connections between individual neurons. At the intra-areal patterns level, it would involve connection bundles or synaptic patches linking local neuronal

populations. At the large scale patterns level, it would focus on connection pathways that consist of millions of individual fibers linking clustered areas of the brain.

2) Functional Connectivity

Functional connectivity refers to the pattern of temporal correlations that exists between distinct neuronal units (Friston. 1993, Friston. 1994). Such temporal correlations are often the result of neuronal interactions along anatomical or structural connections. However, functional connectivity doesn't necessarily imply a physical pathway, because some observed correlations may be due to common input from an external neuronal or stimulus source. Therefore, functional connectivity potentially includes patterns of connectivity that are entirely mediated by the common influence of some external event on distant neural areas. Deviations from statistical independence between neuronal elements are commonly captured in a covariance matrix which may be viewed as a representation of the system's functional connectivity. Although temporal correlations are usually applied to represent statistical patterns in neuronal network, recent studies also took spectral coherence as an indicator of functional connectivity (Bressler et al, 2001).

Anatomical connectivity is a major constraint on the kinds of patterns of functional connectivity that can be generated. On the other hand, functional connectivity can contribute to the shaping of the underlying anatomical structures. This is accomplished either directly through activity dependent synaptic modification or through effects of functional connectivity over longer time scales on an organism's perceptual, cognitive or behavioral capabilities, which in turn affect adaptation and survival.

The structure of brain networks is a result of the combined forces of natural selection and neural activity during evolution and development. Two of the major problems brains have to solve are the extraction of information from inputs and the generation of coherent states that allow coordinated perception and action in real time. Solutions to these problems are reflected in the dual organizational principles of functional segregation and functional integration found throughout the cerebral cortex. The requirement to achieve segregation and integration simultaneously imposes severe constraints on the set of possible cortical connection patterns. Very likely there are many more ways in which structural properties of brain networks impact upon the dynamical and informational patterns neurons can generate and maintain. The dynamic patterns generated by brain networks underlie all of cognition and perception. At least some aspects of vision seem to be embedded in the structural connectivity of parts of the thalamocortical system, and disruptions of the wiring of these networks result in severe and specific alterations of mental and perceptual function. The nature of awareness and consciousness itself may be rooted in the rapid integration of information requiring a structural network capable of sustaining this process (Sporns et al 1991, Singer et al, 1995).

Over the last century, due to the availability of diffusion tensor imaging (DTI), functional connectivity has been widely studied. Much of the study is carried out by examining inter-regional correlations in resting BOLD data (Blood-oxygen-level dependence, which is the MRI contrast of blood deoxyhemoglobin, first discovered in 1990 by Seiji Ogawa (Ogawa, 1990)). This approach is first introduced by Biswal (Biswal et al, 1995), who observed correlations between activity in left and right somatosensory cortex during resting BOLD. Usually, for functional connectivity, the experiments are taken under REST. Temporal correlations in resting data are of special interest because they are not easily explained by externally imposed task

demands. Resting BOLD is more than just the absence of cognitively evoked activity. By contrast, during task performance, the strong correlation between cortex and task sheds no new light on functional connectivity analysis. Another major practical advantage of connectivity studies carried out in resting data is that the same data may be used repeatedly. At this point, a lot of resting BOLD data is available either publicly or through local repositories. In addition, Fox et al. have shown that some of the coherent signal in resting BOLD contributes roughly linearly to task-evoked BOLD. In this way, better understanding of the task independent component of the signal can lead to markedly better sensitivity to detect task-evoked activation (Fox et al, 2006). Culver's group (Zeff et al, 2007) reported functional mapping of the human visual cortex made possible by a high-density DOT (diffuse optical tomography) imaging system. Franceschini et al used near-infrared spectroscopy (NIRS) and diffuse optical imaging (DOI) with 32 source-detector pairs to collect optical data from prefrontal, sensorimotor, and visual cortices in both hemispheres simultaneously. By applying cross-correlation, they were able to generate functional maps of multiple brain regions' responses to brain activation and distinguish brain activation signals from physiological signal including cardiac, respiratory and blood-pressure (Franceschini et al, 2006). Katura et al were able to separate blood-related brain-function measurements in low frequency oscillation (LFO) from physiological noise by using information transfer analysis (Katura et al, 2006). Their work also shed light on functional connectivity study with NIRS, because such analysis of information transfer may be useful in revealing the complex interrelation between elements regulating one another. Therefore, within a specific frequency band such as LFO in brain study, as one of the most important parameters in cross-correlation map, phase study would be meaningful of the spatio-temporal relations between different optical channels, ultimately in functional connectivity.

One point deserves special emphasis here. In this thesis, because of current limited amount of source and detector pairs, our major purpose is to introduce phase analysis methods. Therefore we will mainly focus on task-evoked activation rather than rest. However, the phase analysis methods are designed for future functional connectivity studies, in which we will study in rest or sleeping status and use whole-head helmet and customized ISS machine with large number of channels.

2.4 Underlying Physiological Processes

Using non-invasive optical topography, Taga et al reported spontaneous changes in the cerebral oxygenation state of infants during quiet sleeping (Taga et al, 2000). Their results shed light on our research motivation and method. They used first derivatives of $\Delta[Hb]$ and $\Delta[HbO]$ in order to remove the long-term drift of the baseline of the values.

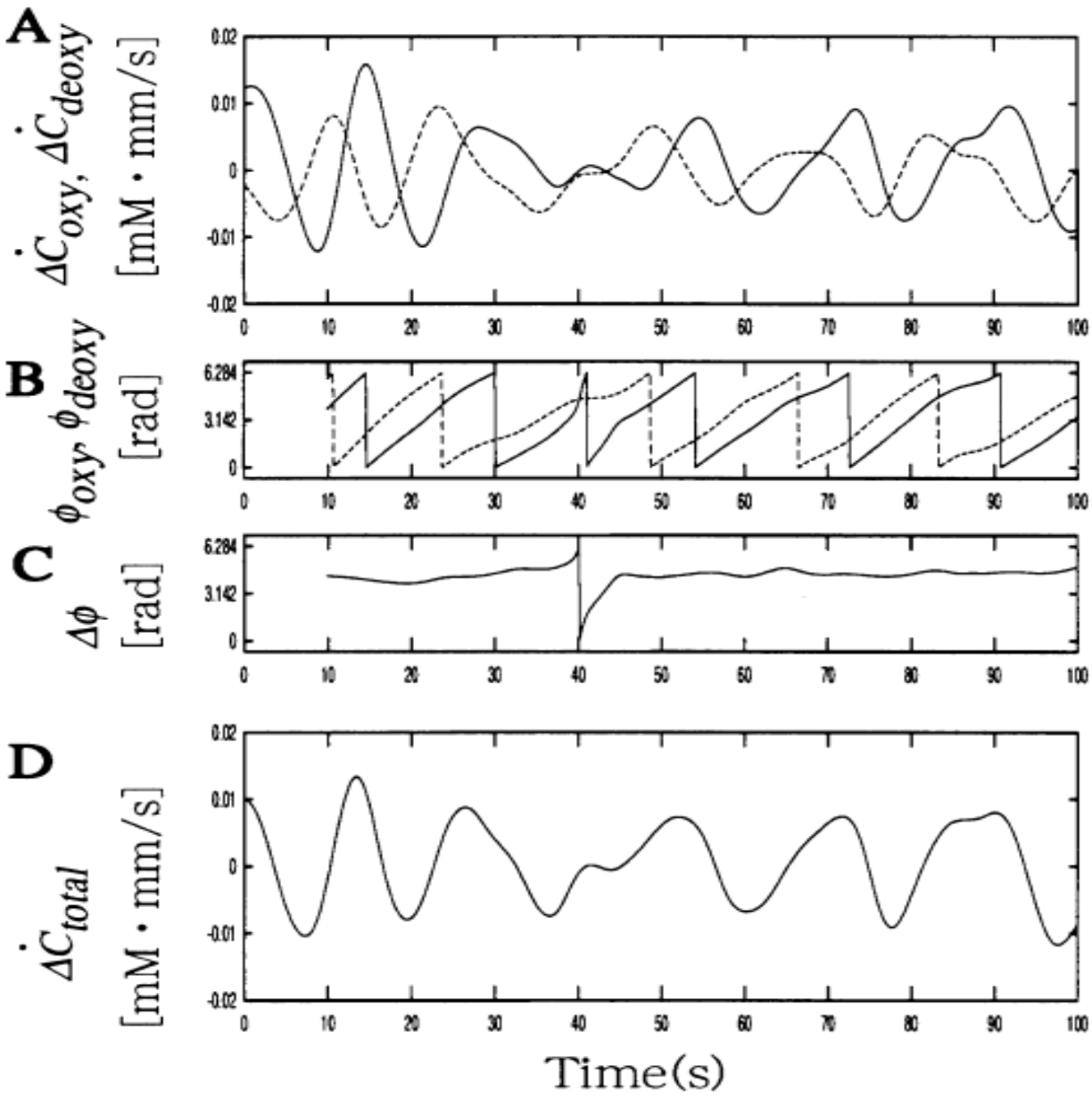

Fig 2.3 from (Taga et al, 2000), (A) the first derivative of $\Delta[HbO]$ and $\Delta[Hb]$. (B) instantaneous phases of changes in HbO and Hb. (C) Relative phase between $\Delta[HbO]$ and $\Delta[Hb]$. (D) the first derivative of the $\Delta[HbT]$

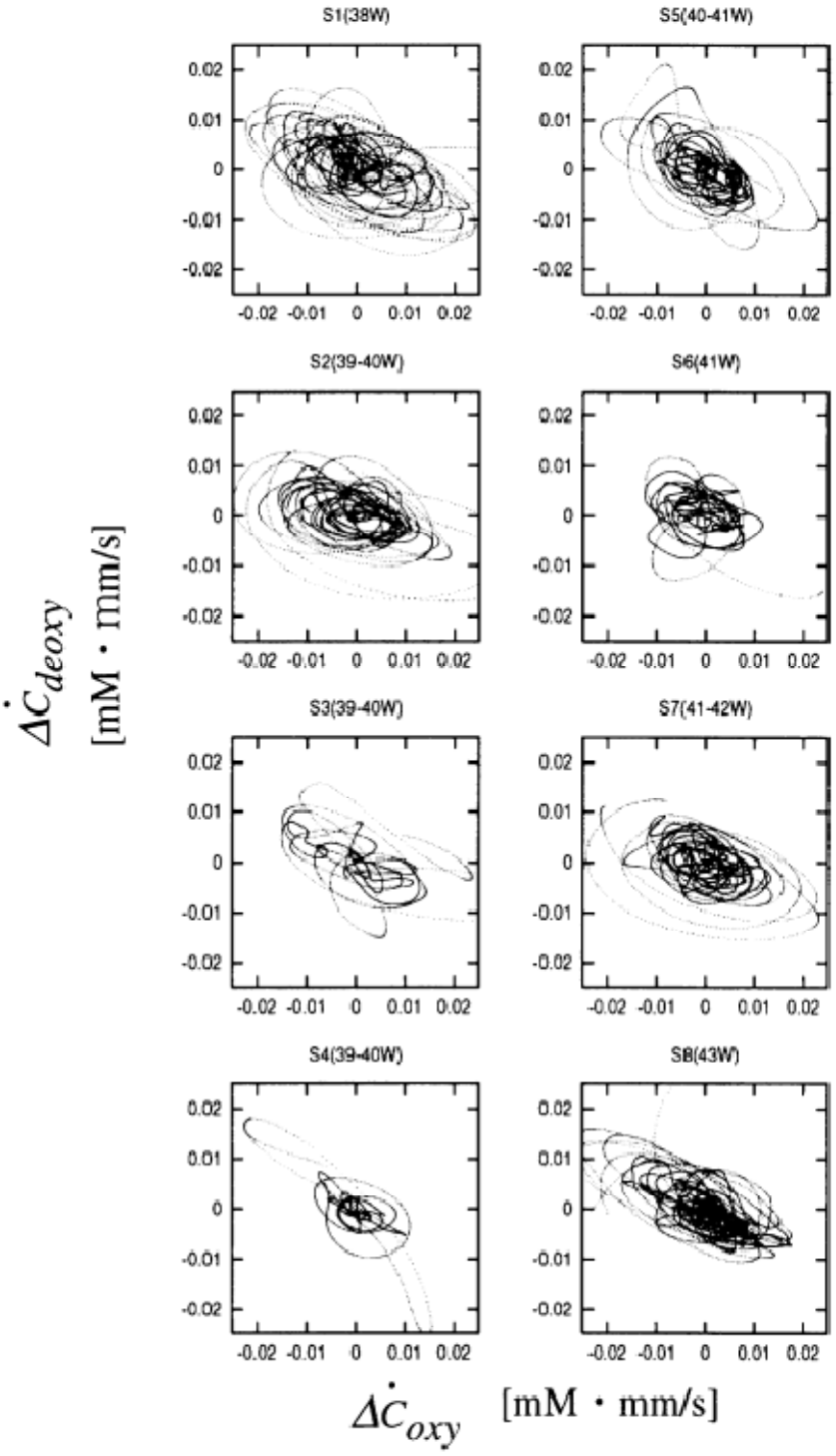

Fig 2.4 from (Taga et al, 2000), phase plane plots of the first derivative of $\Delta[Hb]$ against $\Delta[HbO]$.

Their results in Fig 2.3 and Fig 2.4 clearly showed that the spatially synchronized oscillations of the hemoglobin oxygenation state exist throughout the occipital cortex of neonates. The phase lag of [HbO] relative to [Hb] was stable at around $3\pi/4$. To explain the origins of this phase lag, they suggested that the reason would be the interplay between the vasomotion and the oxygen consumption in relation to brain activity.

In out experiments, we also observed similar phase lag of [Hb] against [HbO], though not a $3\pi/4$ stable value. Nevertheless, such phase lag would serve as an important role in understanding the underlying physiological processes in human brain.

2.5 Summary

In this chapter, we clarified the reason of why we want to focus on phase and develop phase analysis method in our research project, because phase will help us to better understand the cerebral autoregulation, functional connectivity and underlying physiological processes. It is a bridge to connect optical findings and physiological processes. In addition, since low frequency oscillations have the characteristics to reveal the autoregulatory mechanisms in the human brain, we investigate the oscillations of optical and hemoglobin signals in frequency band of LFO around 0.1 Hz.

3. Diffuse near infrared spectroscopy

3.1 Introduction

Our research is based upon near infrared spectroscopy (NIRS), which has been proved as an effective technology in studying the dynamics of physiological processes especially the brain hemodynamics. Noninvasiveness, low-cost and high temporal resolution are some of its typical advantages over traditional clinical functional brain studies such as PET and MRI. In order to make light to have its maximum depth of penetration in tissue, we choose a spectrum window of (600 ~ 900 nm) as the optimal wavelengths for noninvasive functional brain imaging. In this NIRS window, the main absorbers of the brain (i.e. water, oxy- and deoxyhemoglobin) have the minimal absorption. Near-infrared light can reach as far as 2 to 3 cm inside the tissue, therefore also the gray matter, where the most brain functions of conscious level happen. In this chapter, we will introduce the basic interactions between the photons and the tissue, namely scattering and absorption. Then we will introduce the diffusion theory and modified Beer-Lambert Law which is the fundamental of NIRS measurements. Finally, we will discuss the hemodynamic model for the physiological interpretation of in vivo NIRS measurements of the concentration of oxy- and deoxyhemoglobin.

3.2 Absorption and Scattering

The main absorbers of NIRS in human brain are water, oxy- and deoxyhemoglobin. Their absorption spectra are shown in Fig 3.1. in which the concentration of oxy-hemoglobin and deoxy-hemoglobin are set to be 50μM that is a typical value in blood-perfused tissues.

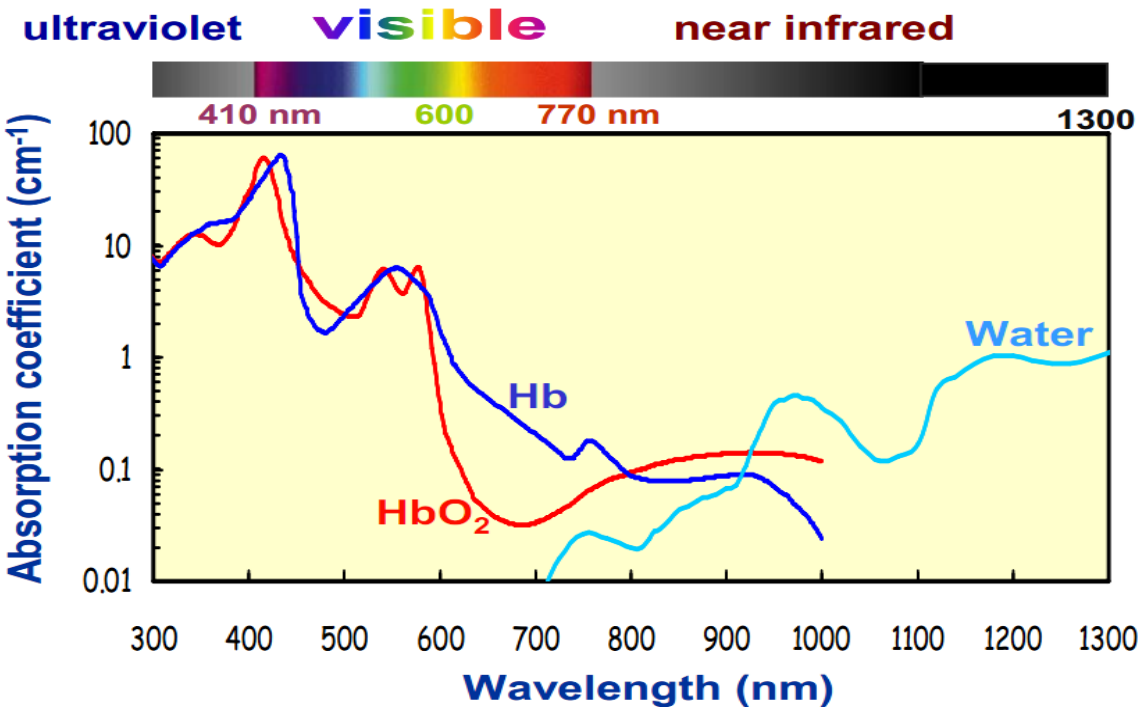

Fig 3.1 Absorption spectra of oxy-hemoglobin (HbO), deoxy-hemoglobin (Hb) and Water (H_2O) from 300 nm to 1300 nm.

We use absorption coefficient μ_a to describe the absorption properties of tissues. It is defined as the inverse of the average photon path length before absorption. The relationship between μ_a and concentrations of n chromophore in the tissue is (Fantini and Franceschini, 2002):

$$\mu_a(\lambda) = \sum_i^n \varepsilon_i(\lambda) \cdot C_i \tag{3.1}$$

in which, μ_a is wavelength dependent absorption coefficient in unit of cm^{-1}; $\varepsilon_i(\lambda)$ is the extinction coefficient of the *i*th chromophore, in unit of $M^{-1}cm^{-1}$; C_i is the concentration of the *i*th chromophore in unit of M. In our studies, we usually focused on the concentration changes of

oxy- and deoxy-hemoglobin ($[HbO]$ and $[Hb]$ respectively), from Eq (3.1) we can get the change of μ_a as:

$$\Delta\mu_a = \varepsilon_{\mathrm{HbO}}\Delta[HbO] + \varepsilon_{Hb}\Delta[Hb] \tag{3.2}$$

The typical value of μ_a in the tissue is 0.02 cm^{-1} – 0.3 cm^{-1} in near-infrared range.

Although within the NIRS spectrum window (600 – 900 nm) the photons are weakly absorbed in tissue, they are highly scattered. The scattering coefficient μ_s is used to describe this scattering optical property. It's defined as the cross-sectional area for scattering per unit volume of medium with unit of cm-1. The inverse of μ_s is the average photon path length between two consecutive scattering events.

However, after few scattering events, the photon would totally lose its memory of the previous direction and becomes isotropic in scattering. Therefore, in order to describe inverse average path length over which the direction of propagation of photon is randomized, we usually use another parameter- reduced scattering coefficientμ_s' to describe the scattering in tissues. It is defined as (Fantini and Franceschini, 2002):

$$\mu_s' = \mu_s(1 - < \cos\gamma >) \tag{3.3}$$

in which $< cos\gamma >$ is the average cosine of the scattering angles γ. Since the most scattering events in tissues are in forward direction, the normal value of $< cos\gamma >$ is 0.8 to 0.9.

The typical value of μ_s' is 2 to 20 cm^{-1}, which is one to two orders of magnitude bigger than μ_a in tissues. Generally, μ_s' is a monotonically decreasing function of the wavelength of the probing light. In Mie scattering where the scattering particles are homogenous spheres, $\mu_s'(\lambda) =$

$a\left(\frac{\lambda}{\lambda_0}\right)^{-b}$ in which a is the reduced scattering coefficient at the reference wavelength λ_0 and b is the scattering power.

3.3 Diffusion Theory

To mathematically understand the photon migration in highly scattering medium, we use the diffusion approximation to the radiative transport equation. If we make the following assumptions: 1) highly scattered medium $\mu_a \ll \mu_s'$ and we consider points of the medium far from the sources and the boundary; 2) isotropic light source; and 3) time scale of the variations of photon density and source are much greater than the average time between isotropic equivalent collisions $\frac{1}{v\mu_s'}$, the diffusion equation in homogeneous media will be reduced to (Fantini and Franceschini, 2002):

$$\frac{\partial U(\vec{r},t)}{\partial t} = D\nabla^2 U(\vec{r},t) - v\mu_a U(\vec{r},t) + S_0(\vec{r},t) \tag{3.4}$$

in which $U(\vec{r},t)$ is the photon density in unit of cm^{-3}; $D = v/[3(\mu_s' + \mu_a)]$ is defined as the diffusion coefficient in unit of cm^2sec^{-1}; v is the speed of light in the medium; $S_0(\vec{r},t)$ is the source distribution of photons. In addition, the photon flux $\vec{J}(\vec{r},t)$, in unit of $sec^{-1}cm^{-2}$, can be obtained by Fick's law

$$\vec{J}(\vec{r},t) = -D\nabla U(\vec{r},t) \tag{3.5}$$

Eq. (3.4) is the diffusion equation in time domain. In the frequency domain, the diffusion equation (3.4) takes the form of the Helmholtz equation

$$(\nabla^2 + k^2)U(\vec{r}) = -S_0(\vec{r})/D \tag{3.6}$$

where $k^2 = (i\omega - v\mu_a)/D$

The diffusion equation is applicable in highly scattering medium, which is the case in many biological tissues, especially in brain. In most of the brain study where NIRS is applied, both source and detector are placed on the surface of the tissue. Because of this arrangement, typically the frequency domain solution of diffusion equation in semi-infinite medium is used. The approaches to solve the diffusion equation in semi-infinite medium are from applying appropriate boundary conditions and replacing the incident pencil beam with single scattering source. The boundary condition for the semi-infinite medium can be satisfied when the photon density U is zero at an extrapolated boundary at some distance $z_b = 2aD^{-1}$ which is in the unit of cm (Fantini and Franceschini, 2002). The parameter a is related to the refractive index mismatch of the two media. To achieve the boundary condition, a negative photon source S_i is placed at the opposite side of the boundary with the actual photon source S_a placed within the medium. The net sum of the photons density from these two sources is zero at extrapolated boundary. In addition to satisfy the boundary condition, we have to make the following assumption. It has been shown that a pencil-like incident beam on the surface can be replaced by a single scattering source lying at depth $z_0 = \frac{1}{\mu_a+\mu_s}$, which is the length of one effective photon mean free path. Therefore, the relations for equations DC and AC photon density, and the phase at the surface are given as follows (Fantini and Franceschini, 2002):

$$U_{dc}^{si} = \frac{2P}{(4\pi)^2 D}\frac{e^{-r\left(\frac{v\mu_a}{D}\right)^{\frac{1}{2}}}}{r^3}\left(1 + r\frac{v\mu_a}{D}\right)(z_b + z_0)$$

$$\cdot\left(z + 3D\left(1 - \frac{(z_b + z_0)^2 + 3z^2}{2r^2}\right)\left(3 + \frac{r^2\frac{v\mu_a}{D}}{1 + r\left(\frac{v\mu_a}{D}\right)^{\frac{1}{2}}}\right)\right) \tag{3.7}$$

$$U_{ac}^{si} = \frac{2P(\omega)}{4\pi D v}\frac{e^{-r\left(\frac{v\mu_a}{2D}\right)^{\frac{1}{2}}V^+}}{r^3}\left\{1 + r\left(\frac{2v\mu_a}{D}\right)^{\frac{1}{2}}V^+ + r^2\frac{v\mu_a}{D}\left(1 + \left(\frac{\omega}{v\mu_a}\right)^2\right)^{\frac{1}{2}}\right\}^{\frac{1}{2}}$$

$$\times (z_b + z_0)\left\{z + 3D\left(1 - \frac{(z_b + z_0)^2 + 3z^2}{2r^2}\right)\right.$$

$$\times\left(2 + \frac{1 + r\left(\frac{v\mu_a}{2D}\right)^{\frac{1}{2}}V^+}{1 + r\left(\frac{2v\mu_a}{D}\right)^{\frac{1}{2}}V^+ + r^2\frac{v\mu_a}{D}\left(1 + \left(\frac{\omega}{v\mu_a}\right)^2\right)^{\frac{1}{2}}}\right) \tag{3.8}$$

$$\left. + r\left(\frac{v\mu_a}{2D}\right)^{\frac{1}{2}}V^+\right\}$$

$$\phi^{si} = r\left(\frac{v\mu_a}{2D}\right)^{\frac{1}{2}}V^- - \arctan\left(\frac{r\left(\frac{v\mu_a}{2D}\right)^{\frac{1}{2}}V^-}{1 + r\left(\frac{v\mu_a}{2D}\right)^{\frac{1}{2}}V^+}\right) \tag{3.9}$$

where superscript si denotes "semi-infinite"; $V^+ = \left(\left(1 + \left(\frac{\omega}{v\mu_a}\right)^2\right) + 1\right)^{\frac{1}{2}}$ and $V^- = \left(\left(1 + \left(\frac{\omega}{v\mu_a}\right)^2\right) - 1\right)^{\frac{1}{2}}$

When photons are injected into the diffusive medium, after hundreds of effectively isotropic scattering events, some of them are absorbed, some of them are scattered out of the tissue, and the rest of them will reach the detector fiber. We define the overlapping paths of these photons as sample volume for the specific source-detector pair, because it describes the most sensitive area for a given source-detector pair.

In the semi-infinite medium such as brain studies in NIRS, the sample volume of a source-detector pair resembles a banana-shape in the tissue as shown in Fig 3.2.

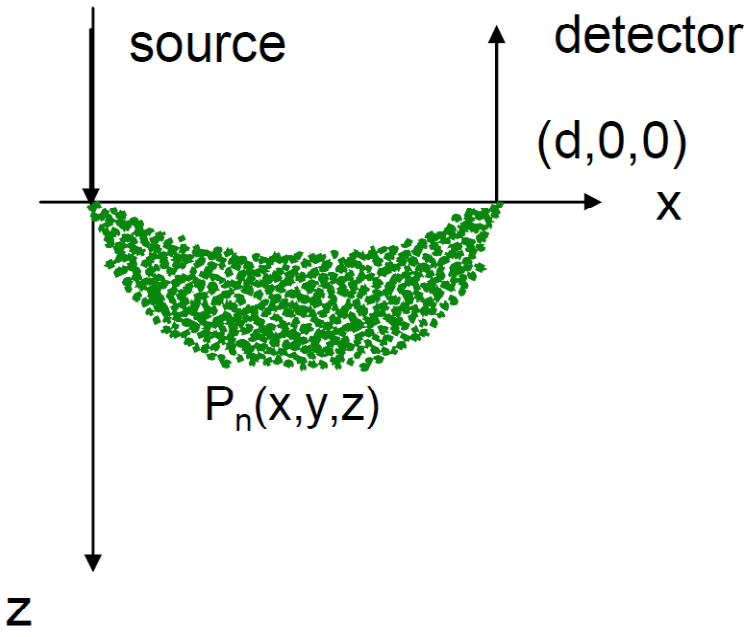

Fig 3.2. Illustration of "banana shape" given by photon hitting-density function with the source and detector at coordinates (0,0,0), (d,0,0) respectively (Feng et al, 1995)

and is given by the photon hitting-density function:

$$P_n(x,y,z) = \frac{z^2 e^{\left\{-\kappa\left[(x^2+y^2+z^2)^{\frac{1}{2}}+((d-x)^2+y^2+z^2)^{\frac{1}{2}}\right]\right\}}}{(x^2+y^2+z^2)^{\frac{3}{2}}((d-x)^2+y^2+z^2)^{\frac{3}{2}}} \times\left\{\kappa(x^2+y^2+z^2)^{\frac{1}{2}}+1\right\}\left\{\kappa[(d-x)^2+y^2+z^2]^{\frac{1}{2}}+1\right\} \quad (3.10)$$

in which, $P_n(x,y,z)$ is the photon hitting density function, which is proportional to the probability density per unit volume that a photon injected at (0,0,0) and detected at (d,0,0). The effective coefficient κ is defined as $\kappa = \sqrt{3\mu_a\mu_s'}$ (Feng et al, 1995).

For a given source-detector pair, the detected photons are known to more likely have traveled through the central area of the banana shape than through its outer portions. The likelihood values over the entire cross-section of the medium add up to one because the measured photons must have come through the medium somewhere. Because photons are more likely to pass through the central regions of banana shape, the measurement is most sensitive to objects found in that area. In brain studies, if the source-detector distance is less than 1 cm, the detected photons on average will only reach a few millimeter of depth so that only scalp and skull are sampled; if the source-detector distance is more than 3 cm, the detected photons will reach 1-2 cm of depth and therefore sample the cerebral cortex.

3.4 Modified Beer-Lambert Law

The Beer-Lambert Law investigates the absorption of light to the properties of the material through which the light is traveling. Without scattering, the Beer-Lambert Law is:

$$A(\lambda) = -\ln\left(\frac{I(\lambda)}{I_0(\lambda)}\right) = \mu_a d \tag{3.11}$$

where $A(\lambda)$ is the absorbance; d is the source detector distance; μ_a is the absorption coefficient; $I(\lambda)$ and $I_0(\lambda)$ are the detected light intensity and the incident light intensity respectively (Fantini and Franceschini, 2002).

If consider both absorption and scattering, the modified Beer-Lambert Law in the highly scattering medium can be expressed as:

$$\Delta A(\lambda) = -\ln\left(\frac{I_{final}(\lambda)}{I_{initial}(\lambda)}\right) = \langle L(\lambda)\rangle \Delta\mu_a(\lambda) \tag{3.12}$$

where $\langle L(\lambda)\rangle$ is the mean path length of detected photons; I_{final} and $I_{initial}$ are the detected light intensity after and before the concentration change. Eq. (3.12) describes the relationship between the change in the concentration of hemoglobin to the change in the detected light intensity. $\Delta\mu_a$ is defined as $\Delta\mu_a = \mu_a(t) - \mu_{a0}$, where μ_{a0} is the baseline absorption coefficient before the concentration change while $\mu_a(t)$ is the absorption coefficient after the change, which is a function of time. $\langle L(\lambda)\rangle$ is the mean path length of detected photons, which is assumed to be time independent (at least in functional studies) depends also on the source-detector distance d:

$$\langle L(\lambda)\rangle = DPF(\lambda) \cdot d \tag{3.13}$$

where DPF is differential path length factor. The DPF can be measured from time domain measurements using ultra-short pulse. In the semi-infinite medium, under the assumption $\frac{\Delta\mu_a}{\mu_{a0}} \ll 1$ and μ_s' is constant, we can get approximated DPF as (Fantini and Franceschini, 2002)

$$DPF = \frac{3\sqrt{\mu_s'}}{2\sqrt{\mu_{a0}}} \frac{d\sqrt{3\mu_{a0}\mu_s'}}{d\sqrt{3\mu_{a0}\mu_s'} + 1} \tag{3.14}$$

In the near-infrared region, the chromophores for absorption are oxy- and deoxy-hemoglobin. Therefore, combining Eq.(3.2) with Eq.(3.12) and Eq.(3.13), we can get (Fantini and Franceschini, 2002)

$$\Delta A(\lambda) = -\ln\left(\frac{I_{final}(\lambda)}{I_{initial}(\lambda)}\right) = (\varepsilon_{HbO}(\lambda)\Delta[HbO] + \varepsilon_{Hb}(\lambda)\Delta[Hb]) \cdot DPF(\lambda) \cdot d \qquad (3.15)$$

If we measure the changes in two wavelengths, particularly λ_1 =690 nm and λ_2 =830 nm in our studies, we could get concentration change of oxy- and deoxy-hemoglobin ($\Delta[HbO]$ and $\Delta[Hb]$ respectively) as (Fantini and Franceschini, 2002):

$$\Delta[HbO] = \frac{\varepsilon_{HbO}(\lambda_2)\frac{\Delta A(\lambda_1)}{DPF(\lambda_1)} - \varepsilon_{HbO}(\lambda_1)\frac{\Delta A(\lambda_2)}{DPF(\lambda_2)}}{d \cdot (\varepsilon_{HbO}(\lambda_2)\varepsilon_{Hb}(\lambda_1) - \varepsilon_{HbO}(\lambda_1)\varepsilon_{Hb}(\lambda_2))} \qquad (3.16)$$

$$\Delta[Hb] = \frac{\varepsilon_{Hb}(\lambda_1)\frac{\Delta A(\lambda_2)}{DPF(\lambda_2)} - \varepsilon_{Hb}(\lambda_2)\frac{\Delta A(\lambda_1)}{DPF(\lambda_1)}}{d \cdot (\varepsilon_{HbO}(\lambda_2)\varepsilon_{Hb}(\lambda_1) - \varepsilon_{HbO}(\lambda_1)\varepsilon_{Hb}(\lambda_2))} \qquad (3.17)$$

Eq. (3.16) and Eq. (3.17) are the key functions we used to calculate the concentration change of hemoglobin in NIRS brain studies.

3.5 Hemodynamic Model of in vivo NIRS measurements

From above sections, we understand that by taking NIRS measurements using two near-infrared wavelengths on a specific source-detector distance we can get the concentration change of deoxy- and oxy-hemoglobin within the tissue volume of banana-shape identified by the source-detector distance. Nevertheless, we have to make appropriate physiological interpretation of these hemoglobin-related measurements.

First of all, we need to establish a model to represent our problem as shown in Fig. 3.3 (Fantini, 2002)

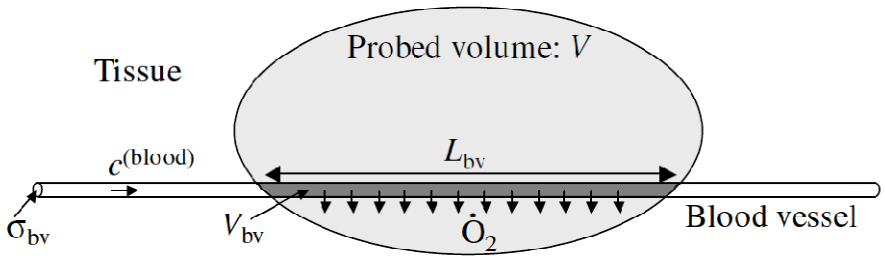

Fig. 3.3 Schematic representation of physiological model.

where $V$is the tissue region probed by NIRS, i.e. the volume that contains most of the photon migration paths from the illumination point to the collection optical fiber. There is a blood vessel with cross-section σ_{bv} cross V with an intersection length L_{bv} and intersection volume V_{bv}. The blood flow in this blood vessel has a speed of $c^{(blood)}$. As the blood flows within volume V, due to the oxygen diffusion to tissue cells, the concentration of oxygen $[O_2]^{(blood)}$in the blood decrease with a rate proportional to the difference between oxygen concentrations in the plasma $[O_2]^{(plasma)}$and in the tissue $[O_2]^{(tissue)}$. This relationship is described in the following equation (Fantini, 2002):

$$\frac{d[O_2]^{(blood)}}{dl} = -\frac{k}{c^{(blood)}}\left([O_2]^{(plasma\,)} - [O_2]^{(tissue)}\right) = -\frac{kr}{c^{(blood)}}[O_2]^{(blood)} \qquad (3.18)$$

where $r = ([O_2]^{(plasma)} - [O_2]^{(tissue)})/[O_2]^{(blood)}$, k is the probability of extraction per unit time for each oxygen molecule, and l is the line coordinate along the blood vessel. By making the assumption that oxygen extraction $\alpha_{O_2} = kr$ and $c^{(blood)}$ are independent of l, we have

$$[O_2]^{(blood)}(l) = [O_2]_0^{(blood)} e^{-\frac{\alpha_{O_2}}{c^{(blood)}} l} \tag{3.19}$$

With the assumption that α_{O_2} is uniform over the length L_{bv} of the blood vessel but associated with changes in $[O_2]^{(tissue)}$ which reflect changes in the cellular metabolic rate of oxygen, the concentration of oxyhemoglobin in the tissue volume V can be written as the average concentration of oxyhemoglobin in the blood times the blood volume fraction V_{bv}/V

$$[HbO]^{(tissue)} = \langle [HbO]^{(blood)} \rangle_V \cdot V_{bv}/V \tag{3.20}$$

Using proportionality between oxyhemoglobin and oxygen concentrations, we can get (Fantini, 2002)

$$[HbO]^{(tissue)} = SO_2|_0^{(blood)} [HbT]^{(blood)} \left(1 - e^{-\frac{\alpha_{O_2} L_{bv}}{c^{(blood)}}}\right) \frac{c^{(blood)} \sigma_{bv}}{\alpha_{O_2} V} \tag{3.21}$$

where $SO_2|_0^{(blood)}$ is the initial oxygen saturation of hemoglobin at $l = 0$, before any oxygen extraction occurs in volume V. $[HbT]^{(blood)} = [HbO]^{(blood)} + [Hb]^{(blood)}$ is the total hemoglobin concentration in the blood, which is independent of l.

With Eq. (3.21), it's straightforward to calculate the following analytical relationship between concentration of hemoglobin and physiological parameters (Fantini, 2002).

$$\begin{aligned} [Hb]^{(tissue)} &= [HbT]^{(tissue)} - [HbO]^{(tissue)} \\ &= [HbT]^{(blood)} \frac{V_{bv}}{V} \left(1 - SO_2|_0^{(blood)} \left(1 - e^{-\frac{\alpha_{O_2} L_{bv}}{c^{(blood)}}}\right) \frac{c^{(blood)}}{\alpha_{O_2} L_{bv}}\right) \end{aligned} \tag{3.22}$$

$$[HbT]^{(tissue)} = [HbT]^{(blood)} \frac{V_{bv}}{V} \tag{3.23}$$

If there're multiple blood vessels (indicating by superscripts (MV)) in the probed volume V, we can make the summation of single-blood-vessel case in Eq.(3.21), (3.22) and (3.23) to obtain the

more general case where the volume V includes arteries, capillaries and veins with the superscripts (a), (c) and (v) respectively as follows (Fantini, 2002):

$$[HbO]^{(tissue)MV} = \left[SO_2|^{(a-blood)} V_{bv}^{(a)} + SO_2|_0^{(c-blood)} \left(1 - e^{-\frac{\alpha_{O_2} L_{bv}^{(c)}}{c^{(c-blood)}}} \right) \frac{c^{(c-blood)} \sigma_{bv}^{(c)}}{\alpha_{O_2}} + SO_2|^{(v-blood)} V_{bv}^{(v)} \right] \frac{[HbT]^{(blood)}}{V} \tag{3.24}$$

$$[Hb]^{(tissue)MV} = \left\{ \left(1 - SO_2|^{(a-blood)}\right) V_{bv}^{(a)} + V_{bv}^{(c)} \times \left[1 - SO_2|_0^{(c-blood)} \left(1 - e^{-\frac{\alpha_{O_2} L_{bv}^{(c)}}{c^{(c-blood)}}} \right) \frac{c^{(c-blood)}}{\alpha_{O_2} L_{bv}^{(c)}} \right] + \left(1 - SO_2|^{(v-blood)}\right) V_{bv}^{(v)} \right\} \times \frac{[HbT]^{(blood)}}{V} \tag{3.25}$$

$$[HbT]^{(tissue)MV} = \left(V_{bv}^{(a)} + V_{bv}^{(c)} + V_{bv}^{(v)} \right) \frac{[HbT]^{(blood)}}{V} \tag{3.26}$$

Physiological analysis of single blood vessel case in Eq. (3.21-23) can be described in the following table:

Physiological change	**Hemoglobin Concentration Change**	**Phase between $\Delta[HbO]$ and $\Delta[Hb]$**
Total hemoglobin concentration in blood $[HbT]^{(blood)} \uparrow$	$[HbO]^{(tissue)} \uparrow$; $[Hb]^{(tissue)} \uparrow$	0°
Blood partial volume $\sigma_{bv} \uparrow$	$[HbO]^{(tissue)} \uparrow$; $[Hb]^{(tissue)} \uparrow$	0°
Initial blood oxygen saturation $SO_2\|_0^{(blood)} \uparrow$	$[HbO]^{(tissue)} \uparrow$; $[Hb]^{(tissue)} \downarrow$	180°
Oxygen utilization rate $\alpha_{O_2} \uparrow$	$[HbO]^{(tissue)} \uparrow$; $[Hb]^{(tissue)} \downarrow$	180°
Speed of blood flow $c^{(blood)} \uparrow$	$[HbO]^{(tissue)} \uparrow$; $[Hb]^{(tissue)} \downarrow$	180°

Tab 3.1. Relationship of physiological parameters change and the phase between the concentration change of oxy- and deoxy-hemoglobin in single blood vessel case

However, Tab 3.1 only explains the simple situation, in observations of most experiments, the phase between $\Delta[HbO]$ and $\Delta[Hb]$ is neither 0° nor 180°. The reasons of these intermediate phase values result from multiple blood vessels or multiple physiological parameters change (Fantini, 2002). In the first case, the superposition of multiple blood vessels would cause different relative contributions of different blood vessels, and further lead to an arbitrary phase difference between $[HbO]^{(tissue)MV}$ and $[Hb]^{(tissue)MV}$; in the second case, there might be multiple physiological change even for single blood vessel (Fantini, 2002). For example, a blood volume increase would associate with a blood flow accelerates. A time lag of the superposition of these in-phase change and out-of-phase changes would result in an intermediate phase difference in hemoglobin concentration. A further interpretation of this arbitrary phase between oxy- and deoxyhemoglobin will be discussed in the next chapter.

3.6 Summary

In this chapter, we introduced the NIRS technology we used in our experiments. Diffusion theory is the fundamental mathematical model in diffusive near-infrared spectroscopy; we showed how from diffusion theory the banana-shape, which is the region of highest sensitivity for the migrating photons, is calculated. Based on the theory, we derived the modified Beer-Lambert law which is the key equation to calculate concentration change of oxy-and deoxy-hemoglobin from detected light intensity change. Finally, we presented a hemodynamic model that can be used to guide the physiological interpretation of oxy- and deoxy-hemoglobin concentration measurements in tissue using NIRS. This model indicates the possible sources of oscillatory components of oxy- and deoxy- hemoglobin concentrations that are in-phase, out-of-phase or arbitrary angle. This model is the foundation stone of our phase analysis of low frequency hemodynamic oscillations.

4. Phase Analysis Method

In this chapter, we will introduce our phase analysis method. There are two major phase analysis method, one is cross-correlation PHASOR method; the other is the phase synchronization analysis. In addition, we will discuss circular or directional statistics, which is the qualified statistical method for phase measurements, rather than traditional statistical method for linear variables.

4.1 Cross-correlation PHASOR Method

The idea of using Phasor notation for hemodynamic oscillations measured with NIRS was first proposed by our group (Zheng et al, 2010). A Phasor is a 2D polar vectors characterized by amplitude A and phase θ.

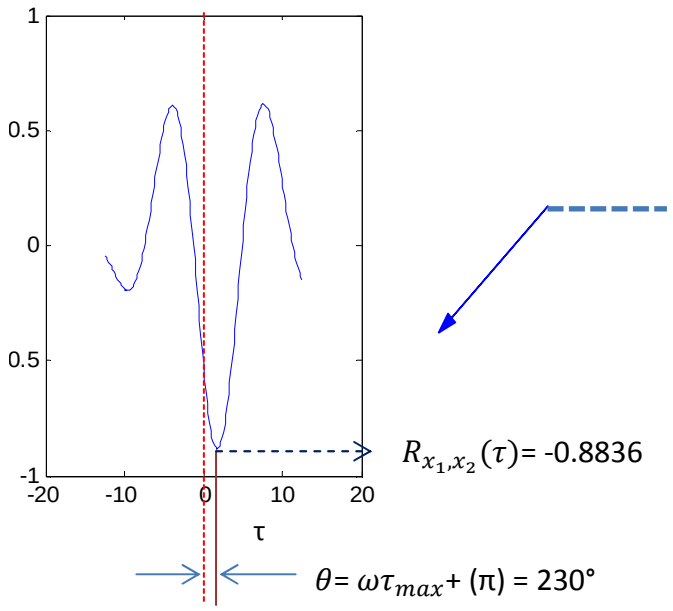

Fig. 4.1. One demo example of how to generate phasors from cross-correlation of signal $x_1(t)$ and $x_2(t)$ filtered around LFO

As explained in Chapter 2, we are interested in hemoglobin concentration oscillations at a specific frequency – low frequency hemodynamic oscillations (LFO) around 0.1 Hz which is meaningful in brain autoregulation, functional connectivity and physiological studies. Filtered with a relative narrow frequency band around LFO, oxy- and deoxy-hemoglobin concentrations are harmonic oscillations at a fixed angular frequency (ω). In addition, in order to minimize the intrinsic phase and amplitude variations and make sure each time-point sampled in experiments corresponding to one phasor or one relative phase, we calculated the phasor at one time-point by isolating a few periods of oscillations within a window which is centered at the specific time-point. To better understand the algorithm we used, here is an example shown in Fig. 4.1. At a given time-point t, we calculate the cross-correlation of LFO filtered oscillations of signal $x_1(t)$ against $x_2(t)$ within a window containing a few periods of oscillations. The exampled plot of cross-correlation is on the left side of Fig. 4.1. There will be a maximum value of $\left|R_{x_1, x_2}(\tau)\right|$, which corresponds to $\tau_{\max}$ in the time axis of the cross-correlation plot. The relative phase of signal $x_1(t)$ and $x_2(t)$ is defined as

$$\theta_{x_1,\ x_2}(t) = \omega\tau_{max}\ [+\pi\ if\ R_{x_1,\ x_2}(\tau_{max}) < 0] \tag{4.1}$$

In the case of Fig.4.1, the relative phase is calculated as 230° because the maximum value of $\left|R_{x_1,\ x_2}(\tau)\right|$ reaches with$R_{x_1,\ x_2}(\tau_{max}) = -0.8836 < 0$. Therefore, the phasor's arrow direction is pointed to $\theta_{x_1,\ x_2}(t) = 230°$ counterclockwise to the horizontal right. If the phasor is used to represent each physical quantity, i.e. oxy- and deoxy-hemoglobin concentration, the phasor amplitude is defined as one half the peak-to-peak ranges of the measured oscillations, so that the length of the arrow is given by $\{\max[x_1(t)] - \min[x_1(t)]\}/2$; note that in this case the phase of one hemoglobin species (oxy-hemoglobin) is set arbitrarily at zero. If the phasor is used to represent the correlation between two signals, the length of the phasor is given by the value of

$\left|R_{x_1,\ x_2}(\tau_{max})\right|$, as shown in Fig. 4.1, the length of phasor is 0.8836 taken 1.0 as the reference length.

One point we need to address here is that the signal $x_1(t)$ and $x_2(t)$ can be either hemodynamic oscillations or physiological signals, which would certainly take the phasor method to much broader application in near-infrared imaging. In specific, the relative phase of the oscillations of deoxy-hemoglobin $[Hb](t)$ and oxy-hemoglobin $[HbO](t)$ is defined in Eq. (4.2) by rewritten from Eq. (4.1):

$$\theta_{[Hb],[HbO]}(t) = \omega\tau_{max}\ [+\pi\ if\ R_{[Hb],[HbO]}(\tau_{max}) < 0] \tag{4.2}$$

The phasor model in tissue measurement can be illustrated in Fig. 4.2. In a tissue model having reduced scattering coefficient and absorption coefficients $\mu_s' = 10\ cm^{-1}$, $\mu_a(690\ nm) = 0.12\ cm^{-1}$ and $\mu_a(830\ nm) = 0.13\ cm^{-1}$ respectively, we consider two cubic regions where [HbO] and [Hb] oscillate around LFO: (a) single region of hemoglobin oscillations: the region is a cube of 5 mm side, centered 5 mm to the right of the incident light point at a depth of 6 mm. (b) double region: one cube has the same size and location as (a), and another cube is 5 mm sided, centered 13 mm to the right of the source point at a depth of 8 mm. The oscillations of [HbO] and [Hb] in tissue region are visually represented by phasors. In Fig.4.2 (a), $\Delta[HbO]_{tissue} = 5\ \mu M$ and $\Delta[Hb]_{tissue} = 1.6\ \mu M$ are in a relative phase of 48.6°. In Fig.4.2 (b), on the left hand side region, $\Delta[HbO]^1_{tissue} = 5\ \mu M$ and $\Delta[Hb]^1_{tissue} = 1.6\ \mu M$ oscillating in phase; on the right hand side region, $\Delta[HbO]^2_{tissue} = 5\ \mu M$ and $\Delta[Hb]^2_{tissue} = 1.6\ \mu M$ out of phase with respect to each other but $\Delta[Hb]^2_{tissue}$ has a relative phase 48.6° with respect to $\Delta[HbO]^1_{tissue}$. The relationship of hemoglobin concentration change in tissue $\Delta[HbO]_{tissue}$ and $\Delta[Hb]_{tissue}$ and

those measured $\Delta[HbO]_{meas}$ and $\Delta[Hb]_{meas}$ can be expressed in Eq. (4.3) and (4.4) (Zheng et al, 2010)

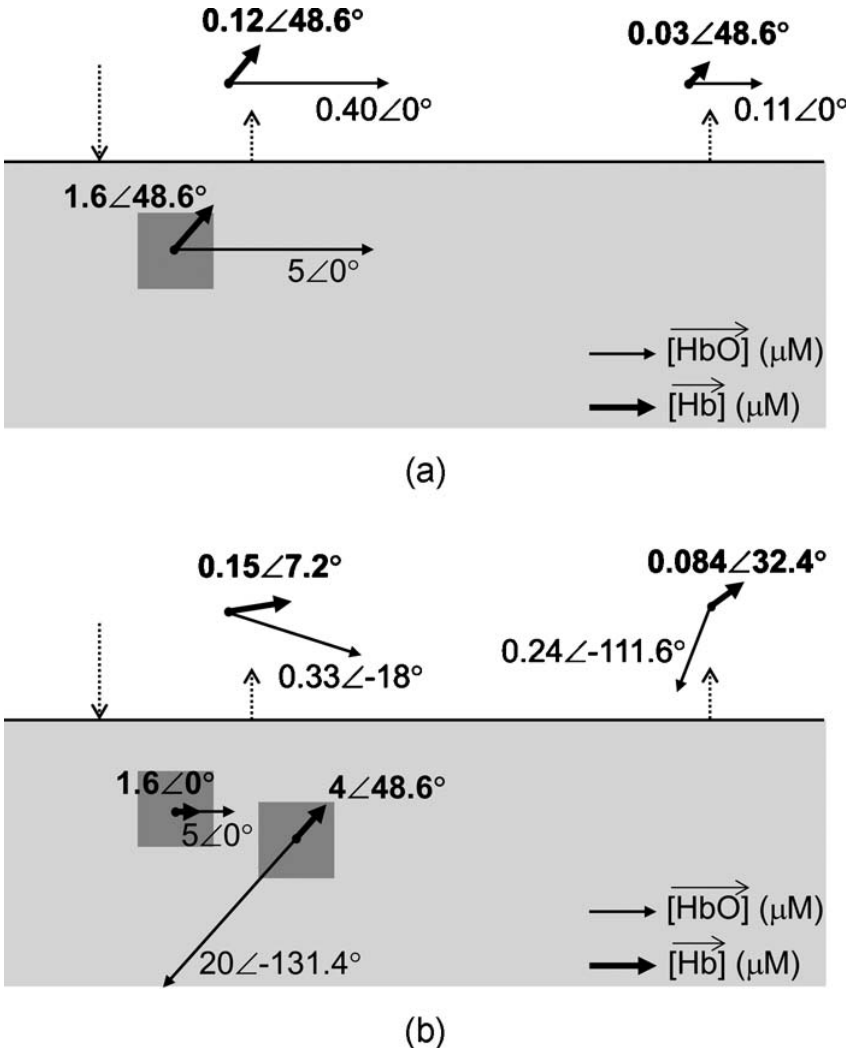

Fig. 4.2. Phasor representation of oscillations in concentrations of deoxyhemoglobin (thick phasors) and oxyhemoglobin (thin phasors) at localized cubic regions in tissue (a) single region and (b) two regions. For the simulations we considered a fixed light incident source position (downward dotted arrow) and two collection detector positions (upward arrows): the nearer one is 1 cm distant from the source and the farther one is 4 cm distant from the source.

$$\Delta[HbO]_{meas} = \frac{1}{D}\sum_{i=1}^{N}\Big\{\varepsilon_{Hb}^{\lambda_1}\varepsilon_{Hb}^{\lambda_2}\Big(k_i^{\lambda_1} - k_i^{\lambda_2}\Big)\Delta[Hb]_{tissue}^{i} + \Big(\varepsilon_{HbO}^{\lambda_1}\varepsilon_{Hb}^{\lambda_2}k_i^{\lambda_1} - \varepsilon_{HbO}^{\lambda_2}\varepsilon_{Hb}^{\lambda_1}k_i^{\lambda_2}\Big)\Delta[HbO]_{tissue}^{i}\Big\} \tag{4.3}$$

$$\Delta[Hb]_{meas} = \frac{1}{D}\sum_{i=1}^{N}\Big\{\Big(\varepsilon_{HbO}^{\lambda_1}\varepsilon_{Hb}^{\lambda_2}k_i^{\lambda_2} - \varepsilon_{HbO}^{\lambda_2}\varepsilon_{Hb}^{\lambda_1}k_i^{\lambda_1}\Big)\Delta[Hb]_{tissue}^{i} - \varepsilon_{HbO}^{\lambda_1}\varepsilon_{HbO}^{\lambda_2}\Big(k_i^{\lambda_1} - k_i^{\lambda_2}\Big)\Delta[HbO]_{tissue}^{i}\Big\} \tag{4.4}$$

where N represents the number of regions considered, N=1 in Fig.4.2(a) and N=2 in Fig.4.2(b); $D = \varepsilon_{HbO}^{\lambda_1}\varepsilon_{Hb}^{\lambda_2} - \varepsilon_{HbO}^{\lambda_2}\varepsilon_{Hb}^{\lambda_1}$ and $k_i^{\lambda_j}$ are the ratios of partial over total mean path length (j=1,2 representing two wavelengths we use)

$$k_i^{\lambda_j} = \frac{\langle l_i^{\lambda_j}\rangle}{\langle L_T^{\lambda_j}\rangle} \tag{4.5}$$

Eq. (4.3) and (4.4) show that $\Delta[Hb]_{meas}$ and $\Delta[HbO]_{meas}$ are the linear combinations of $\Delta[Hb]_{tissue}^{i}$ and $\Delta[HbO]_{tissue}^{i}$. So if $\Delta[Hb]_{tissue}^{i}$ and $\Delta[HbO]_{tissue}^{i}$ in tissue regions are all either in phase or out-of-phase because of the physiological effects listed in Tab. 3.1, the phase difference between $\Delta[Hb]_{meas}$ and $\Delta[HbO]_{meas}$ can only be either in-phase oscillations (0°) or out-of-phase oscillations (180°). However, if there is a time difference between the onset of these physiological effects, the phase shift between $\Delta[Hb]_{meas}$ and $\Delta[HbO]_{meas}$ will be neither 0 nor π. In Fig.4.2 (a), the time difference happens in the same tissue region, which leads to the same intermediate phase difference between $\Delta[Hb]_{meas}$ and $\Delta[HbO]_{meas}$ in both near and far source-detector pairs. In Fig.4.2(b), the time difference happens in two different tissue regions. The left hand side tissue region's in phase oscillation possibly resulted from the increase of arterial blood volume change; while right hand side tissue region's out-of-phase oscillation possibly resulted

from the blood flow velocity increase but has a time delay to the left hand side volume change. These two tissue regions lead to a 25.2° phase shift in near source-detector pair while a 144.0° phase shift in far source-detector pair.

This intermediate phase shift can be further interpreted in vector concepts in Fig.4.3

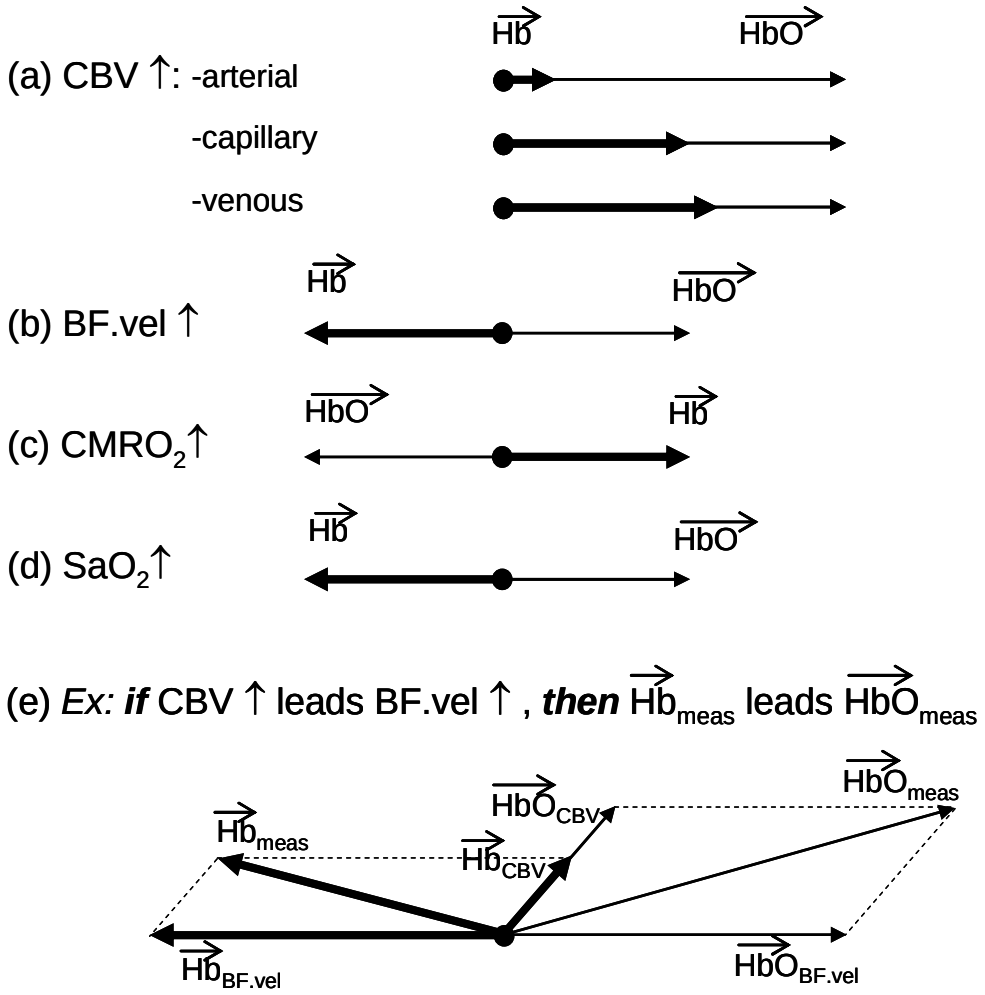

Fig. 4.3. Phasor representation of [Hb] (thick phasors) and [HbO] (thin phasors) in response to physiological signals change.

In Fig.4.3, Increase in (a) cerebral blood volume (CBV) can lead to the in-phase (0°) relationship between $\left[\overrightarrow{Hb}\right]^{i}_{tissue}$ and $\left[\overrightarrow{HbO}\right]^{i}_{tissue}$. Increases in (b) blood flow velocity (BF.vel), (c) cerebral metabolic rate of oxygen ($CMRO_2$), and (d) arterial saturation (SaO_2) can lead to the out-of-phase (180°) difference between $\left[\overrightarrow{Hb}\right]^{i}_{tissue}$ and $\left[\overrightarrow{HbO}\right]^{i}_{tissue}$. Taken the vector sum, in Fig.4.3 (e) we show that how $\left[\overrightarrow{Hb}\right]_{meas}$ and $\left[\overrightarrow{HbO}\right]_{meas}$ phasors can be decomposed in terms of phasors associated with different hemodynamic/metabolic parameters, but they have an intermediate phase shift ~150°. These intermediate phase shifts have been reported by Wolf et al, 2002 and Taga et al, 2000. In this example, measured [Hb] oscillations leading measured [HbO] oscillations are consistent with cerebral blood volume (CBV) changes that lead blood flow velocity (BF.vel) changes.

From Fig.4.3, we can clearly see the advantage of phasor representation that it can lead to a practical characterization and visualization of cerebral hemodynamics and to a more sophisticated approach to the optical study of neurovascular coupling effects.

Based upon the phasor, we can develop a bunch of novel representations of hemodynamic oscillations relationships. Because each time-point corresponds to a phasor between deoxy- and oxy-hemoglobin oscillations, we can generate a phasor developing movie. This changes the static representation of phase relationship to a dynamic/animated demonstration and even real-time monitor in the future. In addition, for phase-distribution in a time range, we can use sophisticated circular statistics to generate a phasor sector of which the average direction is the mean phase and the half sector width is the standard deviation. This phasor sector can be used to classify phase distribution patterns in different time range or during different protocols of mental

activation time in specific. All these phasor analytical tools will be demonstrated in detail in Chapter 6.

4.2 Phase Synchronization Analysis

Another method to obtain phase information from hemodynamic signals is phase synchronization analysis. Phase synchronization is generally defined as a specific relationship between two signals of arbitrary nature, including non-periodic and noisy signals. In our case, the hemodynamic signals filtered by relative narrow frequency band around 0.1 Hz (LFO) can be considered as periodic, quasiharmonic signals. Two periodic non-identical oscillators having phases $\phi_1(t)$ and $\phi_2(t)$ are phase synchronized if there are two integers n and m such that (Toss et al, 1998)

$$|n\phi_1(t) - m\phi_2(t)| < const. \tag{4.6}$$

For periodic oscillators, we can consider it as a modulating signal in Fig.4.4

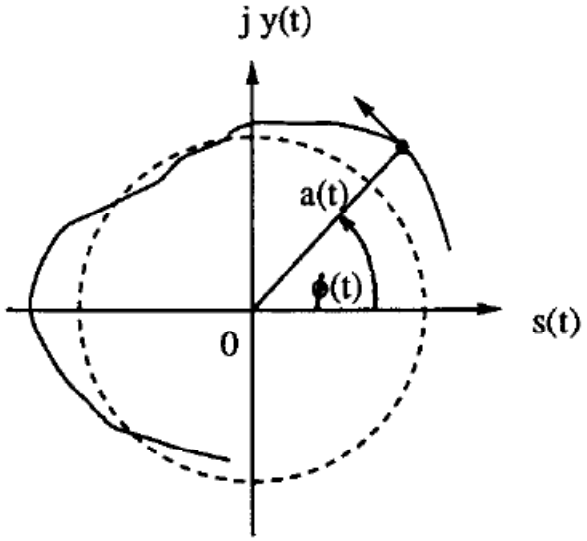

Fig.4.4. Envelope and instantaneous phase of frequency modulated signal. (Boashash, 1992). Frequency Modulated signal is $s(t) = a(t)\cos(\phi(t))$; a(t) is envelop; $\phi(t)$ is phase

The instantaneous frequency at $t = \tau$ is defined as

$$f(\tau) = \frac{1}{2\pi}\frac{d\phi(t)}{dt}\bigg|_{\tau} \tag{4.7}$$

Eq.(4.7) for the pulsation ω becomes:

$$\omega = \overline{\dot{\phi}_k}(t) \tag{4.8}$$

where overbar denotes the time average. If we insert Eq. (4.8) into Eq. (4.6), we have

$$n\omega_1 = m\omega_2 \tag{4.9}$$

Therefore phase synchronization implies frequency synchronization, but the opposite is not generally valid.

For a real function of time $s(t)$, the phase can be defined as the phase of the complex analytical continuation of the given function into the complex plane (Toronov et al. 2000). Using Hilbert Transform, the complex formation of $s(t)$ is $\boldsymbol{S}(t)$

$$\boldsymbol{S}(t) = s(t) + iq(t) = s(t) + i \int_{-\infty}^{\infty} \frac{s(u)}{\pi(t-u)} du \tag{4.10}$$

where $i = \sqrt{-1}$; $s(t)$ itself is the real part of $\boldsymbol{S}(t)$, while $q(t)$ is the imaginary part of $\boldsymbol{S}(t)$.

Therefore, for signal $s_i(t)$, i = 1, 2 we have

$$\phi_i(t) = \arg\left(\boldsymbol{S_i}(t)\right) \tag{4.11}$$

Eq. (4.11) is the equation we used to obtain instantaneous phase value of hemodynamic oscillations filtered around LFO. The relative phase between deoxy-hemoglobin and oxy-hemoglobin is

$$\theta_{[Hb],[HbO]}(t) = n\phi_{[Hb]}(t) - m\phi_{[HbO]}(t) \tag{4.12}$$

where the *n* and *m* are defined as a ratio from Eq. (4.9)

$$n{:}\,m = f_{[HbO]}{:}\,f_{[Hb]} \tag{4.13}$$

where $f_{[HbO]}$ and $f_{[Hb]}$ are the frequency of oxy-hemoglobin oscillation and deoxy-hemoglobin oscillation respectively.

Eq. (4.13) is very important because every time before calculating the phase difference between oxy- and deoxy-hemoglobin using the phase synchronization method, one should identify the ratio *n*: *m* and in turn change the coefficient values in Eq. (4.12). In our study, because we are interested in LFO and oxy- and deoxy-hemoglobin are derived by running a relative narrow band pass filte, the oscillation frequencies are very close. Therefore, we have always assumed that *n*:

m = 1: 1. Similar requirement exists in the Phasor method because the cross-correlation should be taken between two signals with comparable oscillation frequencies. Therefore, in our computer program for phase data analysis, we manually added a condition

$$2:3 < f_{[HbO]}: f_{[Hb]} < 3:2 \tag{4.14}$$

For any two signals, if their frequencies ratio is less than 1.50 and larger than 0.67, we can use cross-correlation phasor and 1: 1 phase synchronization methods to calculate the phase difference; otherwise, an exception returns and the data is discarded. In future work, we should break this restriction and allow any n: m values by using Eq. (4.12) and improve cross-correlation phasor method.

The strength of phase synchronization is described by phase synchronization index (PSI). For random signals (like oxy- and deoxy-hemoglobin) the wrapped phase θ over the interval $(-\pi, \pi)$ has a probability distribution. The sharpness of the probability distribution P_i over N bins can be quantified by Shannon entropy (Toronov et al. 2000).

$$E = -\sum_{i=1}^{N} P_i \ln (P_i) \tag{4.15}$$

where P_i is the probability that a phase value belongs to an angular bin "i" ($i = 1,2, \dots \dots, N$). A uniform distribution has the entropy value $E_{max} = \ln(N)$.

The phase synchronization index (PSI) is designed to characterize the deviation of a distribution from the uniformity

$$PSI = \frac{E_{max} - E}{E_{max}} \tag{4.16}$$

From Eq.(4.16), we have two boundary values of the PSI

$$PSI = \begin{cases} 0 & when\ E = E_{max}:\ uniform\ distribution \\ 1 & when\ E = 0:\ \ \delta\ function\ distribution \end{cases} \tag{4.17}$$

PSI value is the parameter to determine if two signals are phase synchronized or not. One may use large iterations of Gaussian random number simulation to decide the threshold value corresponding to noise.

4.3 Circular Statistics

Circular statistics is devoted to the development of statistical techniques for data on an angular scale. In contrast to a linear scale, there is no designated zero and the definition of high and low values is arbitrary. For example, a phase of 1° is much closer to 359° than to 90°, although mathematically the difference between 90° and 1° is less than 359° and 1°. Another example: in order to calculate the mean value of two phase values: 1° and 359°, if one uses linear statistics, one would get 180°, which is incorrect, since both angles point to a common direction of 0°. In this section, we will briefly introduce the circular statistics we used.

For a sample of the angular variable ψ of size *N*, the angles are first transformed to unit vectors in the two-dimensional plane by

$$r_i = (\cos(\psi_i), \sin(\psi_i)) \tag{4.18}$$

The mean resultant vector $\bar{r}$ is therefore given by

$$\bar{r} = \left(\frac{1}{N} \sum_i \cos(\psi_i), \frac{1}{N} \sum_i \sin(\psi_i) \right) \tag{4.19}$$

From Eq. (4.19) we have two parameters to describe angular average (Fish, 1995)

$$resultant\ vector\ length\colon\ R = \|\bar{r}\|$$
$$circular\ mean\colon\ \bar{\psi} = \arg(\bar{r}) \tag{4.20}$$

The median direction of a sample ψ is the direction for which half of the data points fall on either side. For circular data, we have to find the diameter of the unit circle that divides the whole data points into two equally sized groups. The median is the endpoint of the diameter closer to the center of mass of the data. If the data points are drawn from a uniform distribution or evenly spaced around the circle, there's no well-defined median direction.

The circular variance VAR of the variable ψ is closely related to the length of the mean resultant vector

$$VAR = 1 - R \tag{4.21}$$

Because the mean resultant vector length is in the range of 0 and 1, the circular variance VAR is also bounded in the interval $[0,1]$. If all samples point into the same direction, $R = 1$ and $VAR = 0$; if all sample are spread uniformly around the circle, $R = 0$ and VAR will be 1. Hence, the circular variance VAR is indicative of the spread in a data set.

There are two definitions for standard deviation. First is defined as (Fish, 1995)

$$std = \sqrt{2(1 - R)} \tag{4.22}$$

Second is defined as

$$std_0 = \sqrt{-2\ln R} \tag{4.23}$$

Generally, the first one is preferred, because it is bounded in the interval $[0, \sqrt{2}]$; while the second one ranges from 0 to ∞.

A common question in circular statistics is whether a data sample is distributed uniformly around the circle or has a common mean direction. One of these tests for circular uniformity is Rayleigh test which asks how large the resultant vector length R must be to indicate a non-uniform distribution. It is particularly suited for detecting a unimodal deviation from uniformity. The null hypothesis is

H_0: The population is distributed uniformly around the circle

With alternative hypothesis

H_a: The population is a unimodal distribution

The approximate p-value under H_0 is computed as

$$p = e^{\left\{\sqrt{1+4N+4\left(N^2-R_n^2\right)}-(1+2N)\right\}} \tag{4.24}$$

where $R_n = R \cdot N$. This approximation is valid up to three decimal places for N as small as 10. The Rayleigh test can also be applied to axial data after suitable transformation. Importantly, it assumes sampling from a von Mises distribution.

The von Mises distribution is a continuous probability distribution on the circle. It is similar to the normal distribution wrapped on the circle. It can be considered a circular analogue of the normal distribution. Its probability density function is (Fish, 1995)

$$f(\psi|\mu,\kappa) = \frac{e^{\kappa\cos(\psi-\mu)}}{2\pi I_0(\kappa)} \tag{4.25}$$

where μ is the mean value of sample of ψ; κ is the concentration parameter and $1/\kappa$ is analogous to σ^2 in the normal distribution; and I_0 is the modified Bessel function of order zero.

Circular statistics also has its own statistical test analogue of the two sample t-test or the one-factor ANOVA. It is called Watson-Williams test (Fish, 1995), which assesses the question whether the mean direction of two or more samples are identical or not.

H_0: All of s groups share a common mean direction, i.e. $\overline{\psi_1} = \overline{\psi_2} = \cdots = \overline{\psi_s}$

H_a: Not all s groups have a common mean direction

Rejecting the null hypothesis only provides evidence that not all of the s groups come from a population with equal mean direction, not if all groups have pairwise differing mean directions or evidence of which of the groups differ. The test statistic is calculated by

$$F = K\frac{(N-s)\left(\sum_{j=1}^{s} R_j - R\right)}{(s-1)\left(N - \sum_{j=1}^{s} R_j\right)} \tag{4.26}$$

where R is the mean resultant vector length when all samples are pooled and R_j is the mean resultant vector length computed on the j-th group alone. The correction factor $K = 1 + \frac{3}{8\kappa}$, where κ is the maximum likelihood estimate of the concentration parameter of a von Mises distribution with resultant vector length r_w. r_w is the mean resultant vector length of the s resultant vector r_j computed for each group individually. The obtained value of the test statistic is then compared to a critical value at the δ level obtained from $F_{\delta(1),1,N-2}$ (which can be found in a table of F test).

The Watson-Williams test assumes underlying von Mises distribution with equal concentration parameter, but has proven to be fairly robust against deviations from these assumptions. The sample size for each individual sample should be at least 5. And bin widths should be no larger than 10°.

There is a multi-sample test for equal median directions, which is a circular analogue to the Kruskal-Wallis test.

H_0: Any of s groups share a common median direction, i.e. $\hat{\psi}_1 = \hat{\psi}_2 = \cdots = \hat{\psi}_s$

H_a: Not all s groups have a common median direction

The test statistic is computed as

$$P = \frac{N^2}{M(N-M)} \sum_{i=1}^{s} \frac{m_i^2}{n_i} - \frac{NM}{N-M} \tag{4.27}$$

where n_i is the number of samples in each group. We first compute the total median direction $\hat{\psi}$ by pooling all groups. Then we compute the number m_i of samples within the i-th group, whose angular distance $d(\psi_j^i, \hat{\psi})$ to the total median is negative, where ψ_j^i indicates the j-th sample from the i-th group. The result of Eq.(4.27) is compared to the upper $1-\delta$-percentile of a χ_{s-1}^2 distribution. This statistical test also requires the sample size for each group greater than 10.

4.4 Summary

In this chapter, we introduced the phasor concept used to describe the phase relationship of oxy- and deoxy-hemoglobin and also for describing the phase relationship of physiological parameters. From the phasor representation, we can develop various derivatives for experimental data demonstration. The phasor is a novel approach to near-infrared functional imaging and we will use it in the following chapters. Besides phasor, phase synchronization analysis also provides a way to analyze the phase relationship of hemodynamic signals. The instantaneous frequency and phase approach together with the phasor method offers two effective tools of real-time phase

analysis. Because of the angular characteristics of phases, we have to use the circular statistics tools instead of linear statistics.

5. Experimental Methods

5.1 Instrumentation

The optical instrument was a near-infrared optical spectrometer from ISS, Inc., Champaign, IL (OxiplexTS). In our studies, there are two detector channels (A and B) and a total of 16 laser diodes, 8 emitting at a wavelength of 690 nm and 8 at 830 nm. The wavelengths choice is based upon the absorption spectra window in Fig. 3.1. All sources and detectors are coupled to optical fibers. The source and detector fibers are 3 m long with 0.4 and 3 mm in core diameter respectively. They were arranged on the optical helmet (in Fig. 5.1) according to two circular arrays with the detectors at the centers and the laser sources at four locations of the perimeters. The source-detector distance is 3 cm for all 8 source-detector pairs. The source and detector fibers were firmly held in the pads on the helmet and somewhat flexible to adapt to the curved surface of the subjects' forehead. The helmet is fixed by an adjustable bolt. Each probe received one detector fiber (from channel A for the right forehead side and from channel B for the left side) and four pairs of individual source fibers (each pair consisting of one fiber for 690 nm and one fiber for 830 nm). The connection of sources and detectors are schematically shown in Fig. 5.1. The acquisition rate of the optical system was set to 6.25 Hz, so that we collected on data point every 160 millisecond. With the same sampling rate we also monitored arterial oxygen saturation and heart rate by means of a pulse oximeter (Nellcor N-200) and also the respiration by means of a chest gauge (Sleepmate/Newlife Technologies).

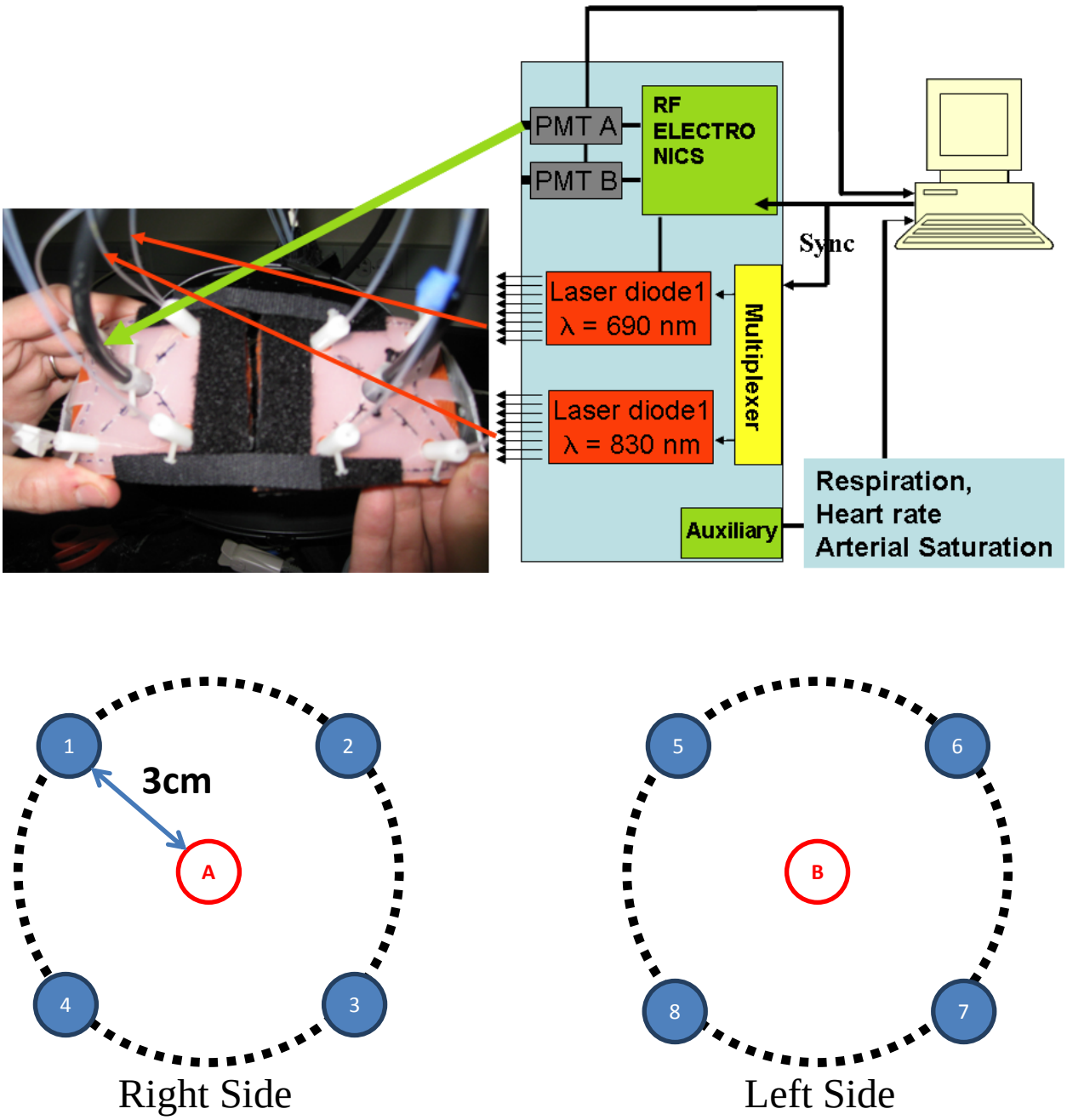

Fig. 5.1. (Upper Left) the optical helmet with the source (transparent) and detector (black) fibers. (Upper Right) schematic of the experimental apparatus. (Bottom) arrangement of sources and detectors, the source ids are clockwise on either side, detector A is placed on the right side of the forehead; detector B on the left side

5.2 Experimental Protocol

Rotating Cube Experiment

Five healthy subjects completed seven cognitive tasks where they viewed five sides of a rotating cube on a computer screen. The side faces of the cube consisted of sections of different colors. In the experiment, the cube presented to the subject had either uniform gray or three/four sections of different colors, and the number of colored sections defined the level of mental workload. Some subjects were challenged with workload 0 (uniform gray) and workload 3 (three colors), while some subjects were challenged with workload 0 and workload 4 (four colors). The experimental schematic was shown in Fig. 5.2.

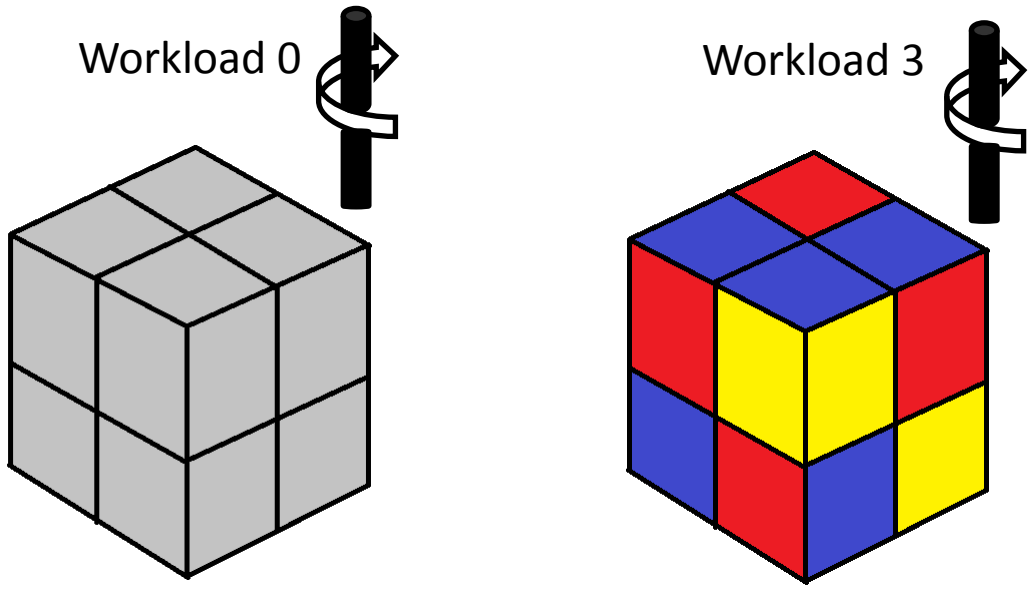

Fig. 5.2. Schematic of rotating cube presented to the subjects, (Left) workload 0 with a uniform gray color; (Right) workload 3 with a three different colors.

During each task, the subjects were asked to count the total number of sections of each color in the five cube sides (lateral and top sides) and their final answer was recorded either by vocal or manually input by arrow buttons on keyboard for verification. Each lateral face of the cube was presented to the subjects for 8 seconds; then the cube underwent a 90° rotation lasting about 3 seconds and stopped when the next lateral face was facing the subject. The process was repeated three times for a total rotation angle of 270° during which four lateral faces of the cube were shown to the subjects. Four extra seconds were finally allowed at the end of the last rotation for the examinations of the colored sections on the top face. The period of time during which five cube sides were presented to the subjects, which lasted 45 seconds, defined a workload period. Workload 0 is a uniform gray colored cube rotating in the same way as in workload 3 but subjects were asked to clear their minds and not to engage in any particular mental task. Each workload was followed by a 40 seconds of rest, for a total trial period of 85 seconds. Two different workload levels (0, 3) or (0,4 for some subjects) were presented randomly six times to the subjects, for a total measurement duration of about 20 minutes including one to three minutes of initial baseline.

Finger Tapping Experiment

One subject completed two finger tapping tasks in different days. The helmet setup was similar to the one in Fig. 5.1, but the source-detector pairs were located on the motor cortex instead of frontal hemispheres as shown in Fig. 5.3. The subject was asked to sit comfortably on the chair with right hand naturally put on the table. After a three to four minutes baseline, the subject started using one's thumb finger to tap in sequence the first, middle, ring, little, ring, middle, first

finger forth and back. This finger tapping workload lasted for 2 minutes and followed by a 2 minutes rest. These trials repeated by 5 times while we collected heart rate, respiration and pulse simultaneously.

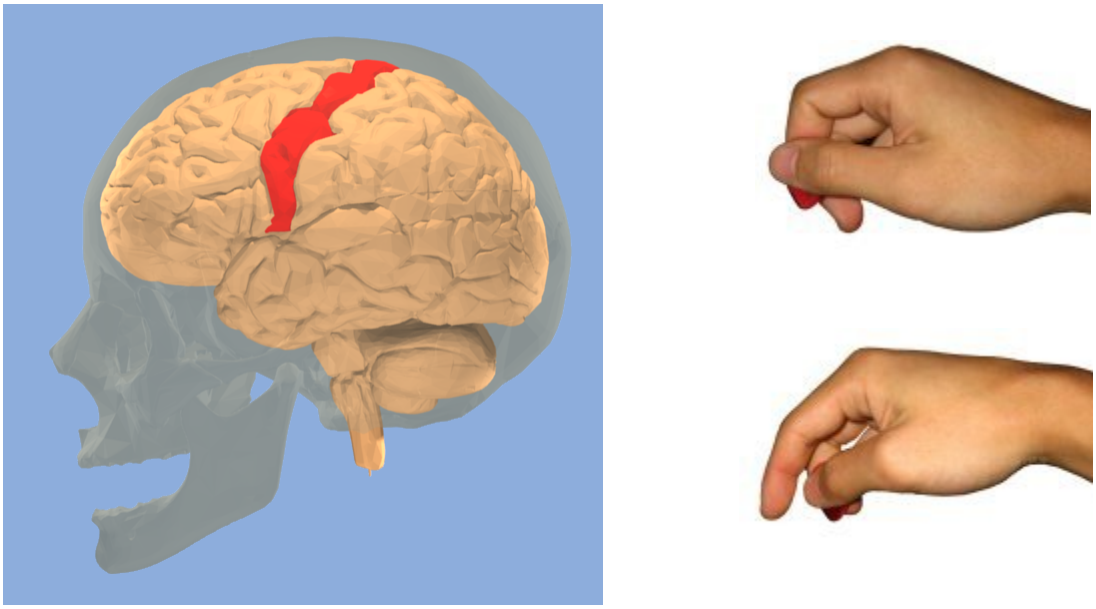

Fig. 5.3. (Left) Motor cortex location (dark red) on the human brain. (Right) The finger tapping: thumb taps other four fingers in a sequence of first, middle, ring, little, ring, middle, first… forth and back.

6. Results

The continuous intensities of the optical data were processed by calculating an average rest value, defined as I_0, in order to apply the modified Beer-Lambert Law (described in Chapter 3.4) to translate intensity changes into absorption changes. The changes of oxy-hemoglobin $\Delta[HbO]$ and deoxy-hemoglobin concentrations $\Delta[Hb]$ were calculated from the data at 3 cm source-detector distance by assuming differential path-length factors (DPF, derived from Eq. 3.15) of 6.5 and 5.8 at the wavelengths of 690 nm and 830 nm respectively. After the temporal trends of $\Delta[HbO]$ and $\Delta[Hb]$ were detrended with a third order polynomial algorithm, we computed a folding average to the 6 repetitions of workload 0 and workload 4 respectively. We studied the statistical significance of the points in the folding average by using a modified t-test at the level of significance $\alpha = 5\%$, which offers a heuristic method to control the rate of statistical errors of type I (false positives) when the data points are correlated (Sassaroli et al. 2008). The results of folding averages for rotating cube experiments are shown from Fig. 6.1 to Fig. 6.7. In each figure, the folding average relative to changes in oxy-hemoglobin concentration $\Delta[HbO]$ is located on the left panel and the relative to changes in deoxy-hemoglobin concentration $\Delta[Hb]$ is located on the right panel. Every panel shows eight near-infrared channels from left to right and upper to lower. The detailed arrangement of sour-detector channels can be found in Fig. 5.1.

The results for finger tapping are shown from Fig. 6.8 to Fig. 6.9. The labels are the same as rotating cube. However, due to the hair at the motor cortex location, signals from channel 1, 2, 3, 4 and 6 are too weak to be detected. The subject was asked to perform finger tapping using right hand, so channel 5, 7 and 8 detected relative strong optical signal changes in finger tapping workload.

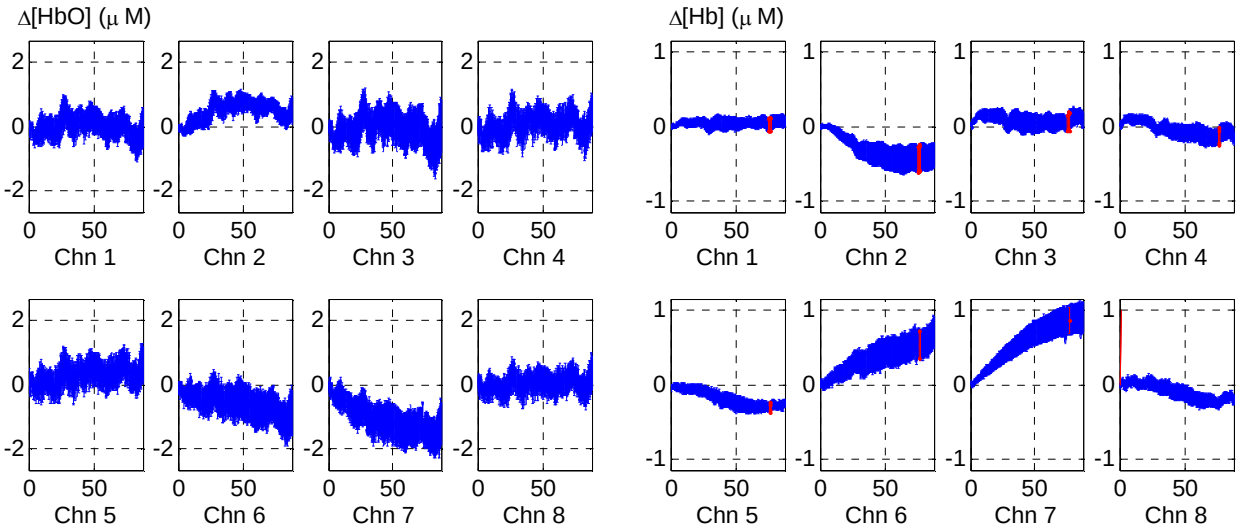

Fig. 6.1 (A). Folding average of changes in $\Delta[HbO]$ on left panels and of changes in $\Delta[Hb]$ on right panels measured for 6 repeated Rotating Cube workload 0 on Subject A (trial 1). X-axis is the time in seconds, 45 sec workload 0 followed by 40 sec rest

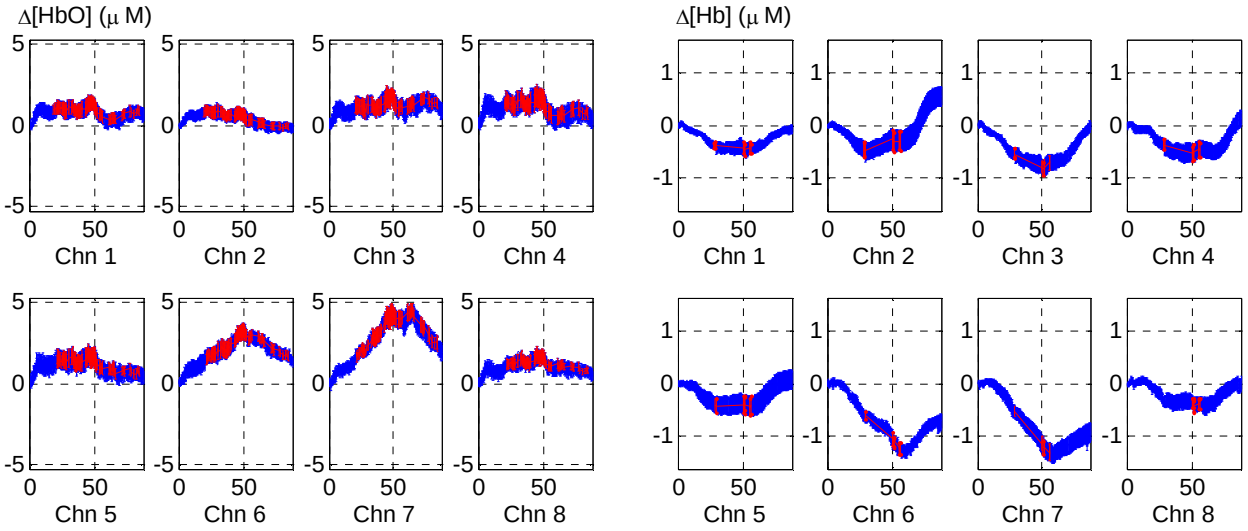

Fig. 6.1 (B). Folding average of changes in $\Delta[HbO]$ on left panels and of changes in $\Delta[Hb]$ on right panels measured for 6 repeated Rotating Cube workload 4 on Subject A (trial 1). X-axis is the time in seconds, 45 sec workload 4 followed by 40 sec rest

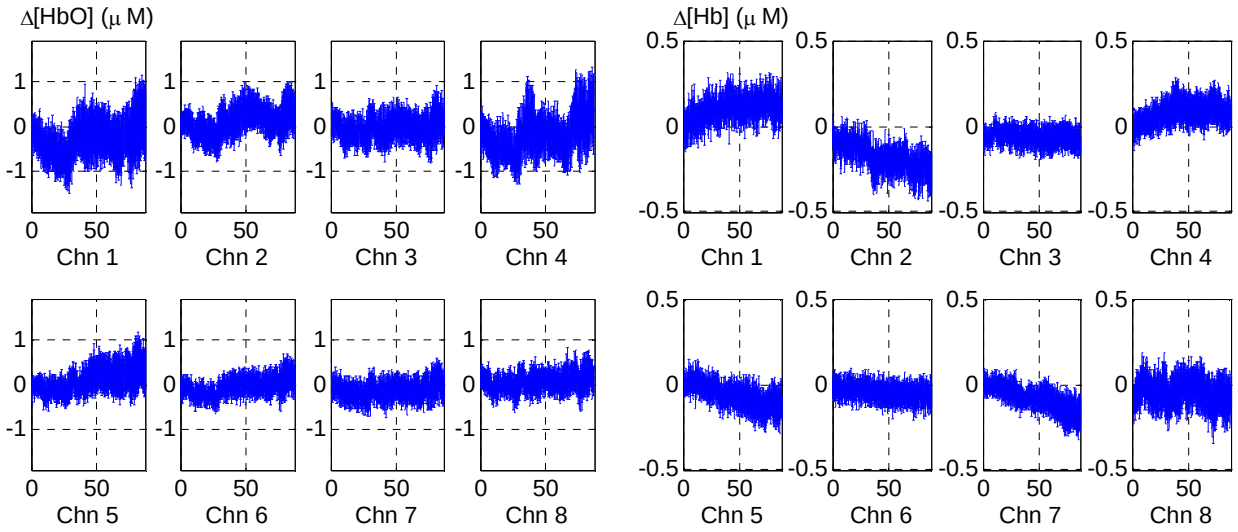

Fig. 6.2 (A). Folding average of changes in $\Delta[HbO]$ on left panels and of changes in $\Delta[Hb]$ on right panels measured for 6 repeated Rotating Cube workload 0 on Subject A (trial 2). X-axis is the time in seconds, 45 sec workload 0 followed by 40 sec rest

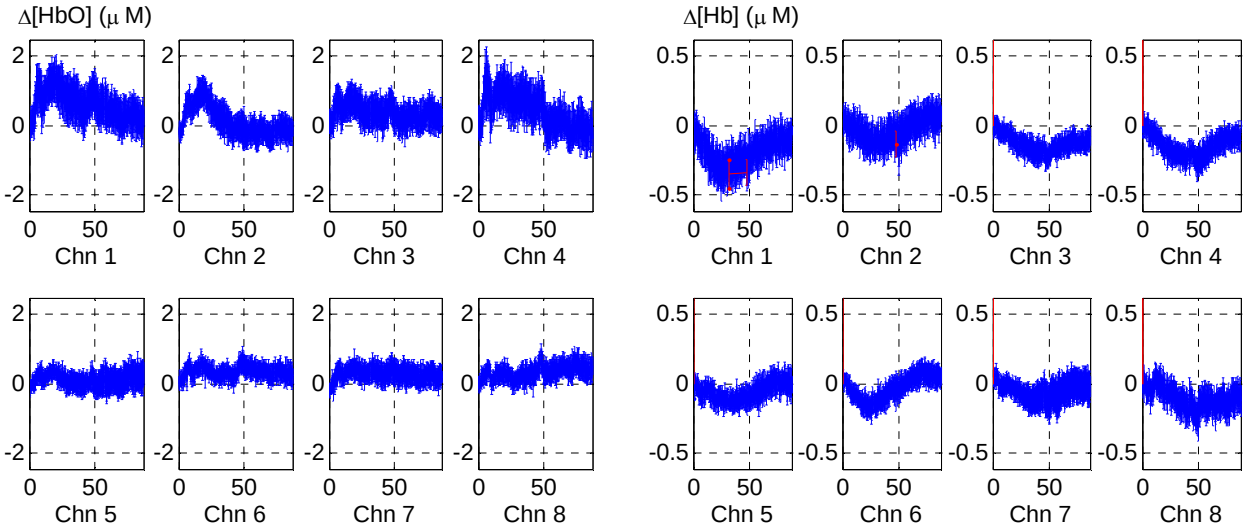

Fig. 6.2 (B). Folding average of changes in $\Delta[HbO]$ on left panels and of changes in $\Delta[Hb]$ on right panels measured for 6 repeated Rotating Cube workload 4 on Subject A (trial 2). X-axis is the time in seconds, 45 sec workload 4 followed by 40 sec rest

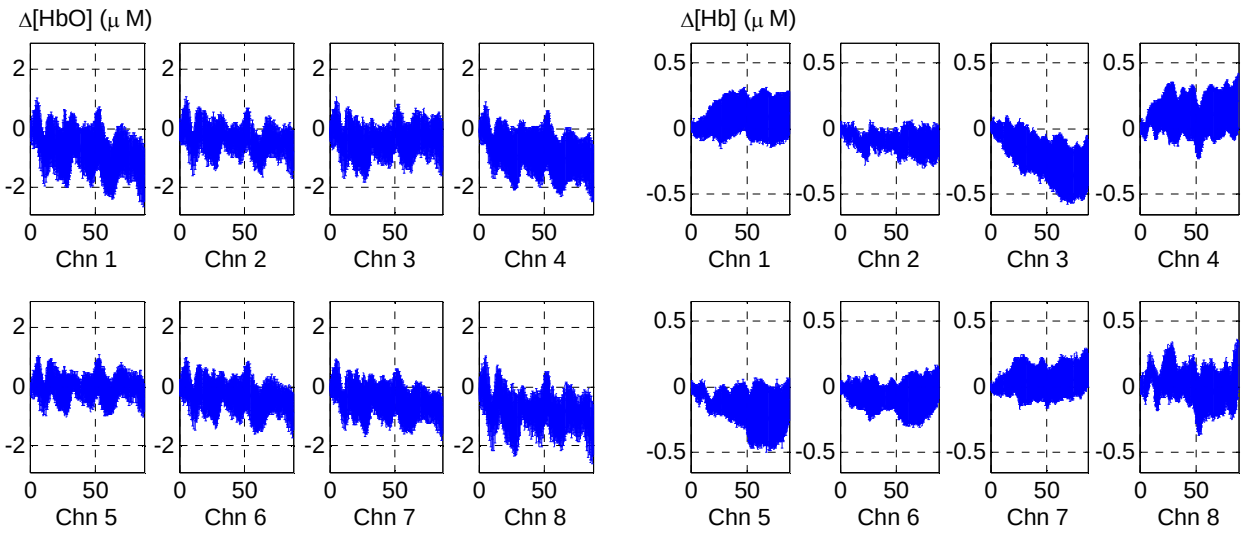

Fig. 6.3 (A). Folding average of changes in $\Delta[HbO]$ on left panels and of changes in $\Delta[Hb]$ on right panels measured for 6 repeated Rotating Cube workload 0 on Subject B. X-axis is the time in seconds, 45 sec workload 0 followed by 40 sec rest

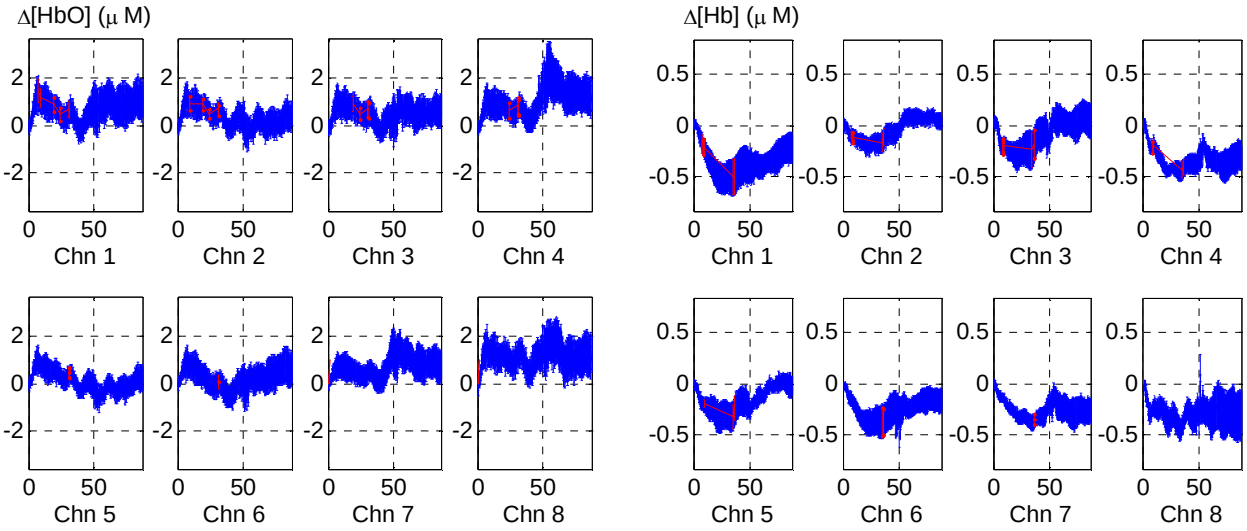

Fig. 6.3 (B). Folding average of changes in $\Delta[HbO]$ on left panels and of changes in $\Delta[Hb]$ on right panels measured for 6 repeated Rotating Cube workload 4 on Subject B. X-axis is the time in seconds, 45 sec workload 4 followed by 40 sec rest

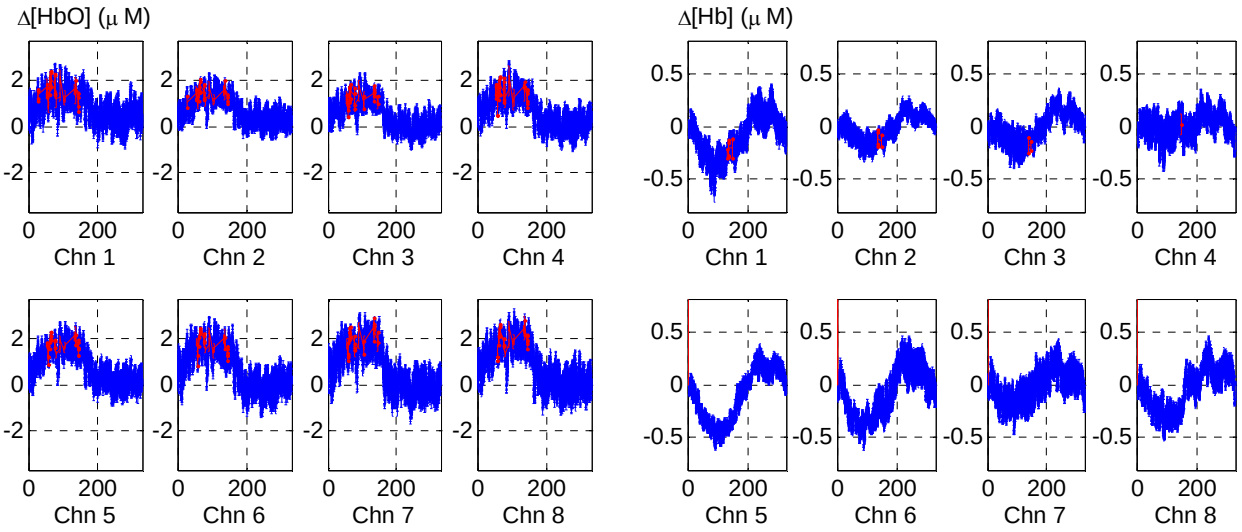

Fig. 6.4 (A). Folding average of changes in $\Delta[HbO]$ on left panels and of changes in $\Delta[Hb]$ on right panels measured for 6 repeated Rotating Cube workload 0 on Subject C. X-axis is the time in seconds, 135 sec workload 0 followed by 180 sec rest

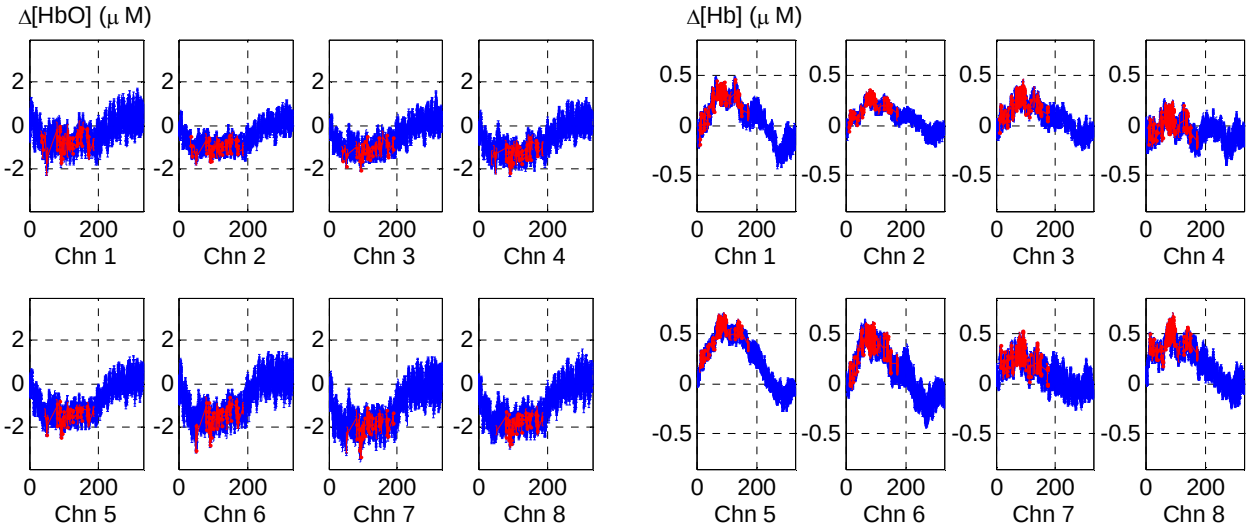

Fig. 6.4 (B). Folding average of changes in $\Delta[HbO]$ on left panels and of changes in $\Delta[Hb]$ on right panels measured for 6 repeated Rotating Cube workload 3 on Subject C. X-axis is the time in seconds, 135 sec workload 3 followed by 180 sec rest

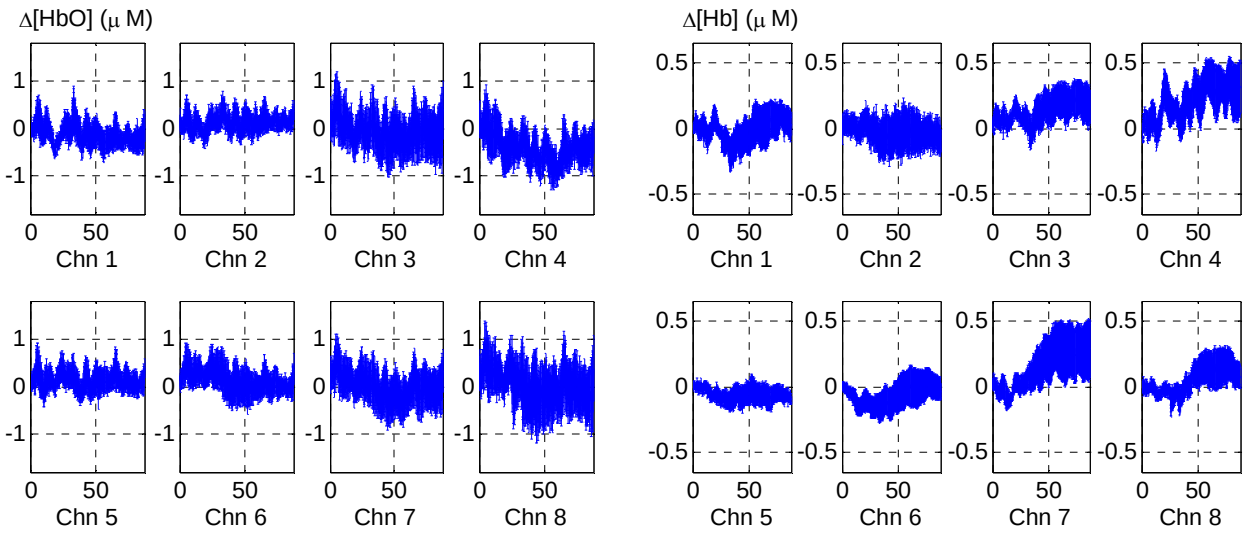

Fig. 6.5 (A). Folding average of changes in $\Delta[HbO]$ on left panels and of changes in $\Delta[Hb]$ on right panels measured for 6 repeated Rotating Cube workload 0 on Subject D (trial 1). X-axis is the time in seconds, 45 sec workload 0 followed by 40 sec rest

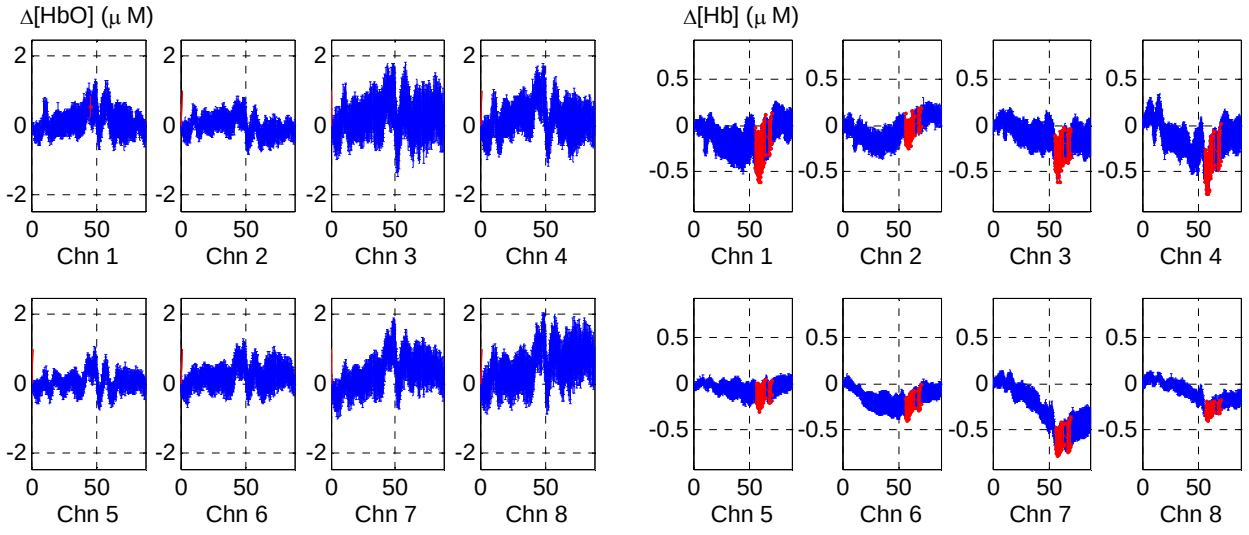

Fig. 6.5 (B). Folding average of changes in $\Delta[HbO]$ on left panels and of changes in $\Delta[Hb]$ on right panels measured for 6 repeated Rotating Cube workload 4 on Subject D (trial 1). X-axis is the time in seconds, 45 sec workload 4 followed by 40 sec rest

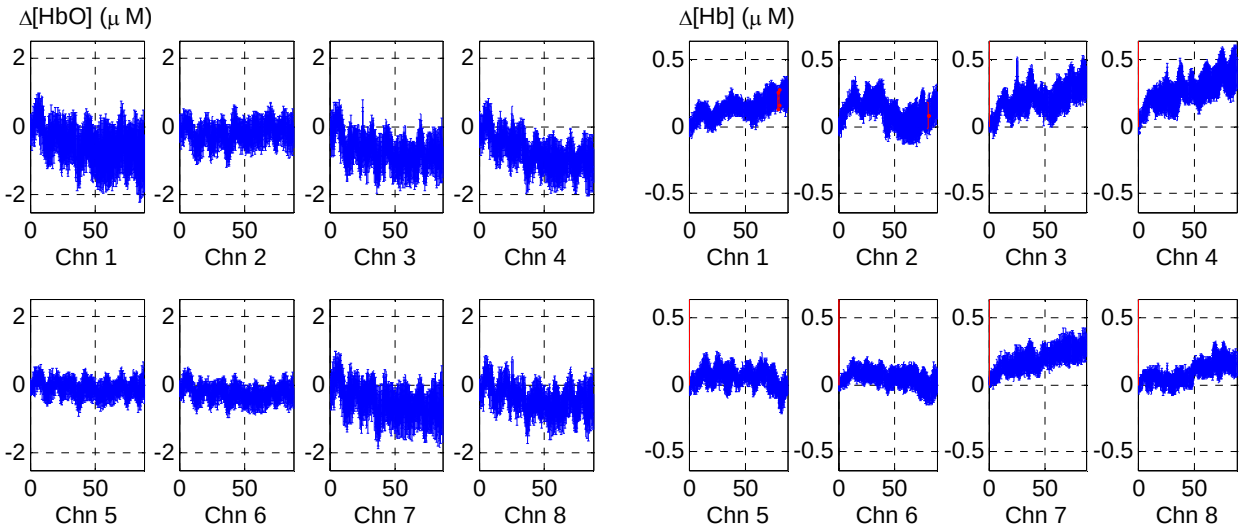

Fig. 6.6 (A). Folding average of changes in $\Delta[HbO]$ on left panels and of changes in $\Delta[Hb]$ on right panels measured for 6 repeated Rotating Cube workload 0 on Subject D (trial 2). X-axis is the time in seconds, 45 sec workload 0 followed by 40 sec rest

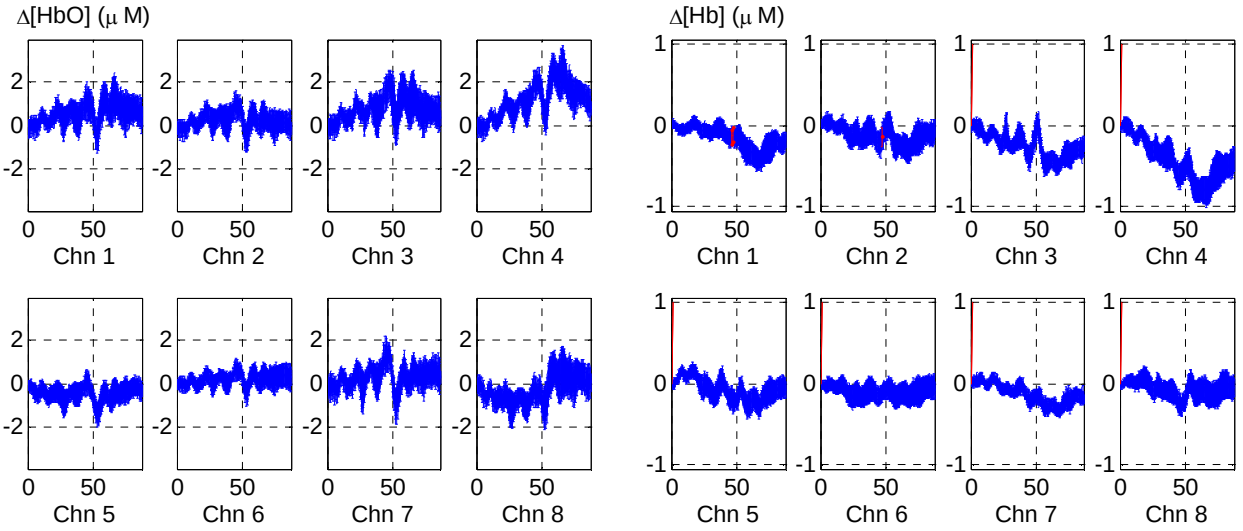

Fig. 6.6 (B). Folding average of changes in $\Delta[HbO]$ on left panels and of changes in $\Delta[Hb]$ on right panels measured for 6 repeated Rotating Cube workload 4 on Subject D (trial 2). X-axis is the time in seconds, 45 sec workload 4 followed by 40 sec rest

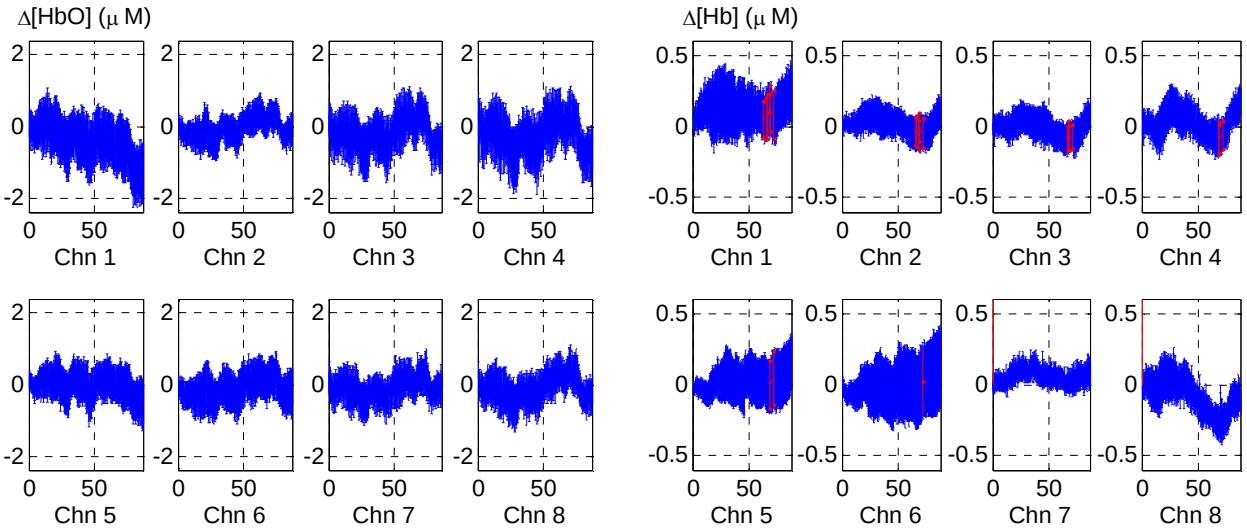

Fig. 6.7 (A). Folding average of changes in $\Delta[HbO]$ on left panels and of changes in $\Delta[Hb]$ on right panels measured for 6 repeated Rotating Cube workload 0 on Subject E. X-axis is the time in seconds, 45 sec workload 0 followed by 40 sec rest

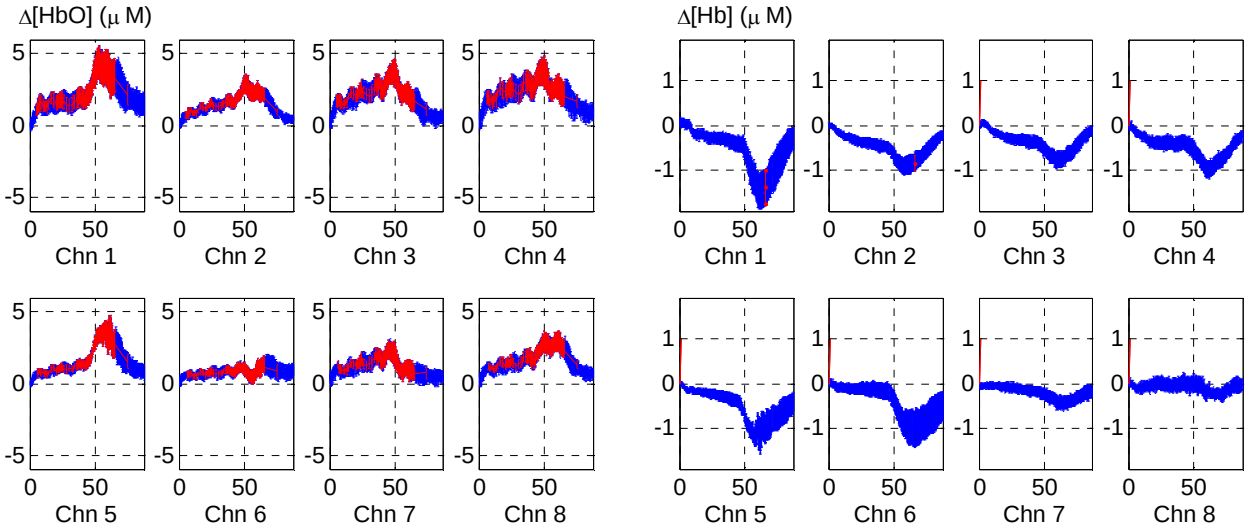

Fig. 6.7 (B). Folding average of changes in $\Delta[HbO]$ on left panels and of changes in $\Delta[Hb]$ on right panels measured for 6 repeated Rotating Cube workload 4 on Subject E. X-axis is the time in seconds, 45 sec workload 4 followed by 40 sec rest

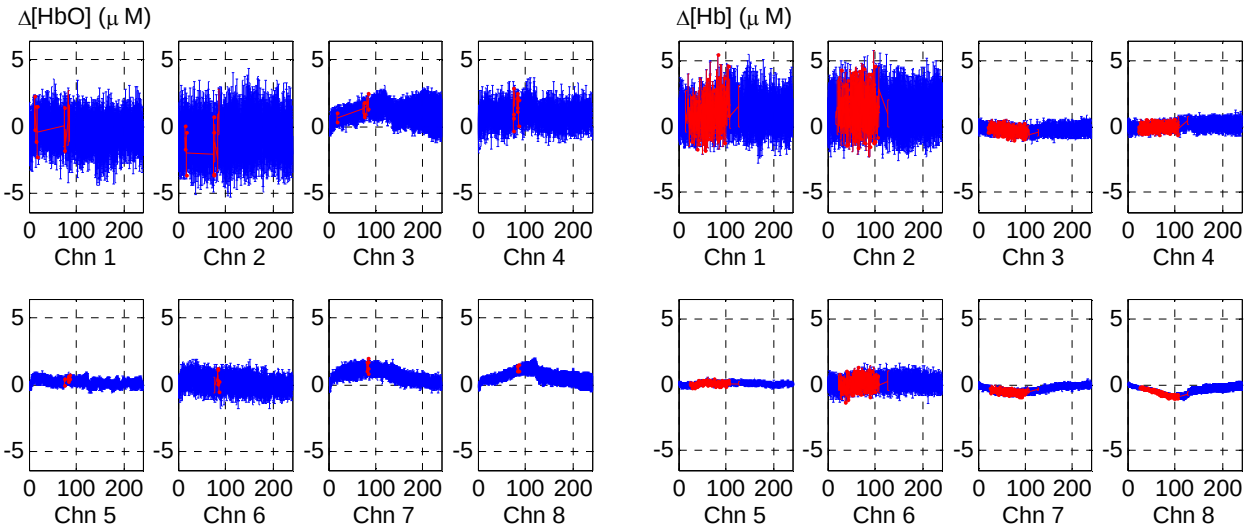

Fig. 6.8. Folding average of changes in $\Delta[HbO]$ on left panels and of changes in $\Delta[Hb]$ on right panels measured for 5 repeated finger tapping on Subject A (trial 1). X-axis is the time in seconds, 120 sec finger tapping followed by 120 sec rest. Channel 5, 7 and 8 are valid

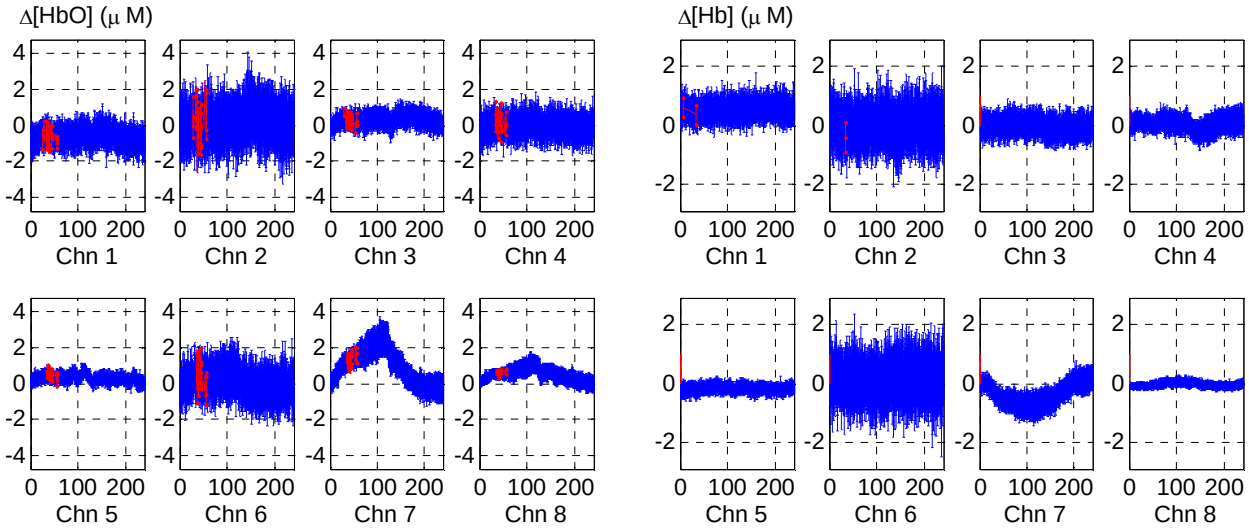

Fig. 6.9. Folding average of changes in $\Delta[HbO]$ on left panels and of changes in $\Delta[Hb]$ on right panels measured for 5 repeated finger tapping on Subject A (trial 2). X-axis is the time in seconds, 120 sec finger tapping followed by 120 sec rest. Channel 5, 7 and 8 are valid

After folding average, the temporal trends of $\Delta[HbO]$ and $\Delta[Hb]$ are bandpass filtered at the LFOs (0.05 to 0.10 Hz) by an elliptic bandpass filter. The frequency response of the bandpass filter is shown in Fig. 6.10.

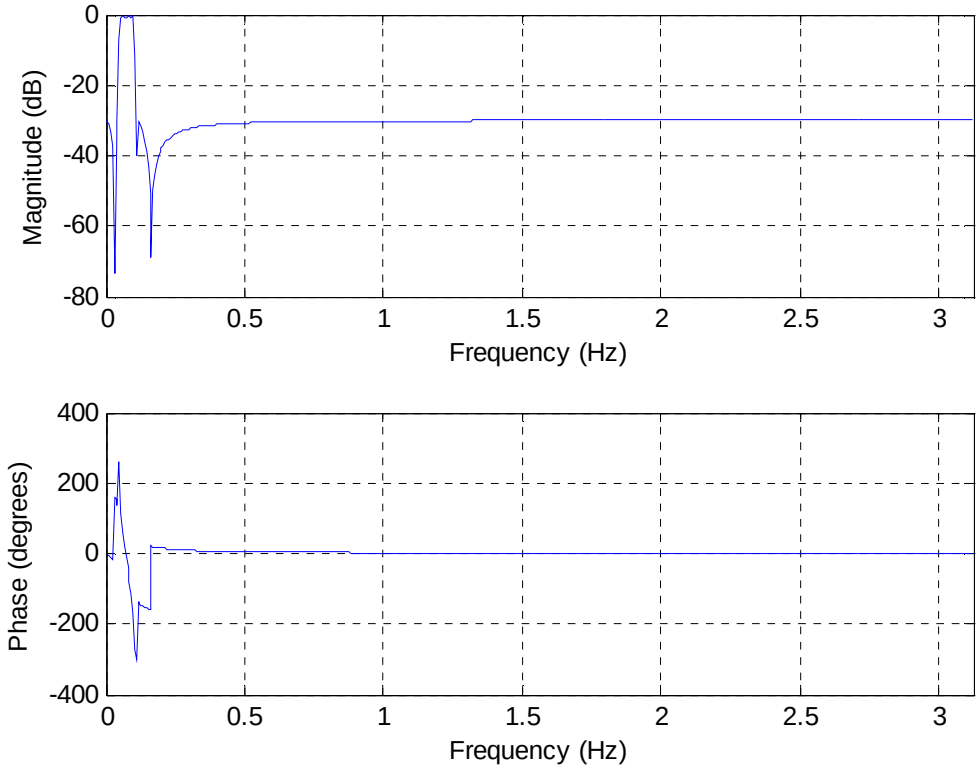

Fig. 6.10. The magnitude (dB) and phase response of bandpass filter (0.05 to 0.10 Hz)

Figure. 6.11 shows a piece of data for example from channel 8 on subject A rotating cube trial 1. In the upper subplot are shown the raw oxyhemoglobin change in thin and red and raw deoxy-hemoglobin change in thick and black; in the lower subplot are shown in the same time scale, $\Delta[HbO]$ and $\Delta[Hb]$ after band passed filtered in the band (0.05, 0.10) Hz. Comparing before and

after the elliptic bandpass filter, we can see that the characteristics oscillations around 0.10 Hz in the raw data are preserved and enhanced in the filtered data.

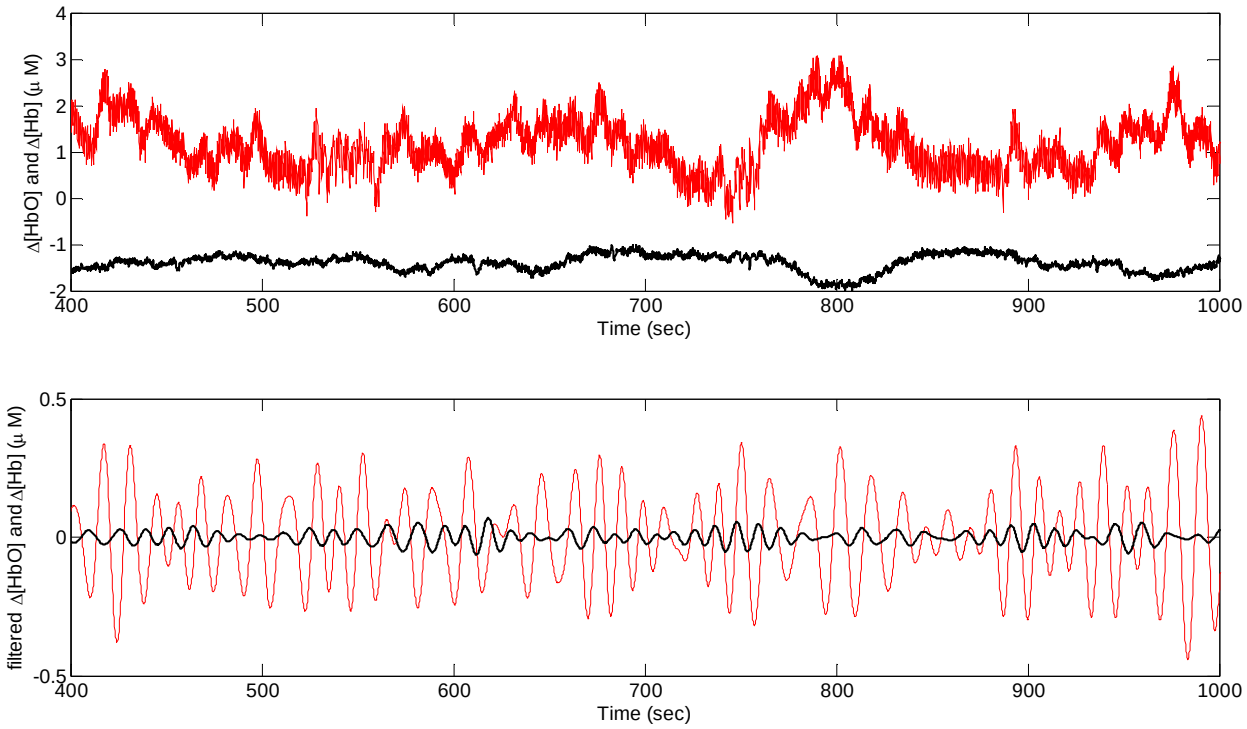

Fig. 6.11. Example of raw data (top) and bandpass filtered (0.05, 0.10) Hz data (bottom) from rotating cube experiment. Thin red plot is change of oxy-hemoglobin concentration $\Delta[HbO]$ while thick black plot is change of deoxy-hemoglobin concentration $\Delta[Hb]$

Based on the hemodynamic oscillations filtered around LFO, we can use the phase method discussed in the previous chapters to investigate the phase difference between deoxy-hemoglobin and oxy-hemoglobin concentration changes. In phase synchronization analysis method, we applied the Hilbert transform to both filtered $\Delta[Hb]$ and $\Delta[HbO]$ to get the complex form, then

we used Eq. (4.11) to get the phase value of $\Delta[Hb]$ and $\Delta[HbO]$. After assuming the frequencies of $\Delta[Hb]$ and $\Delta[HbO]$ are close or n: m ~ 1: 1, we can use Eq. (4.12) to calculate the phase difference $\theta_{[Hb],[HbO]}$. This is also called instantaneous phase value. On the other hand, after isolating 20 sec oscillations centered around each time point in the filtered $\Delta[Hb]$ and $\Delta[HbO]$, we used the phasor cross-correlation method explained in Fig. 4.1 to calculate the phase difference $\theta_{[Hb],[HbO]}$ by finding $\tau_{max}$and the corresponding phase value of the cross-correlation between $\Delta[Hb]$ and $\Delta[HbO]$. The hemodynamic oscillations in Fig. 6.11 can be investigated by cross-correlation phasor method and phase synchronization analysis method to get the phase difference shown in Fig. 6.12:

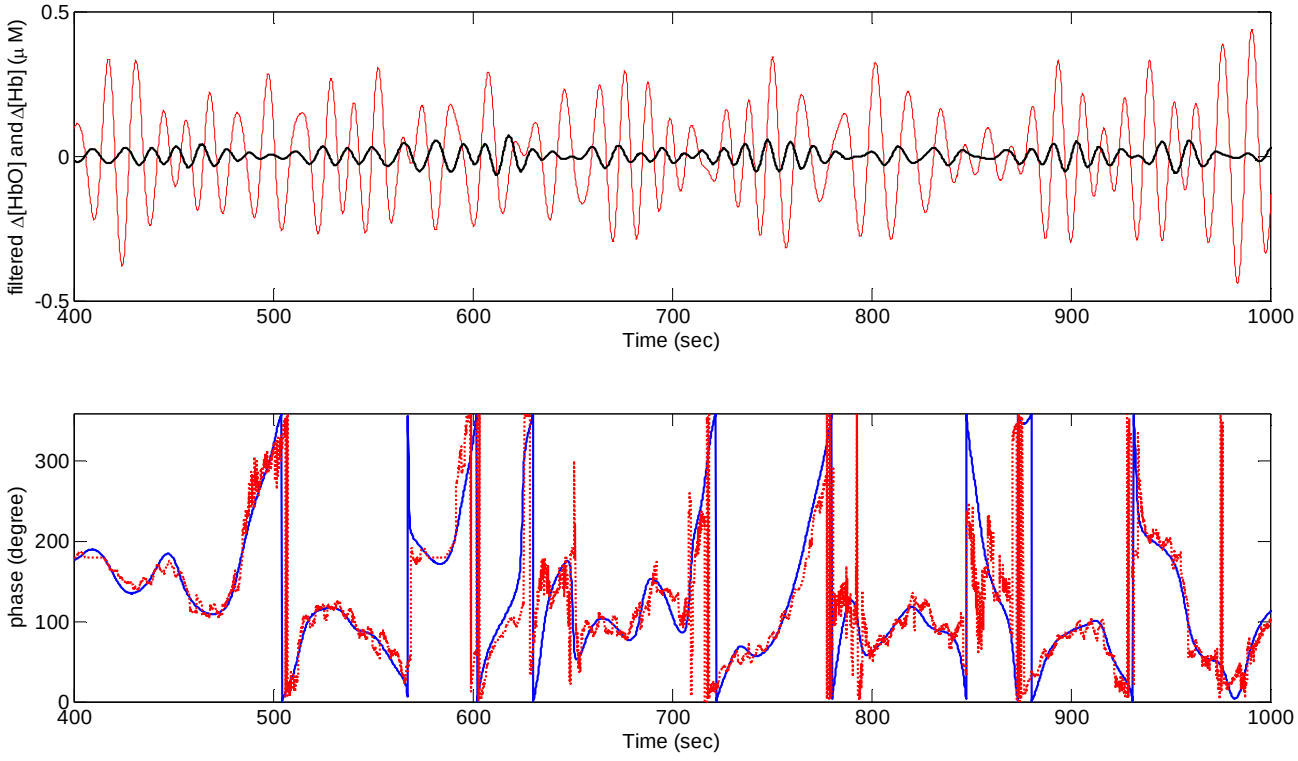

Fig. 6.12. Example of how phasor and PSI analysis method work. These plots refer to the same data (and the same temporal section) of Fig. 6.11. Upper subplot is the filtered $\Delta[Hb]$ in thick black plot and filtered $\Delta[HbO]$ in thin red plot.

Lower subplot is the corresponding phase difference between $\Delta[Hb]$ and $\Delta[HbO]$ in degree: blue and solid plot is calculated by PSI analysis method while red and dot plot is calculated by phasor method.

From Fig.6.12, we can see that the results from cross-correlation phasor method and phase synchronization analysis method match each other very well. Rather than studying the single phase value, we would like to investigate the phase distribution during workload 0 and workload 4, respectively. Also we would like to compare the phase distributions in task and rest and find out if there is any correlation in phase changes and the stimulus (either cognitive challenge or finger tapping). We introduced a circular histogram in which the entire 360° angle is divided into 36 bins; each bin contains the frequency rate of the phase values located around a circle. Therefore, for all the experiments, we calculated the $\Delta[Hb]$ and $\Delta[HbO]$, phase distribution of workload 0 and workload 4 according to both methods (phasor method and PSI method). From Eq. (4.14), we discarded the point where the relative ratio of frequency between deoxy- and oxy-hemoglobin is either less than 2/3 or more than 3/2. We applied a Rayleigh test on circular statistics (Chapter 4) on the processed phase distribution to check if it is uniform or not. If the distribution is not uniform, we draw a red arrow in the center of the circular histogram map, of which direction is the mean value of the phase distribution and length is the resultant average length. On the contrary, if the distribution is uniform, we draw a blue arrow. Of course, the blue arrow usually is much shorter than the red arrow since the resultant length of uniform distribution is close to zero.

Phase distributions in all experiments are shown as follow. Note that Fig. 6.20 and Fig. 6.21 only show the results from Channel 5, 7 and 8 because other channels have low Signal/Noise ratio.

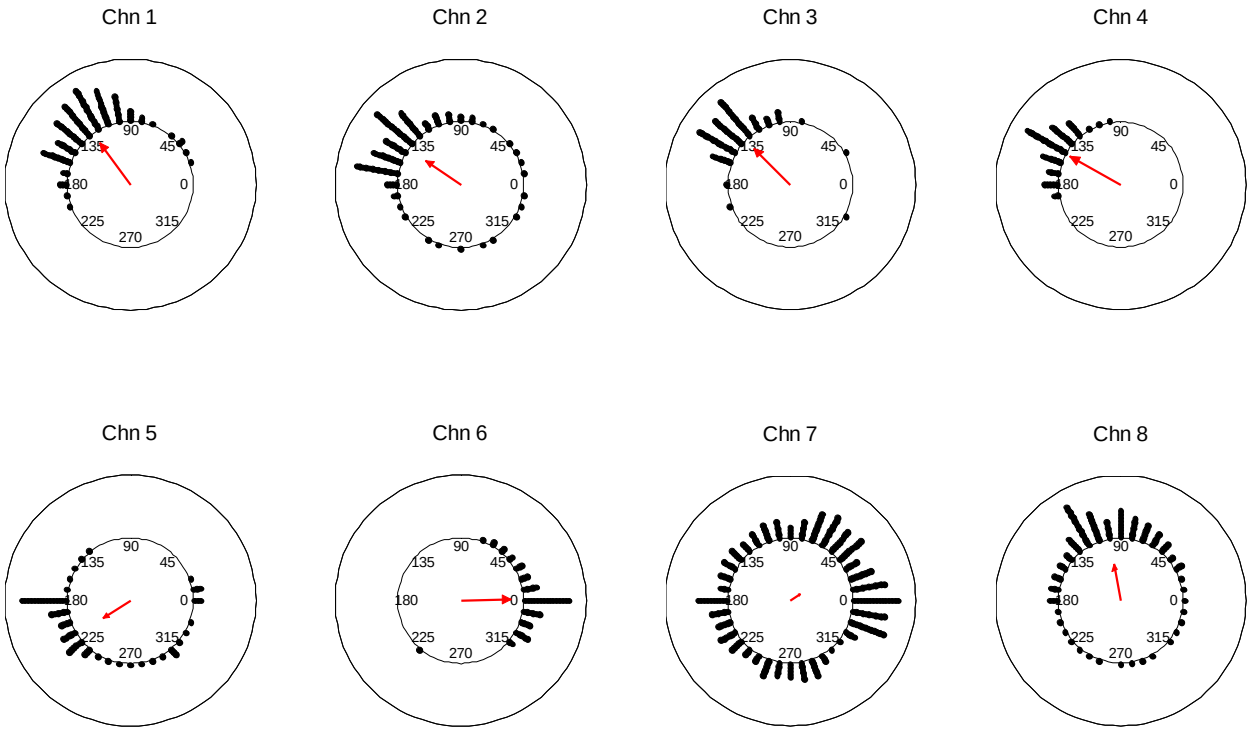

Fig. 6.13 (A). Circular histogram of workload 0 on Subject A (trial 1) by Phasor method

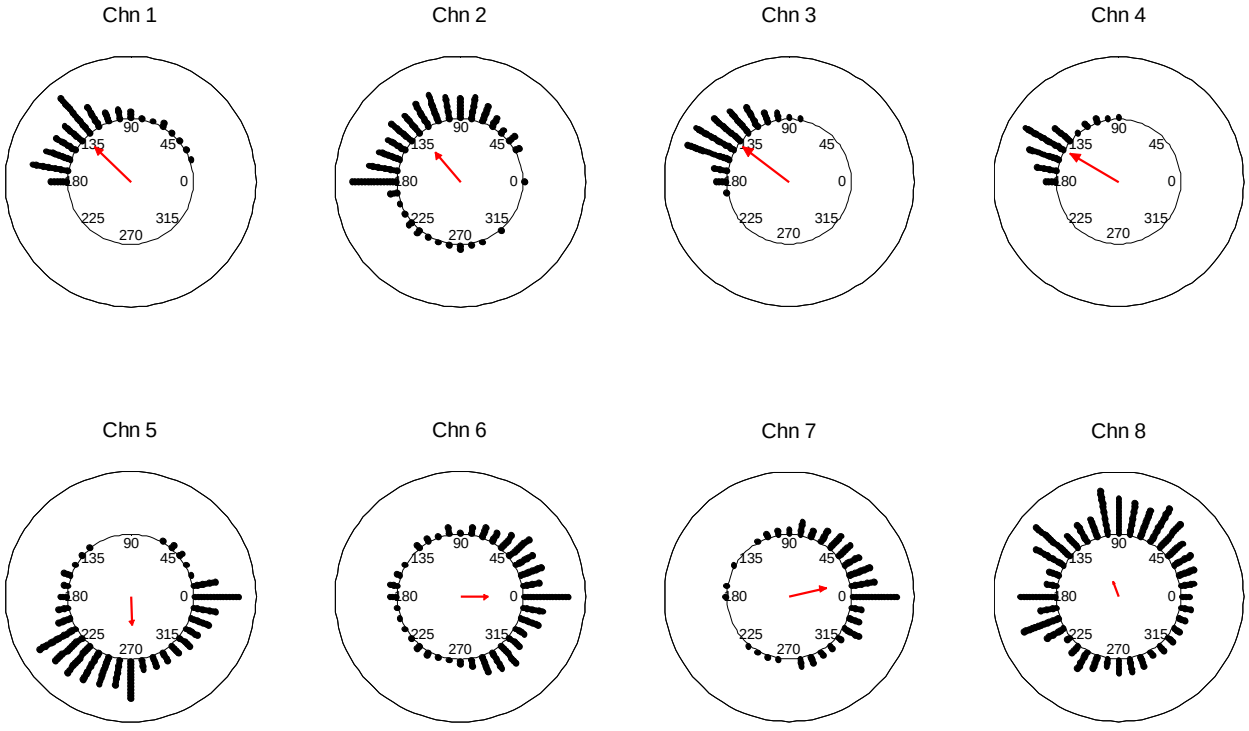

Fig. 6.13 (B). Circular histogram of workload 4 on Subject A (trial 1) by Phasor method

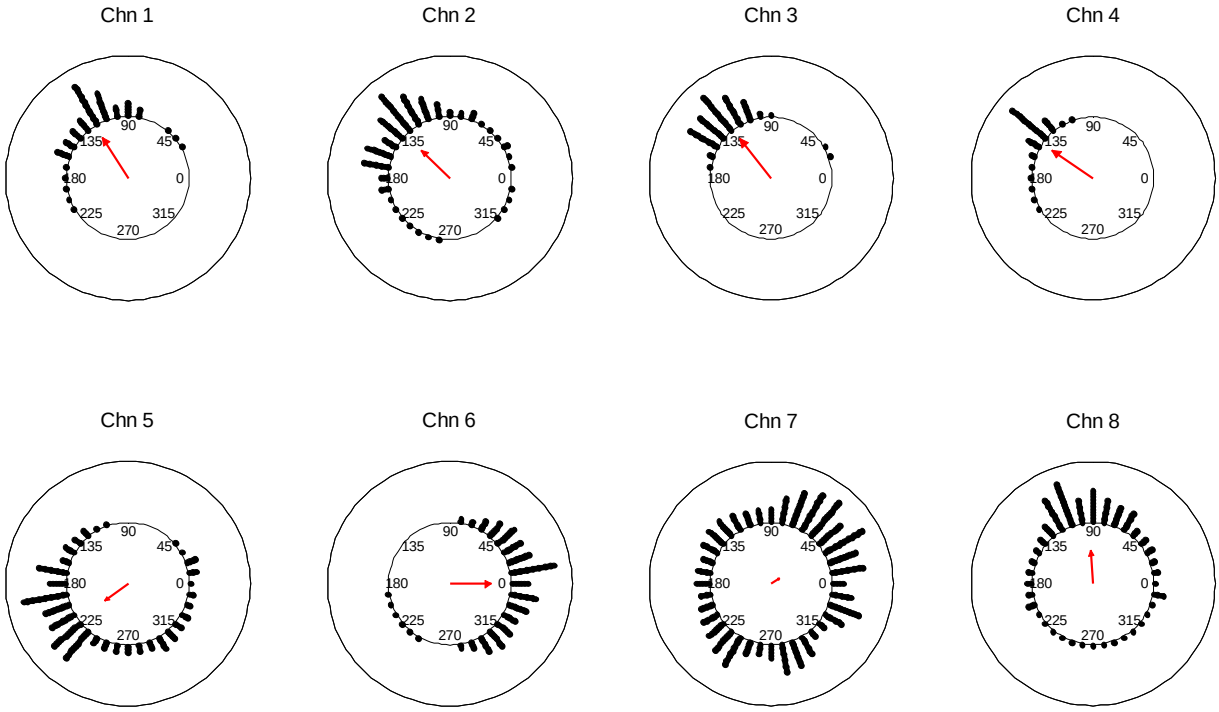

Fig. 6.13 (C). Circular histogram of workload 0 on Subject A (trial 1) by PSI method

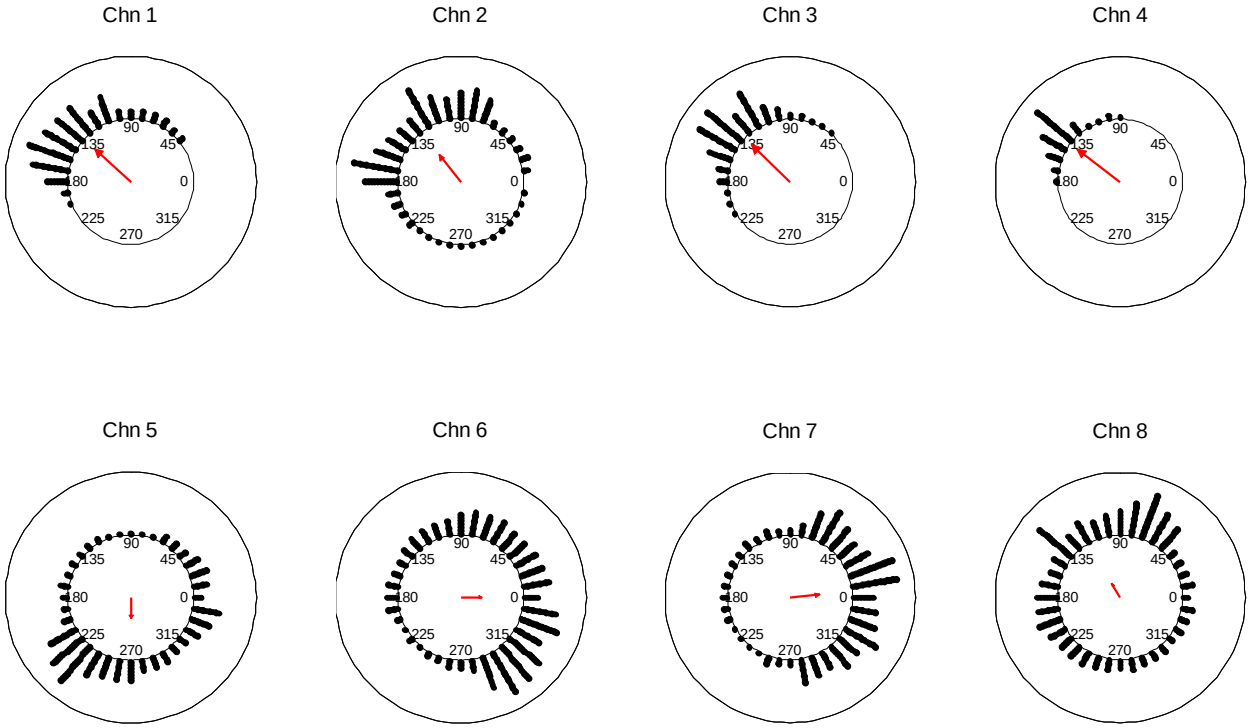

Fig. 6.13 (D). Circular histogram of workload 4 on Subject A (trial 1) by PSI method

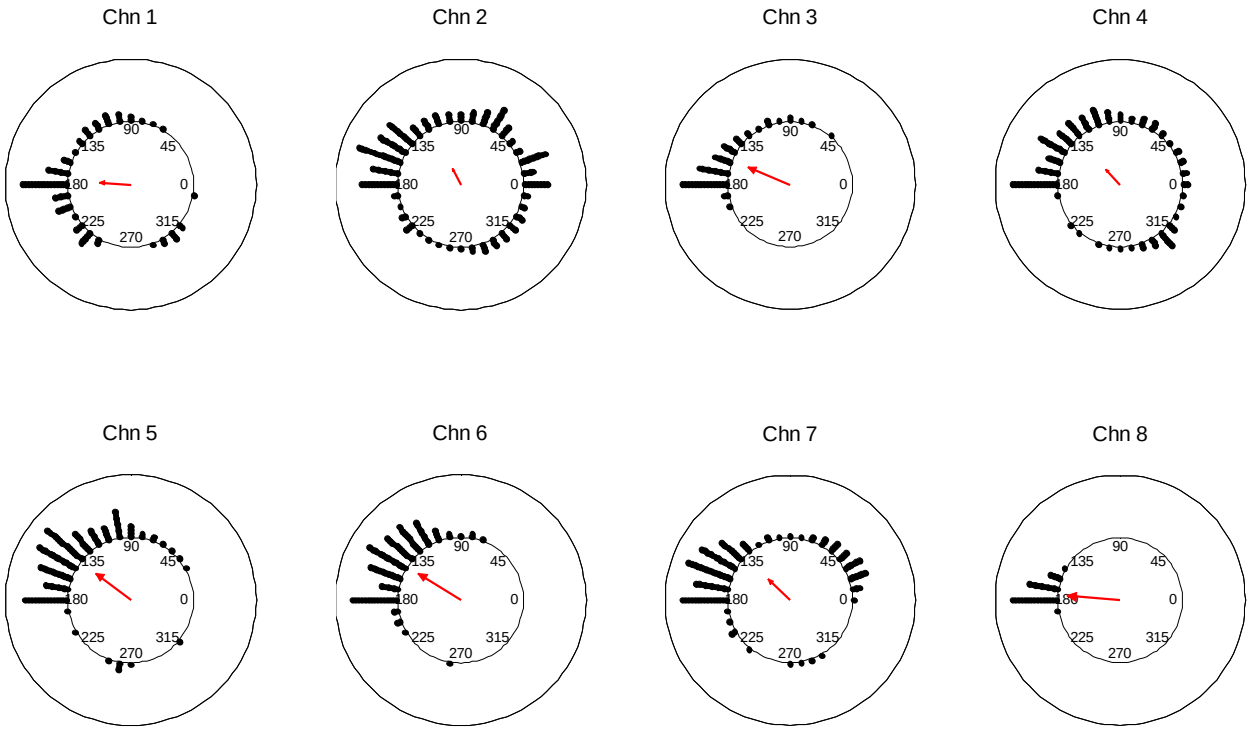

Fig. 6.14 (A). Circular histogram of workload 0 on Subject A (trial 2) by Phasor method

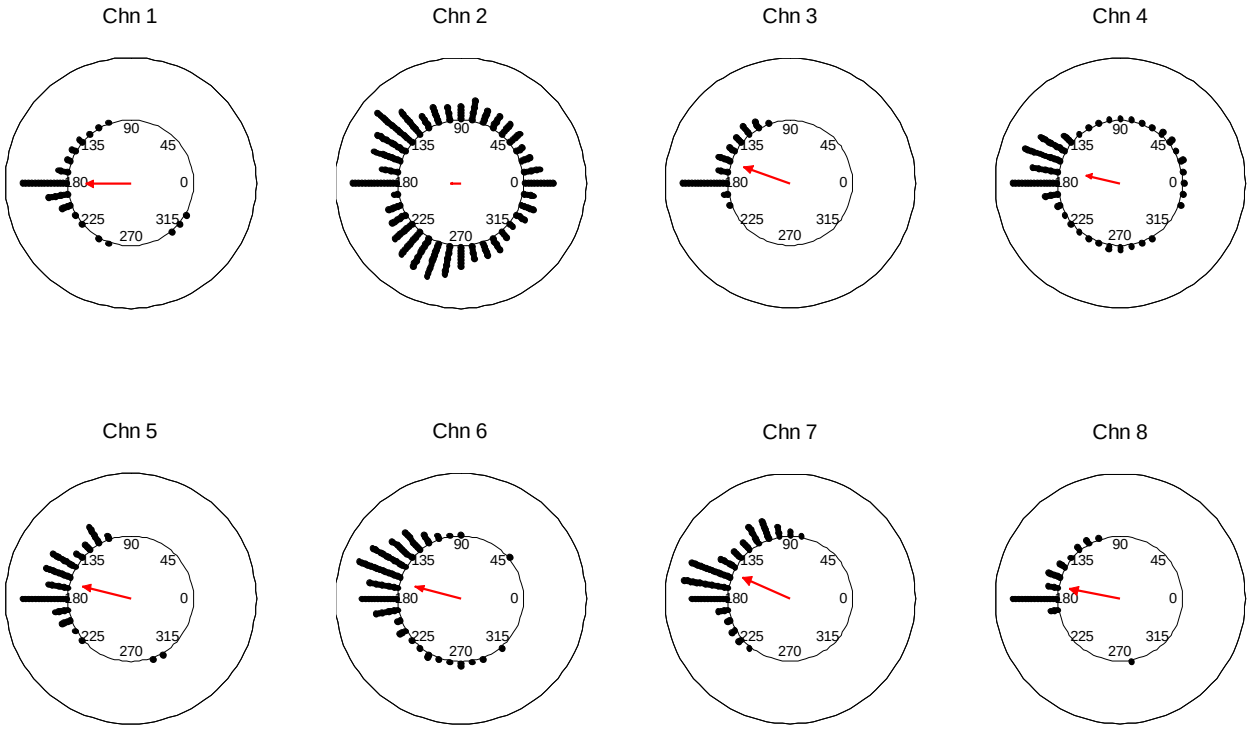

Fig. 6.14 (B). Circular histogram of workload 4 on Subject A (trial 2) by Phasor method

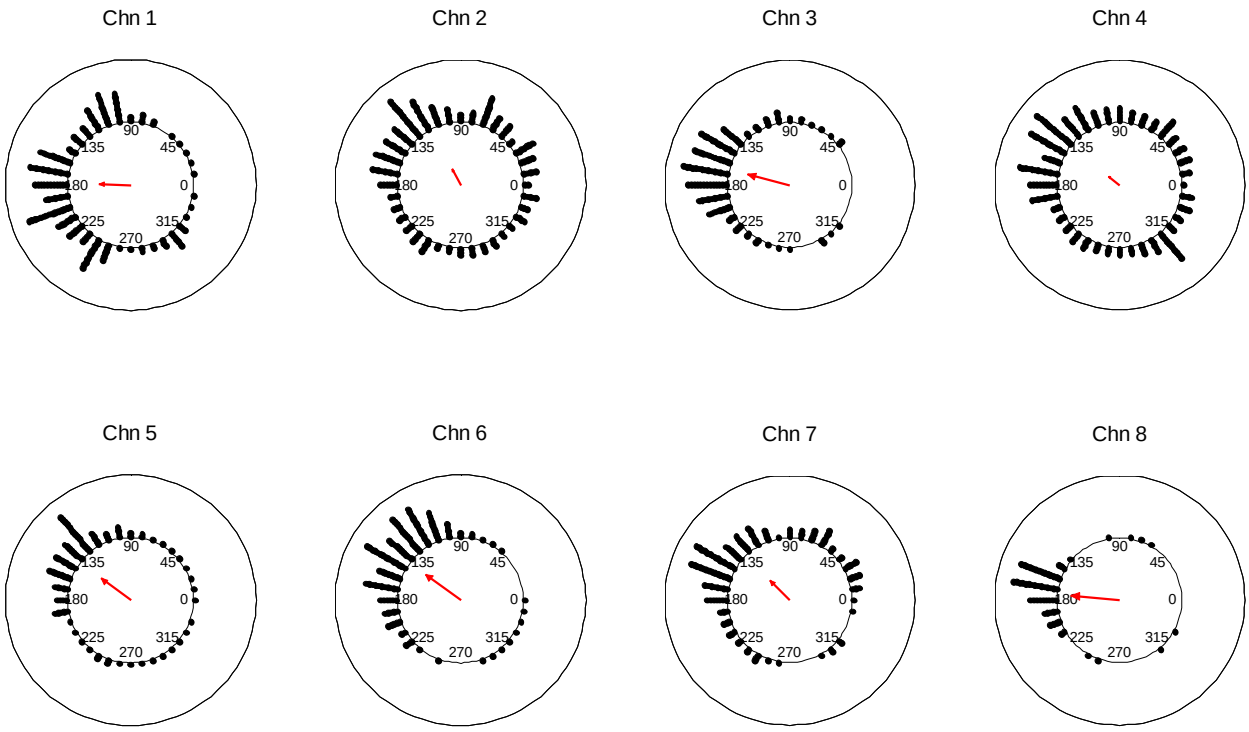

Fig. 6.14 (C). Circular histogram of workload 0 on Subject A (trial 2) by PSI method

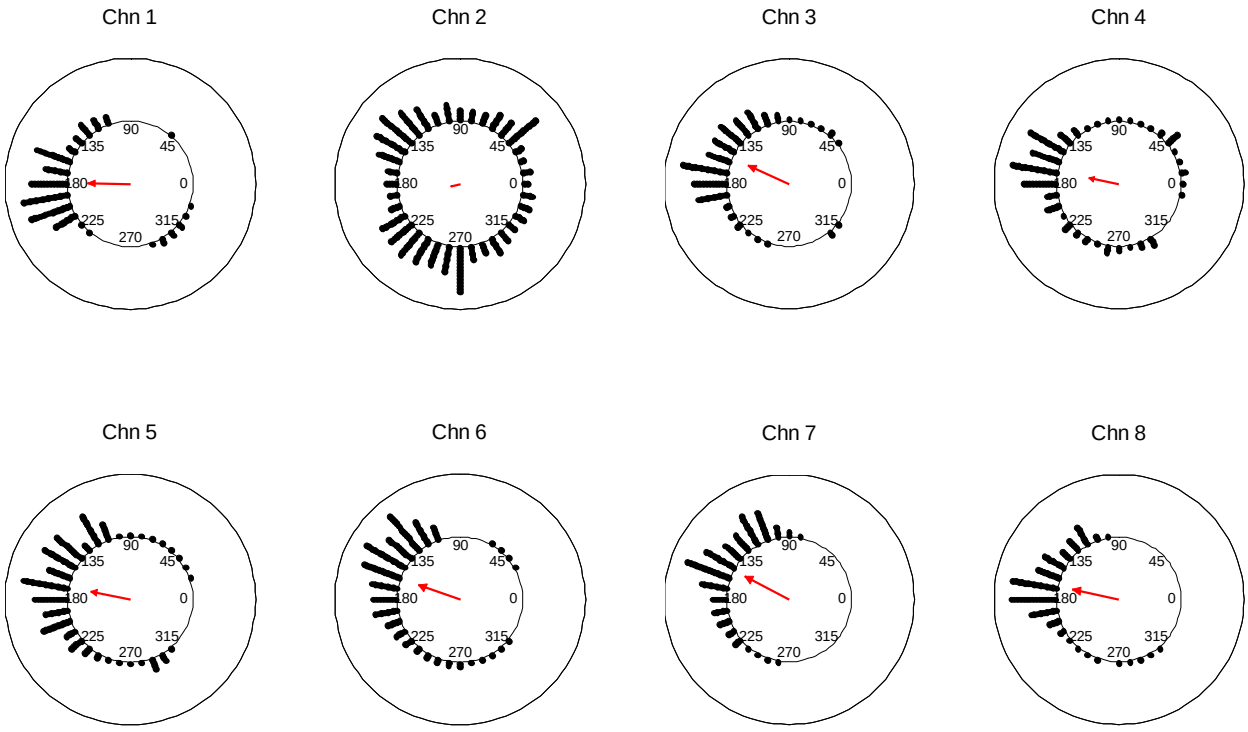

Fig. 6.14 (D). Circular histogram of workload 4 on Subject A (trial 2) by PSI method

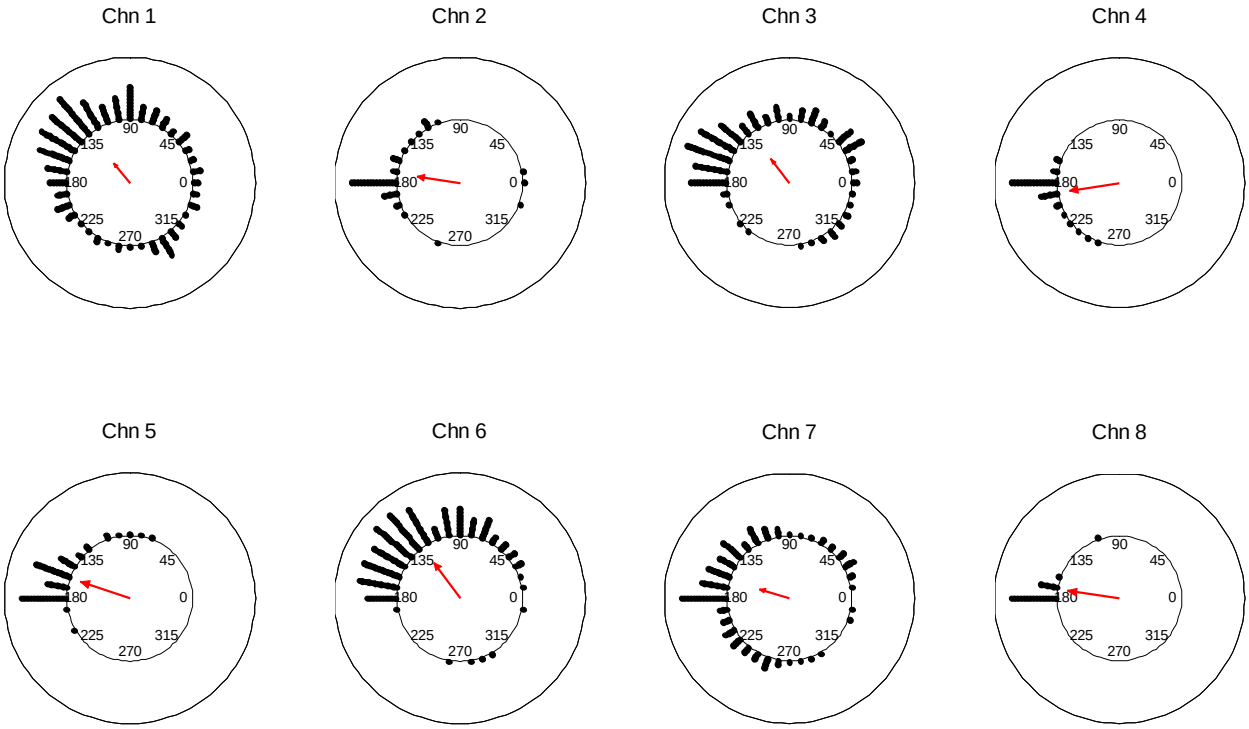

Fig. 6.15 (A). Circular histogram of workload 0 on Subject B by Phasor method

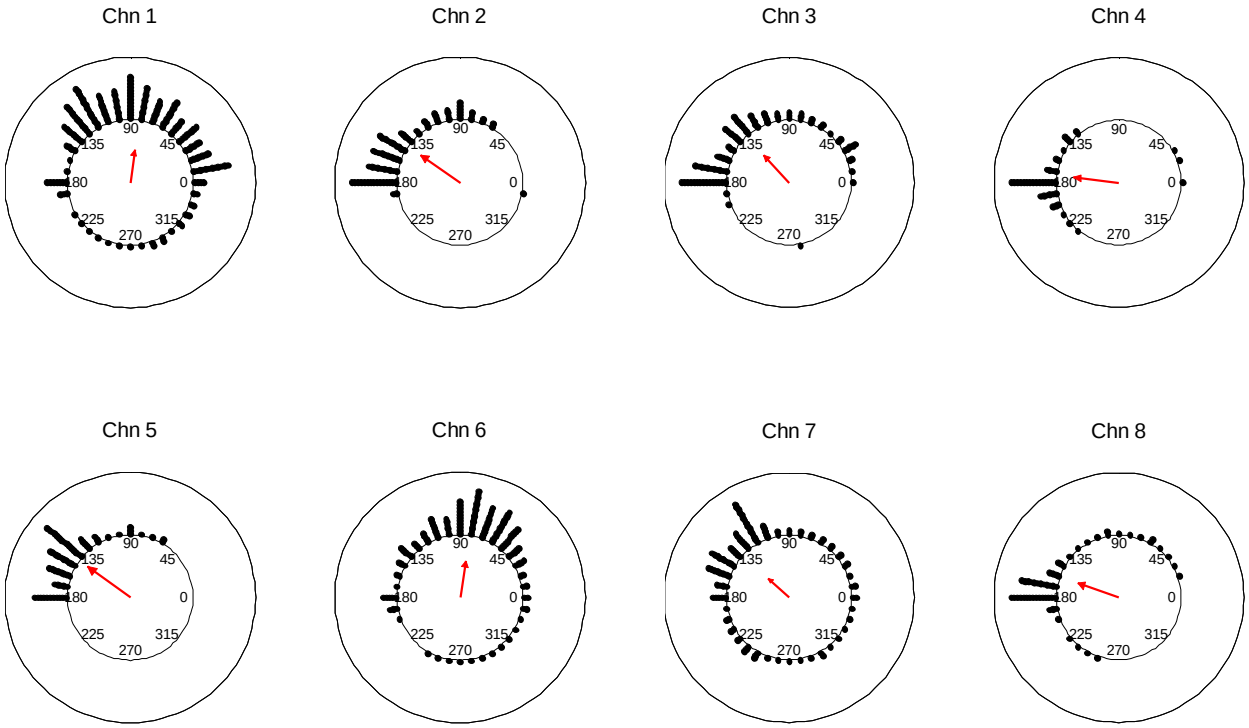

Fig. 6.15 (B). Circular histogram of workload 4 on Subject B by Phasor method

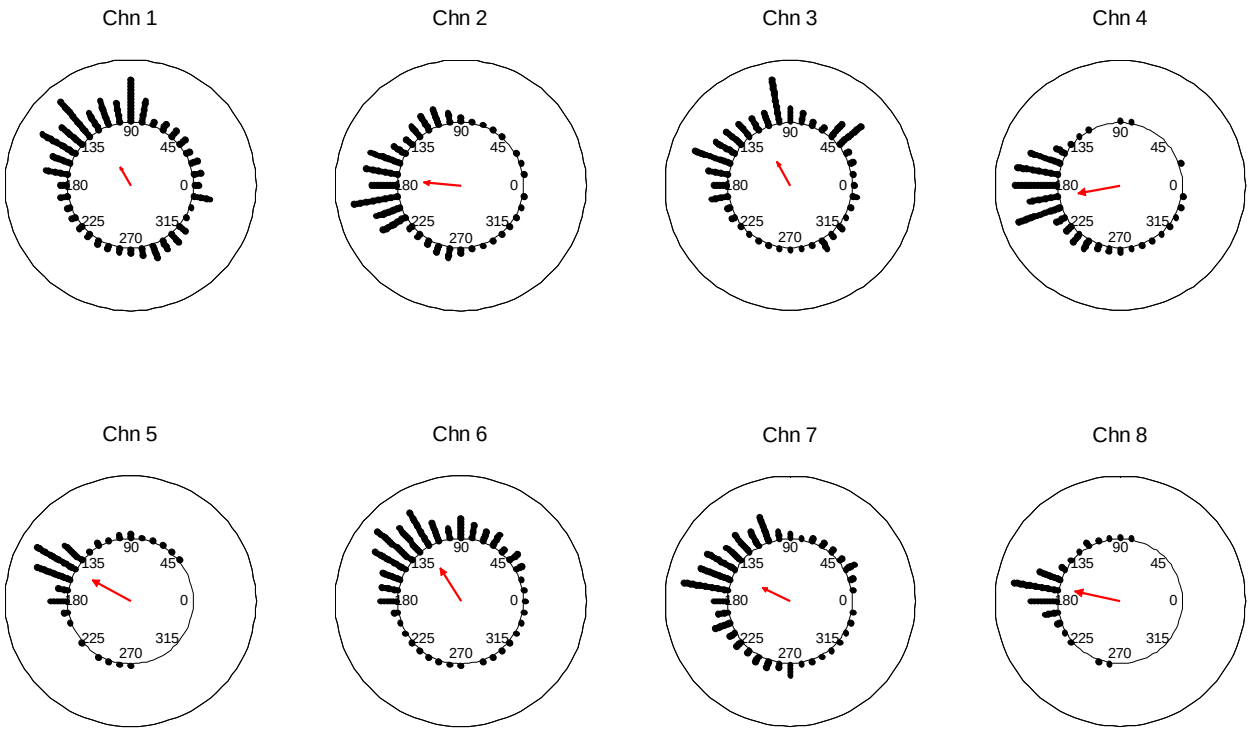

Fig. 6.15 (C). Circular histogram of workload 0 on Subject B by PSI method

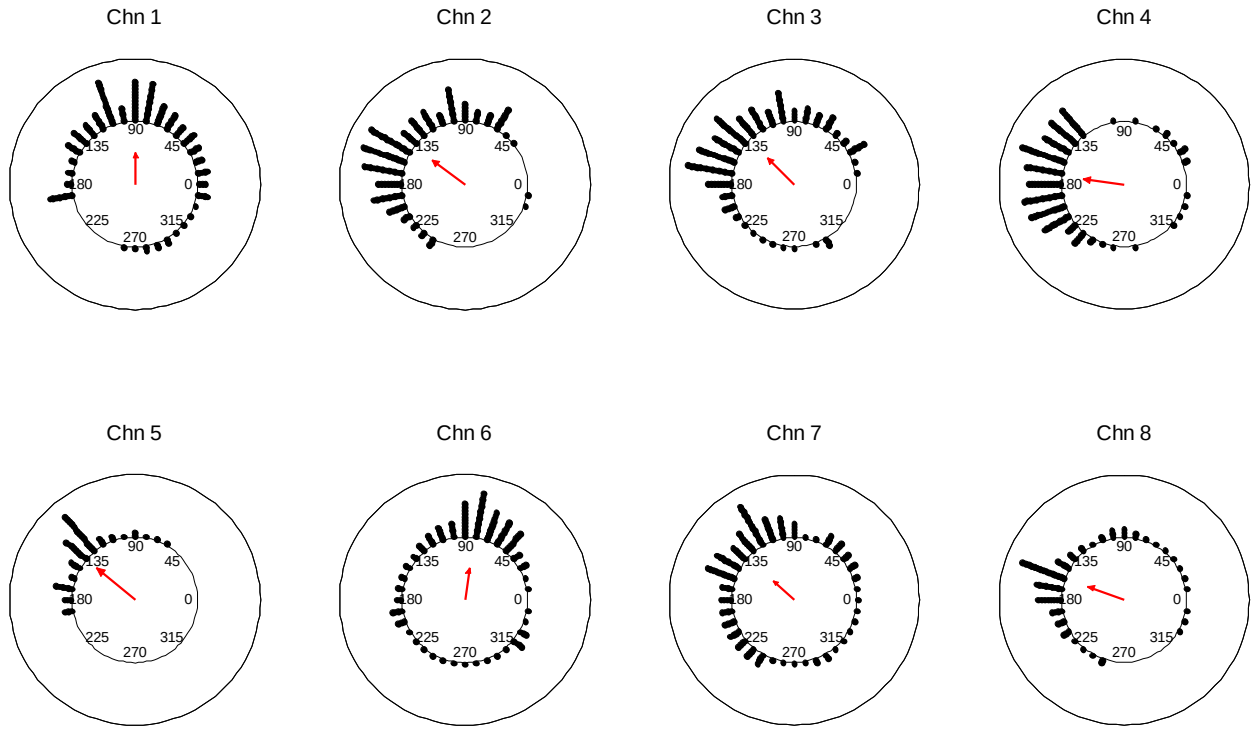

Fig. 6.15 (D). Circular histogram of workload 4 on Subject B by PSI method

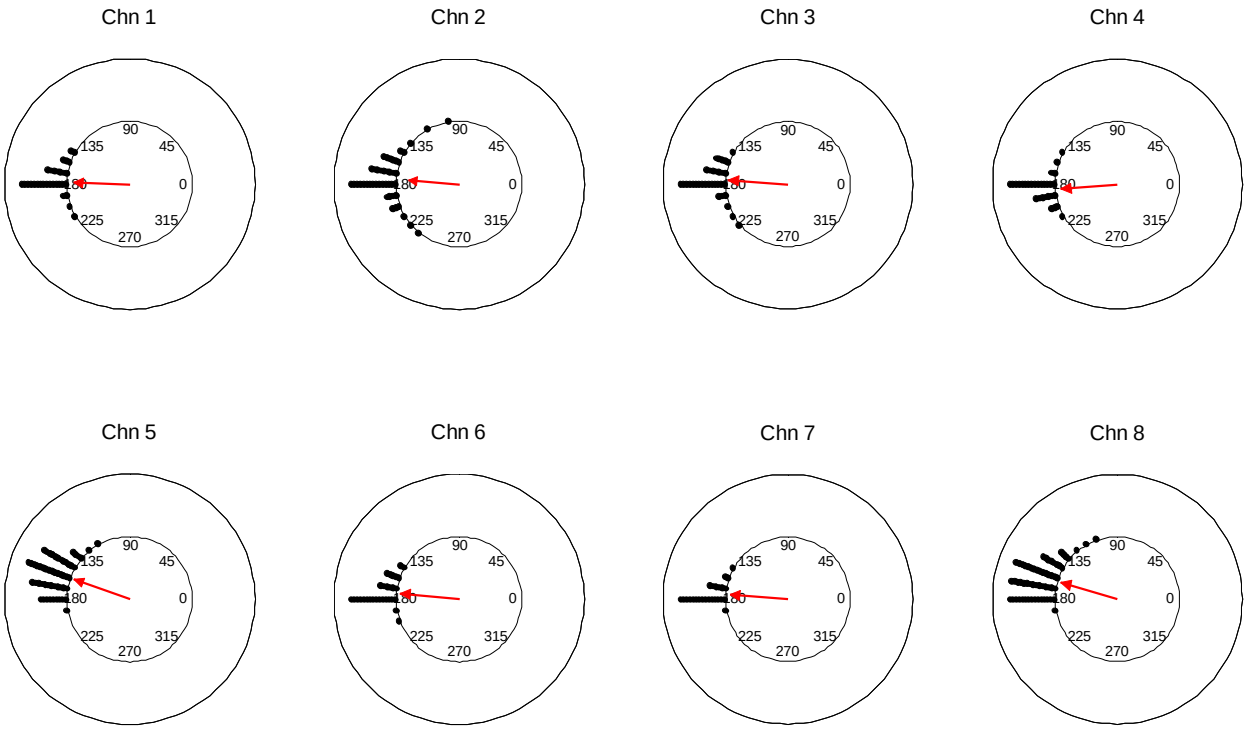

Fig. 6.16 (A). Circular histogram of workload 0 on Subject C by Phasor method

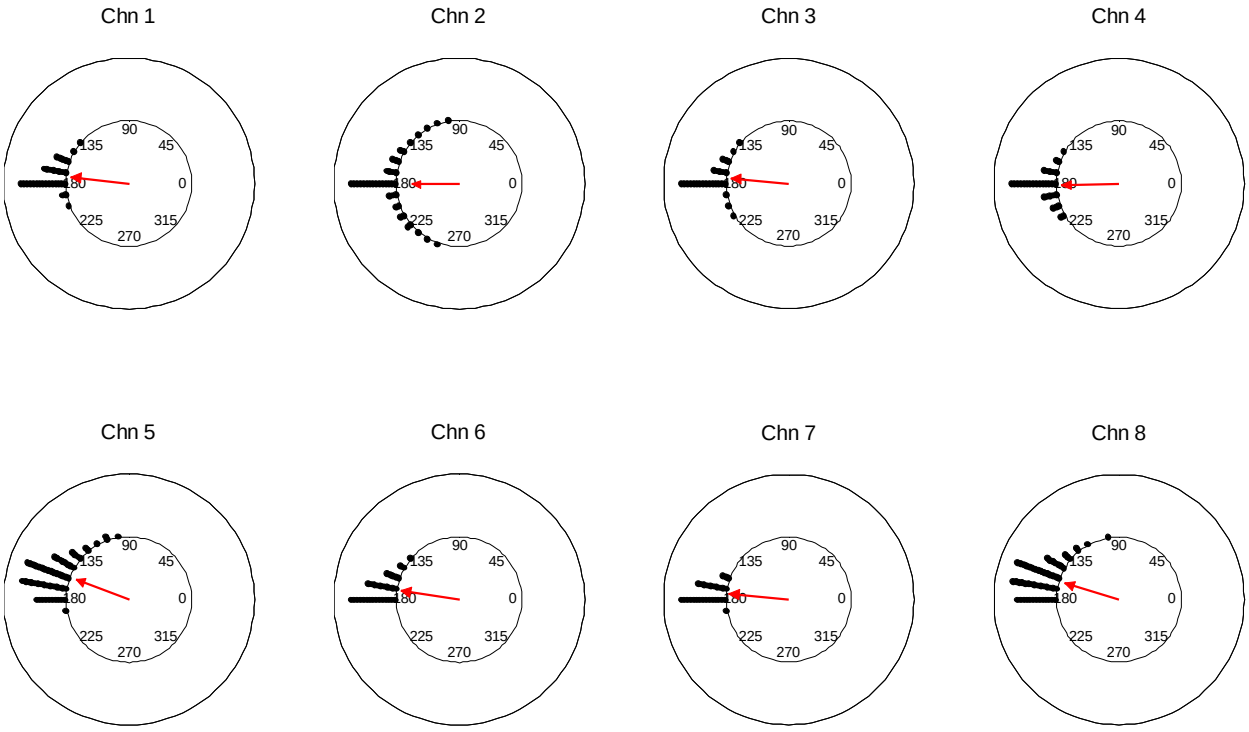

Fig. 6.16 (B). Circular histogram of workload 3 on Subject C by Phasor method

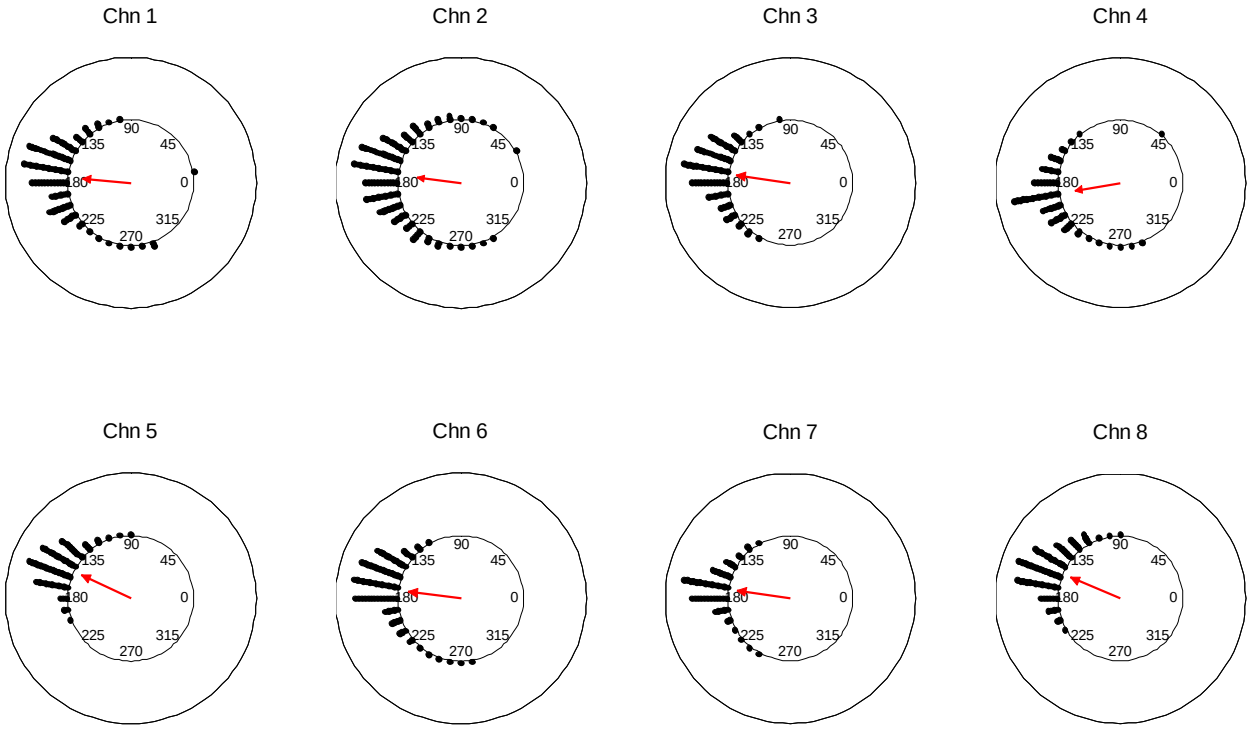

Fig. 6.16 (C). Circular histogram of workload 0 on Subject C by PSI method

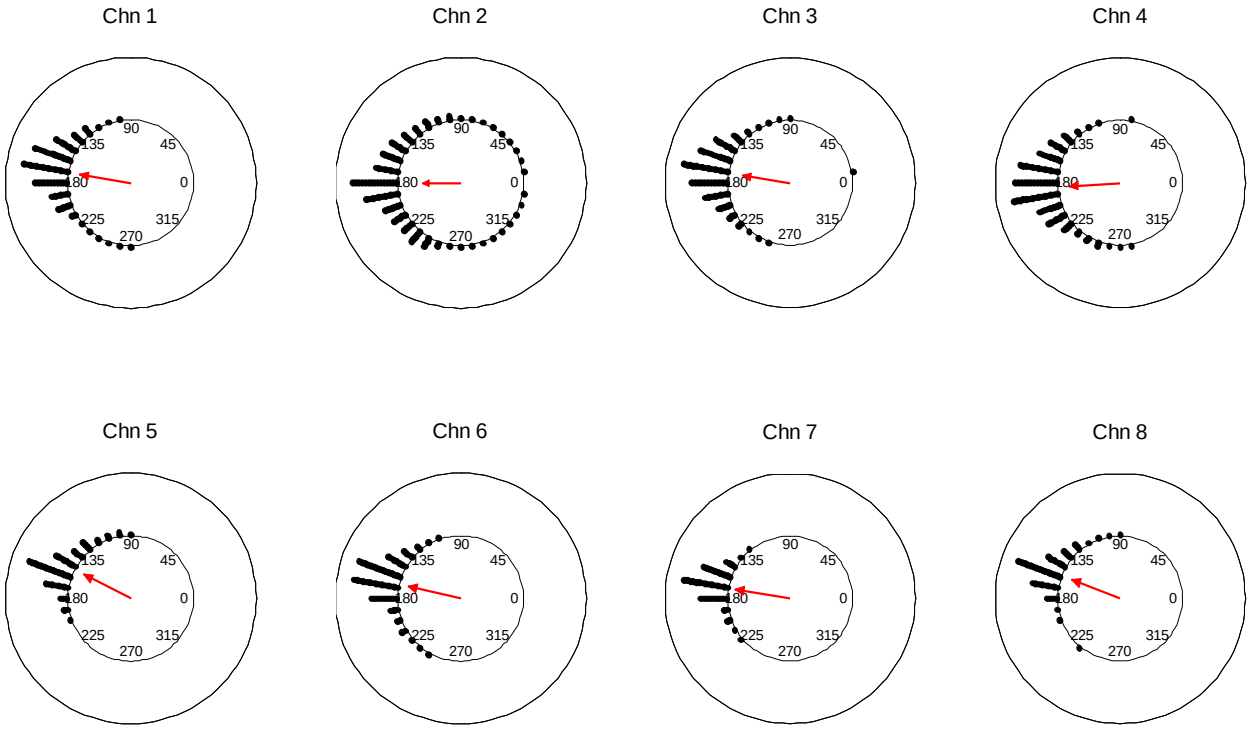

Fig. 6.16 (D). Circular histogram of workload 3 on Subject C by PSI method

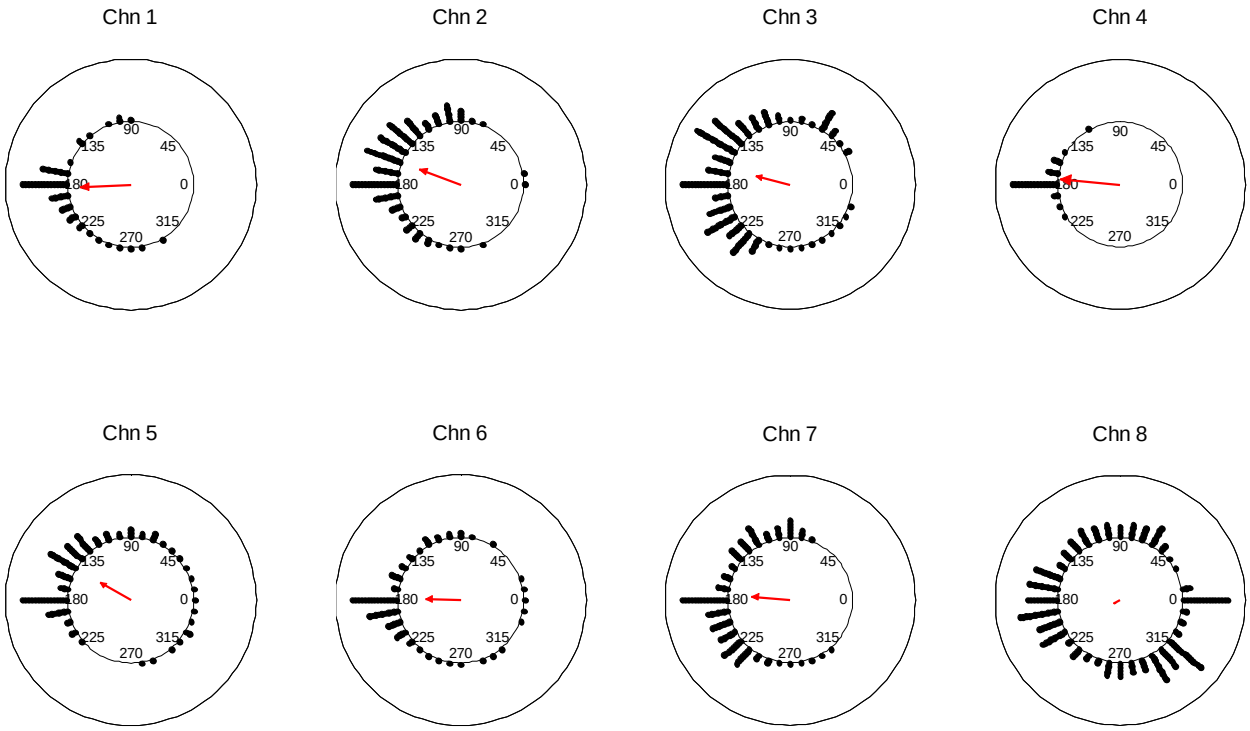

Fig. 6.17 (A). Circular histogram of workload 0 on Subject D (trial 1) by Phasor method

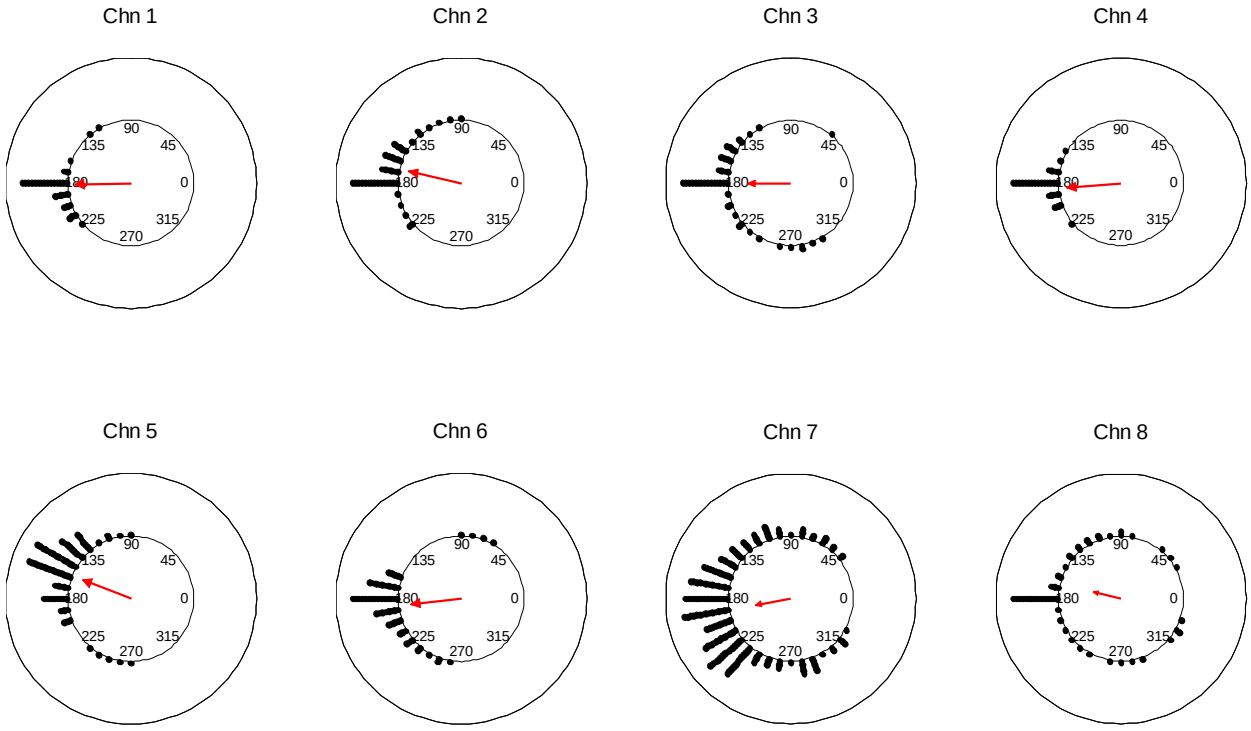

Fig. 6.17 (B). Circular histogram of workload 4 on Subject D (trial 1) by Phasor method

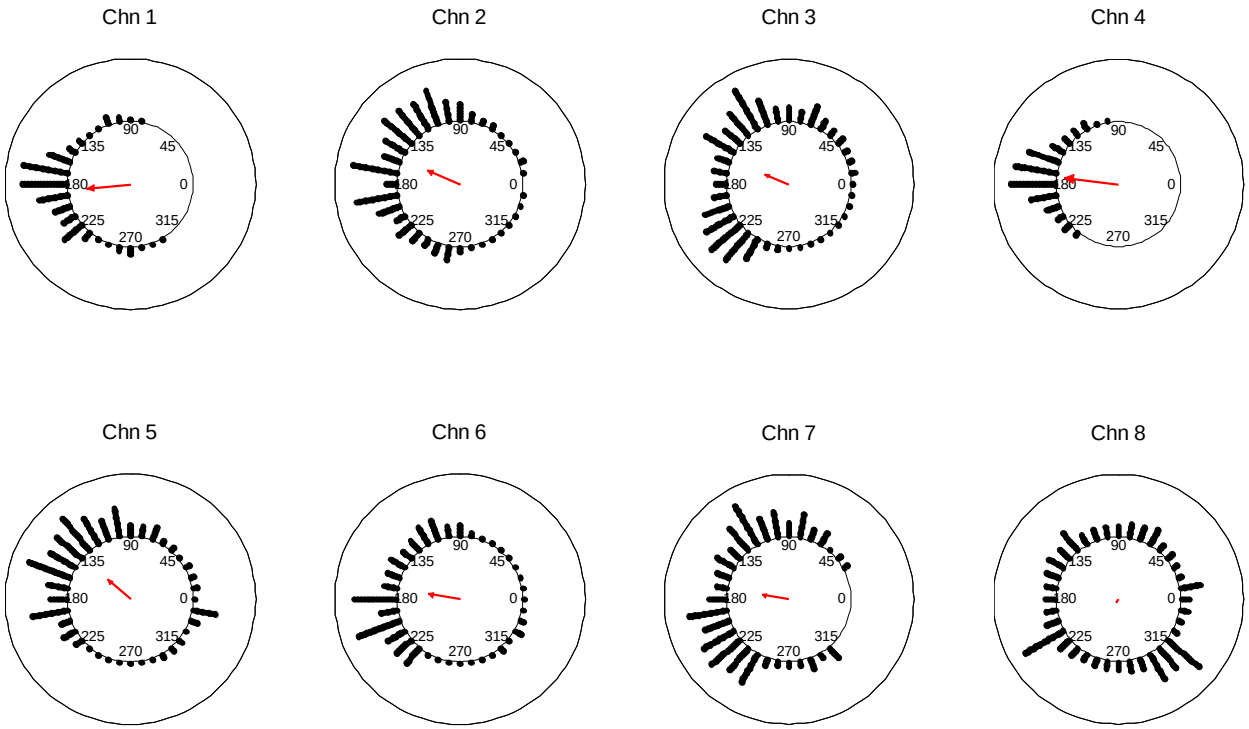

Fig. 6.17 (C). Circular histogram of workload 0 on Subject D (trial 1) by PSI method

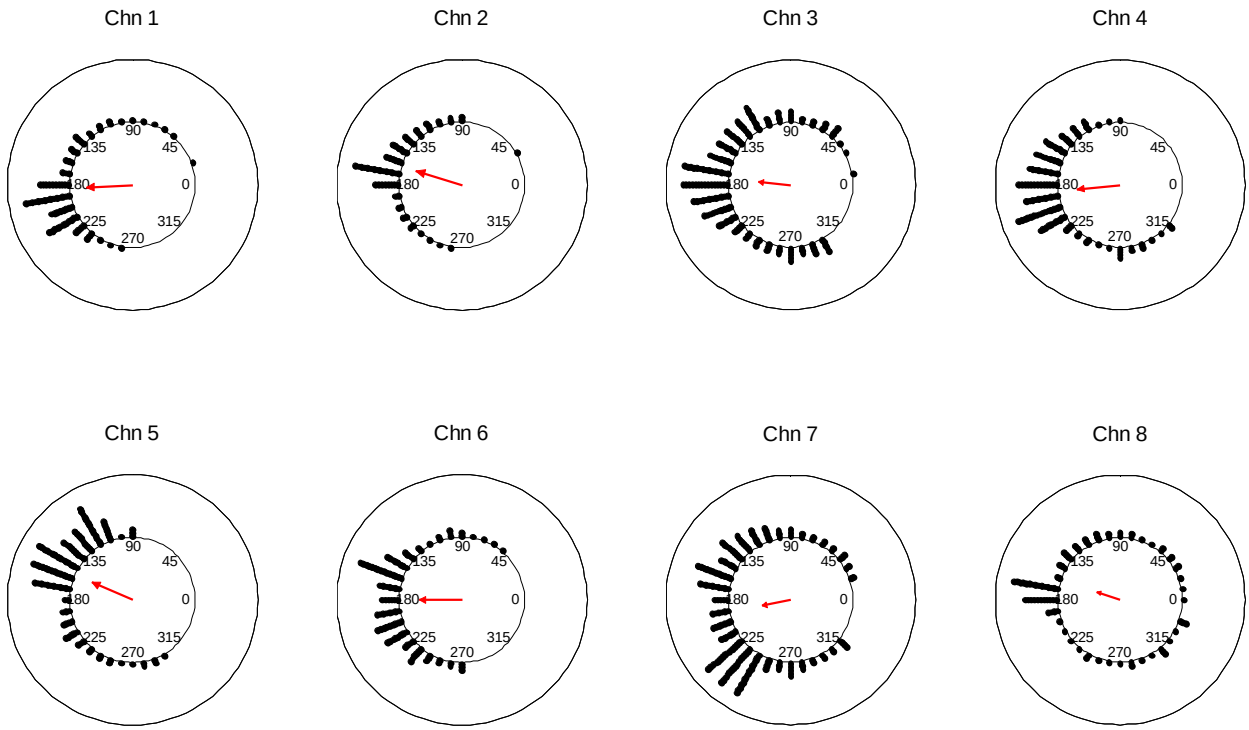

Fig. 6.17 (D). Circular histogram of workload 4 on Subject D (trial 1) by PSI method

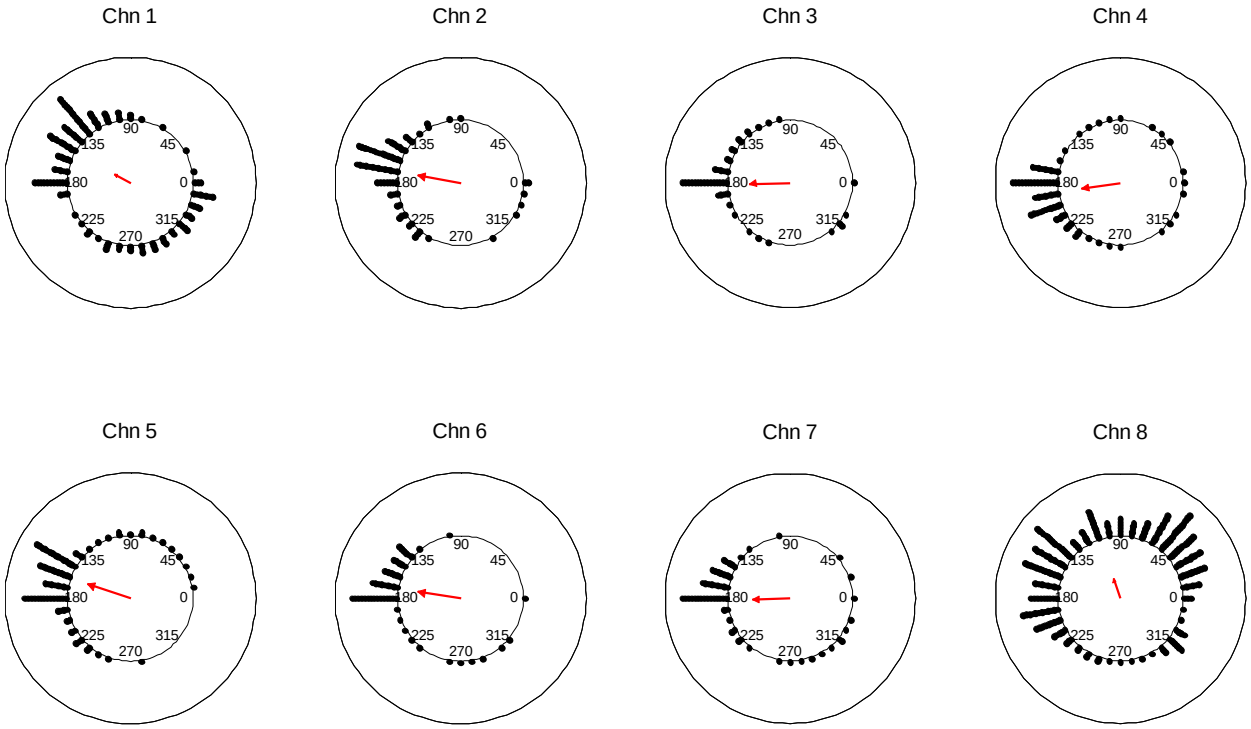

Fig. 6.18 (A). Circular histogram of workload 0 on Subject D (trial 2) by Phasor method

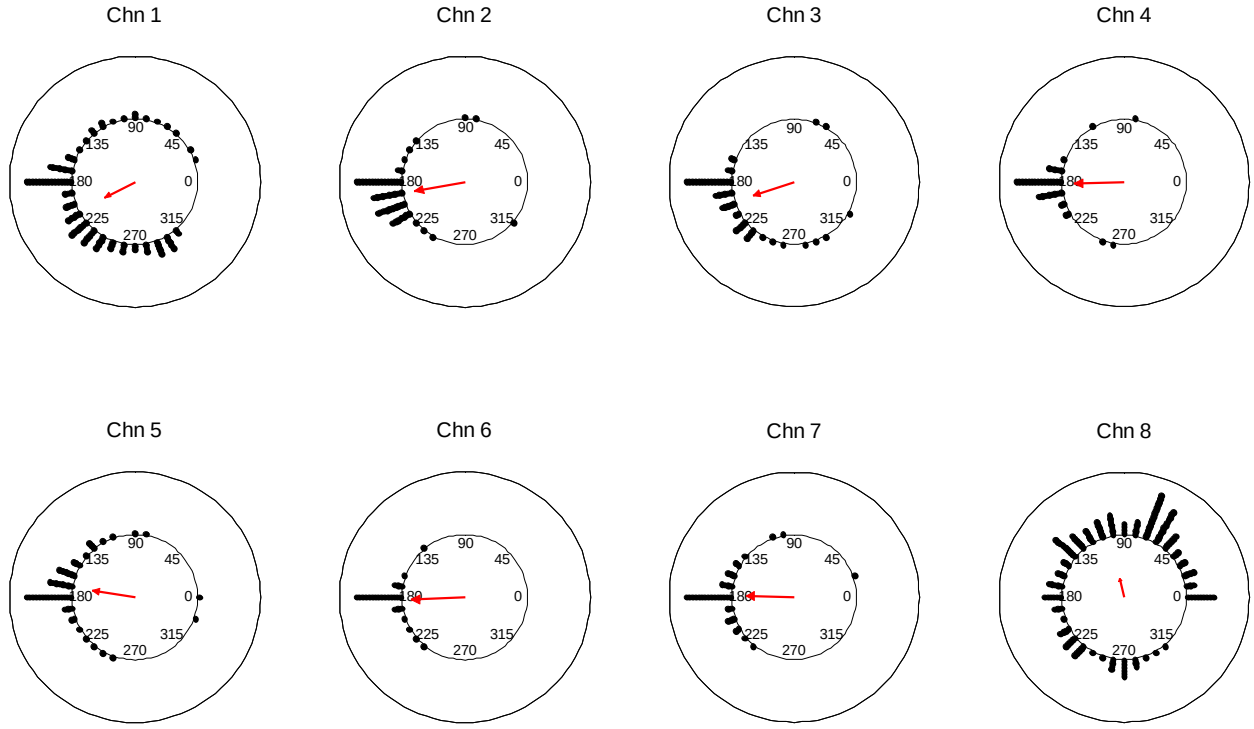

Fig. 6.18 (B). Circular histogram of workload 4 on Subject D (trial 2) by Phasor method

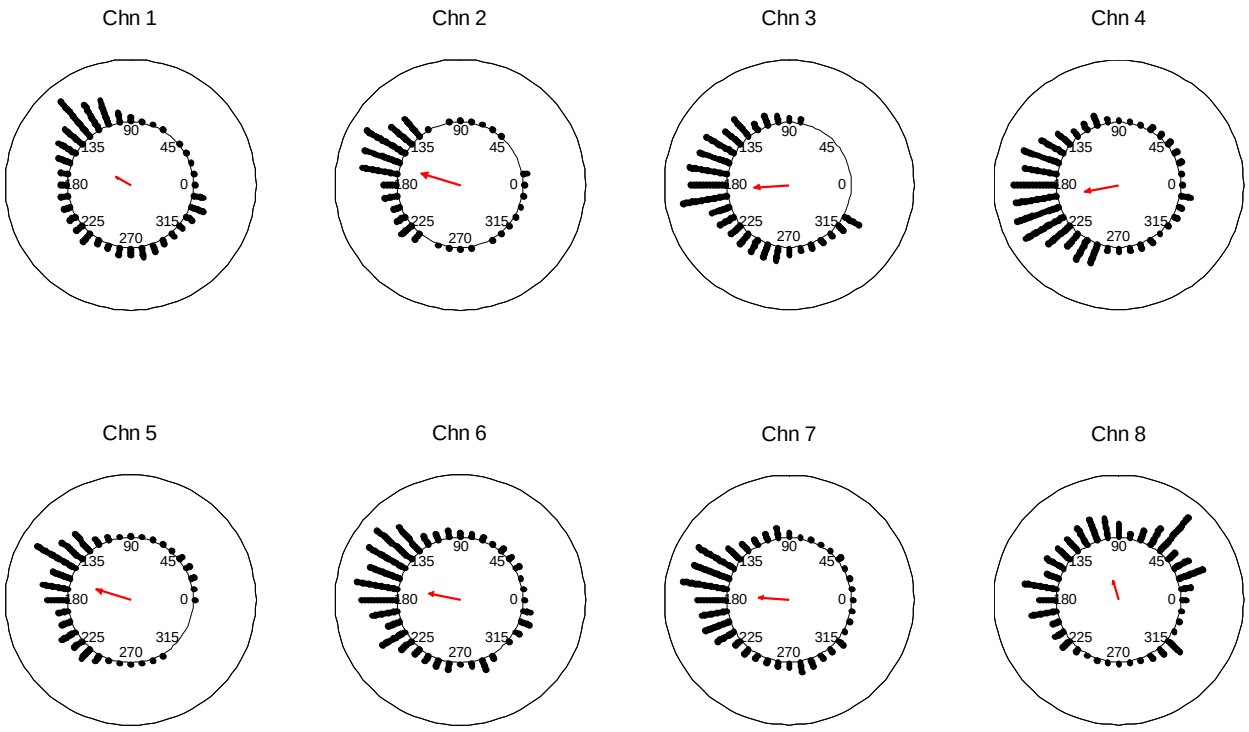

Fig. 6.18 (C). Circular histogram of workload 0 on Subject D (trial 2) by PSI method

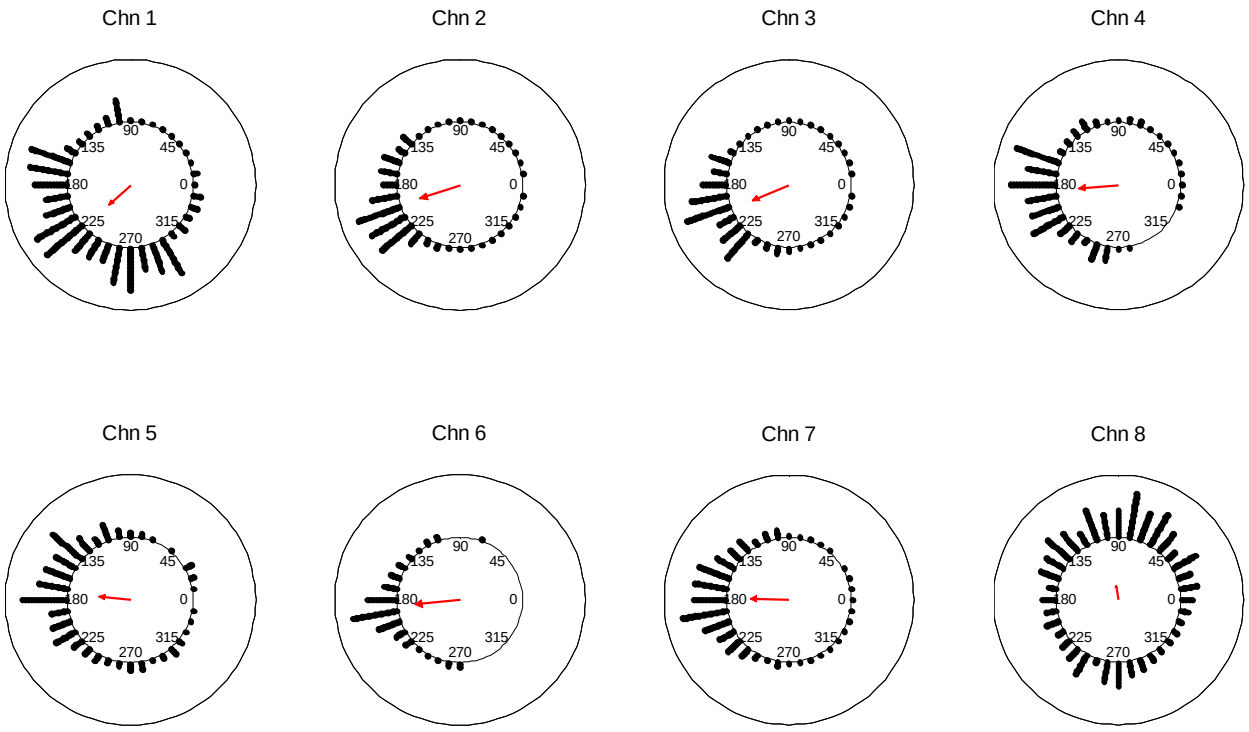

Fig. 6.18 (D). Circular histogram of workload 4 on Subject D (trial 2) by PSI method

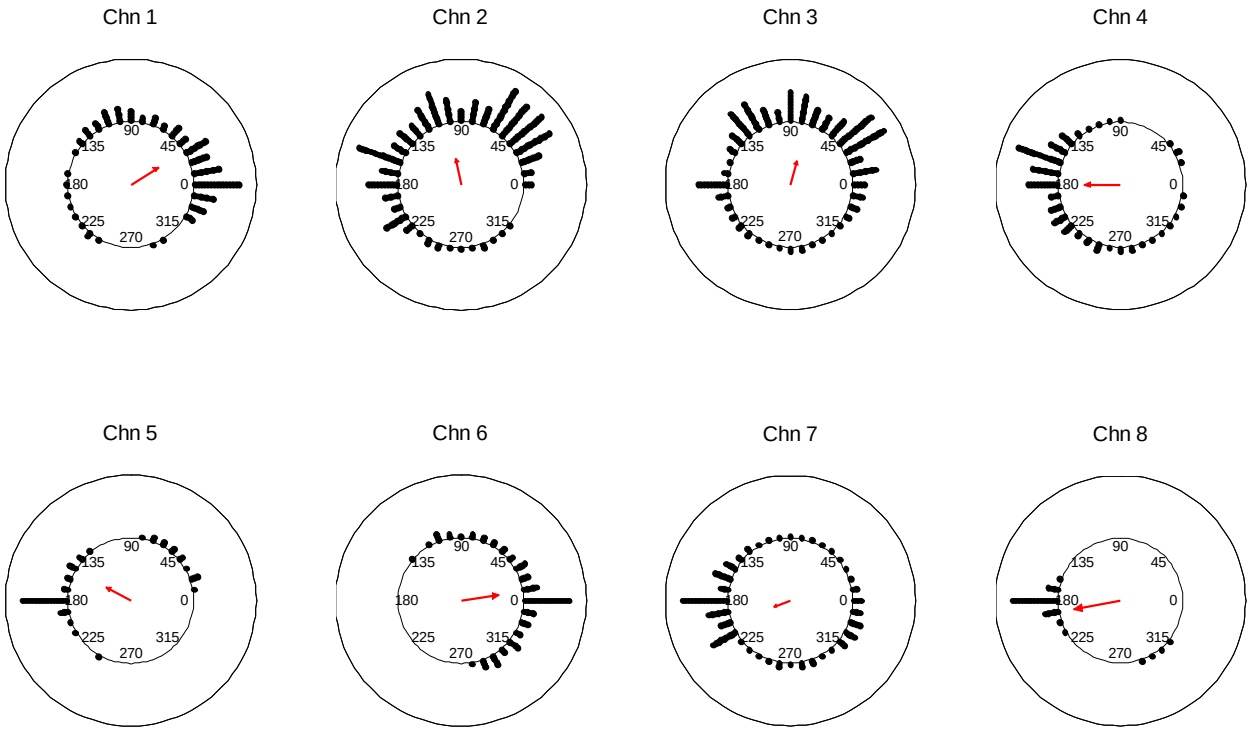

Fig. 6.19 (A). Circular histogram of workload 0 on Subject E by Phasor method

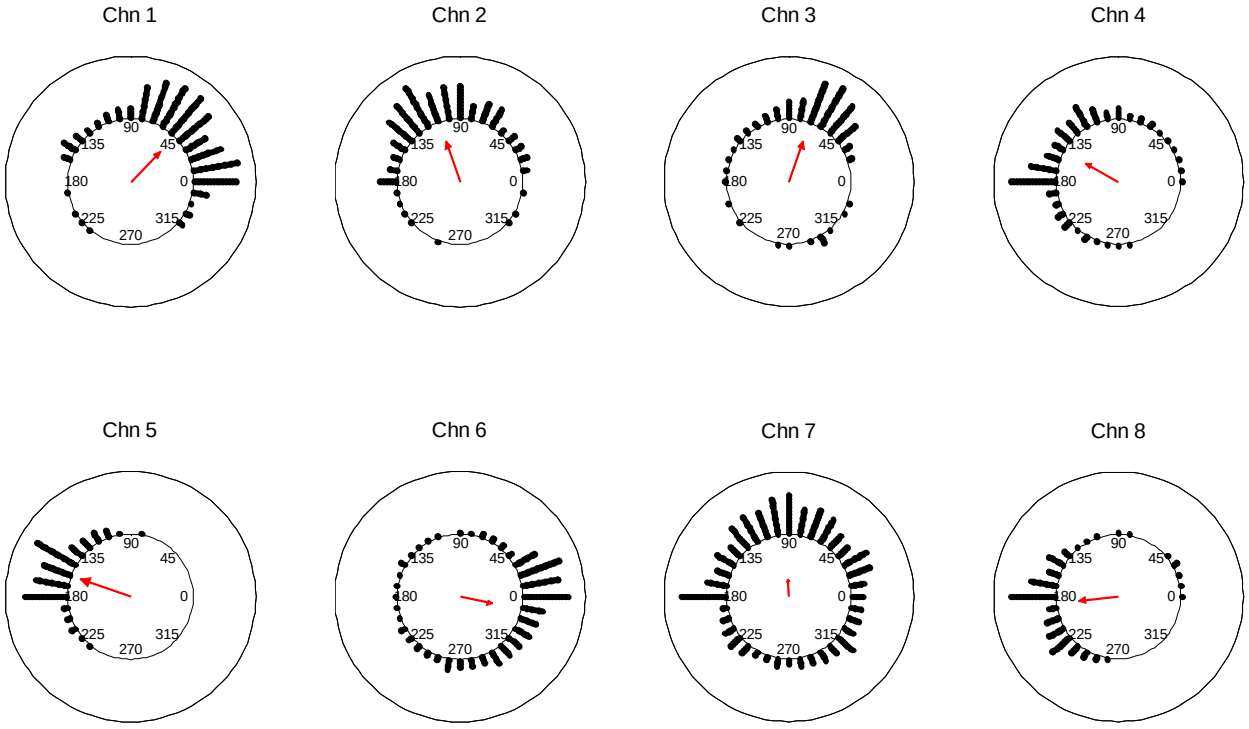

Fig. 6.19 (B). Circular histogram of workload 4 on Subject E by Phasor method

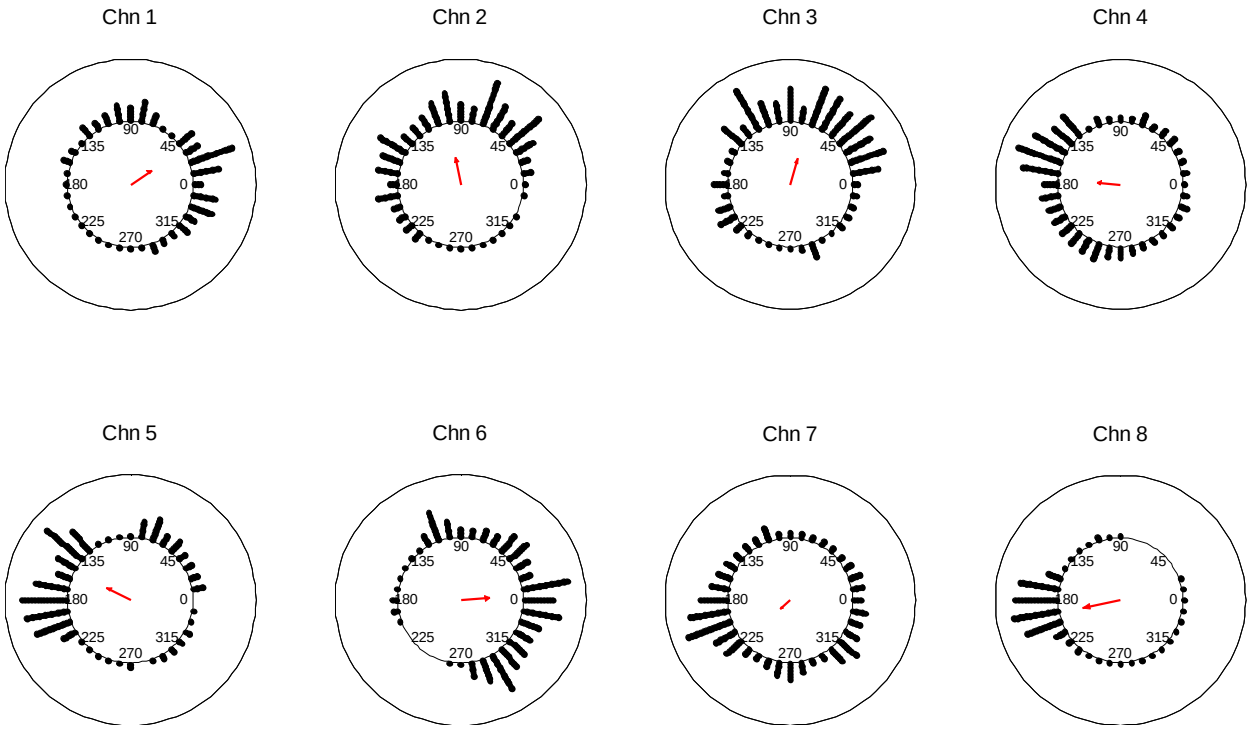

Fig. 6.19 (C). Circular histogram of workload 0 on Subject E by PSI method

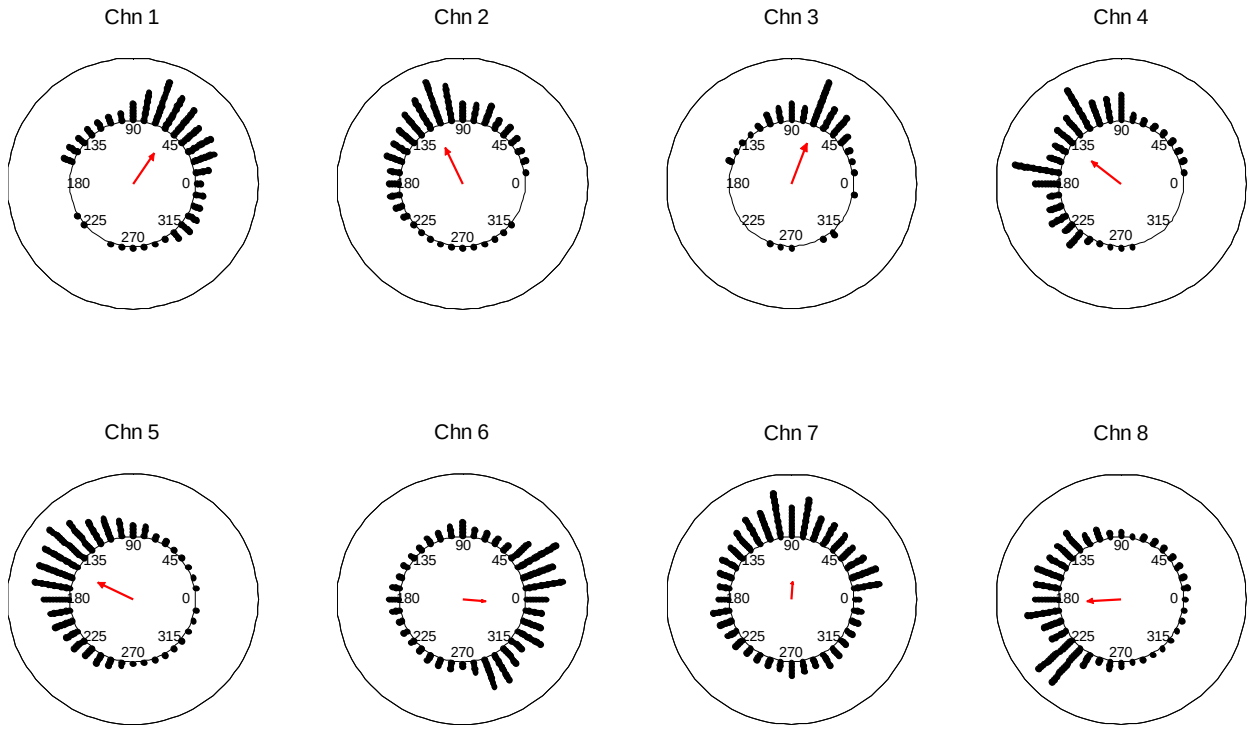

Fig. 6.19 (D). Circular histogram of workload 4 on Subject E by PSI method

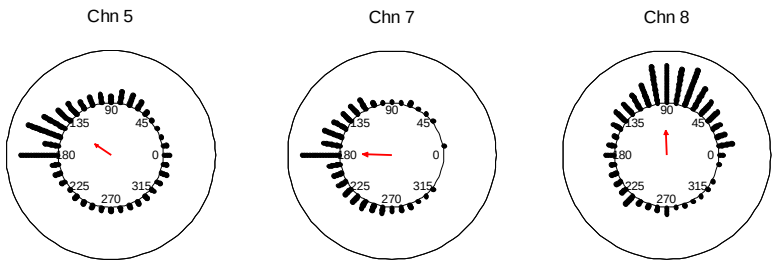

Fig. 6.20 (A). Circular histogram of rest on Subject A (trial 1) by Phasor method

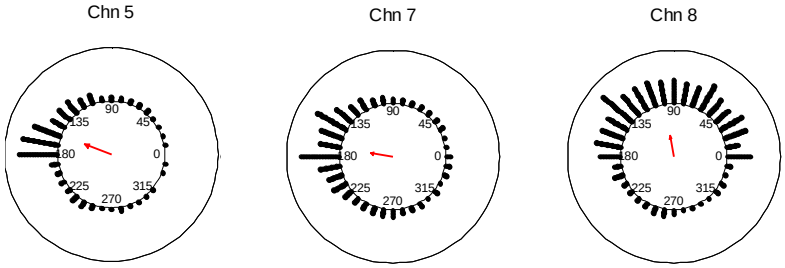

Fig. 6.20 (B). Circular histogram of finger tapping on Subject A (trial 1) by Phasor method

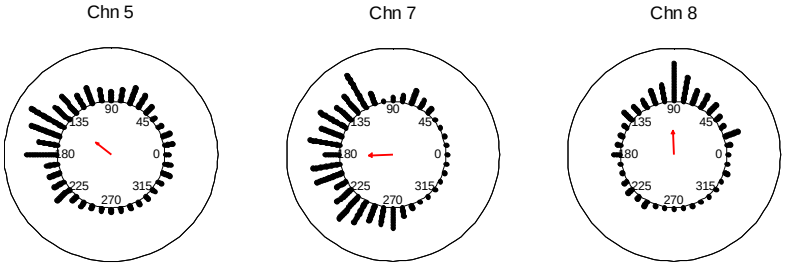

Fig. 6.20 (C). Circular histogram of rest on Subject A (trial 1) by PSI method

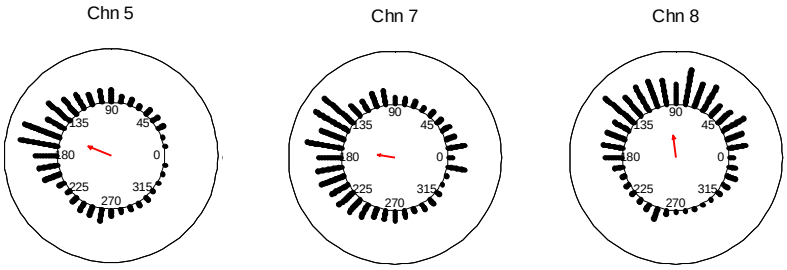

Fig. 6.20 (D). Circular histogram of finger tapping on Subject A (trial 1) by PSI method

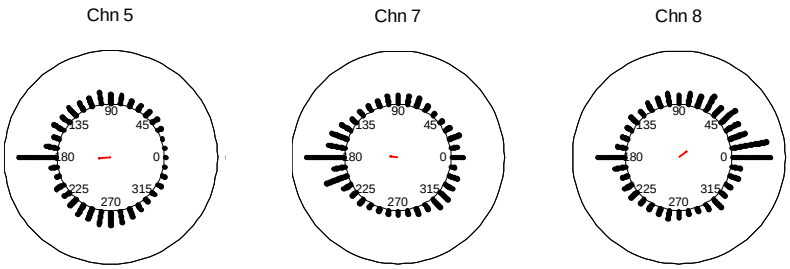

Fig. 6.21 (A). Circular histogram of rest on Subject A (trial 2) by Phasor method

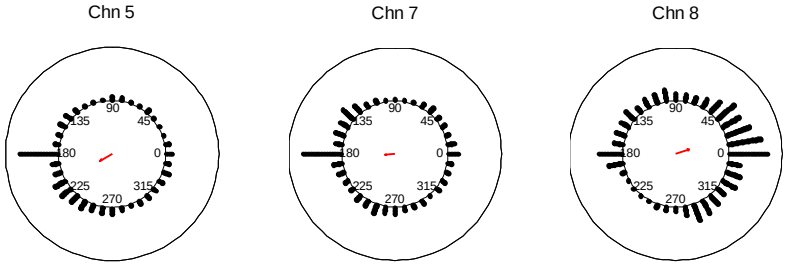

Fig. 6.21 (B). Circular histogram of finger tapping on Subject A (trial 2) by Phasor method

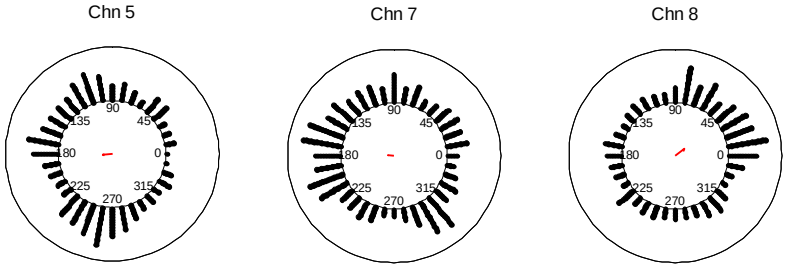

Fig. 6.21 (C). Circular histogram of rest on Subject A (trial 2) by PSI method

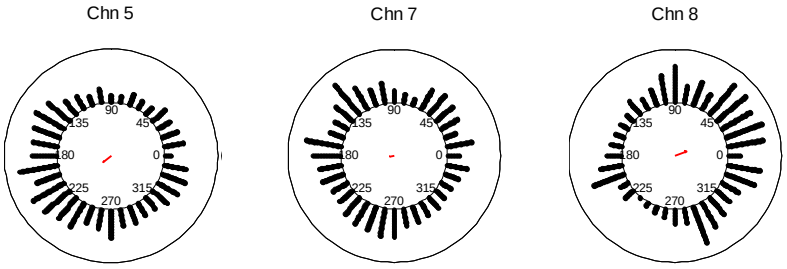

Fig. 6.21 (D). Circular histogram of finger tapping on Subject A (trial 2) by PSI method

Another representation of the phase distribution is the phasor-sector, of which the pie chart width denotes the standard deviation of phases defined in Eq. (4.22), the arrow direction is the average phase value and the arrow length is the resultant mean vector length. Results are shown below:

Only PSI result shown in table due to similar results of PSI and Phasor							
Subject ID	s-d Channel ID	Workload	Average Phase (degree)	Resultant Vector Length	Standard Deviation (degree)	p-value of Rayleigh /Uniform Test	p-value of Watson-Williams Test/circular ANOVA Test
Subject A (trial 1) – Rotating Cube	1	Wkl0	121.6	0.79	37.3	0.0000	0.0000
		Wkl4	137.4	0.78	38.2	0.0000	
	2	Wkl0	135.6	0.65	47.8	0.0000	0.0025
		Wkl4	129.4	0.56	54.0	0.0000	
	3	Wkl0	128.6	0.83	33.5	0.0000	0.0000
		Wkl4	136.6	0.86	30.1	0.0000	
	4	Wkl0	145.9	0.82	34.5	0.0000	0.0059
		Wkl4	142.8	0.88	28.1	0.0000	
	5	Wkl0	216.9	0.48	58.3	0.0000	0.0000
		Wkl4	272.0	0.34	65.8	0.0000	
	6	Wkl0	359.3	0.68	45.3	0.0000	0.4223
		Wkl4	1.3	0.34	65.4	0.0000	
	7	Wkl0	29.4	0.17	73.9	0.0000	0.0000
		Wkl4	5.4	0.48	58.2	0.0000	
	8	Wkl0	94.0	0.55	54.1	0.0000	0.0000
		Wkl4	120.7	0.26	69.5	0.0000	
Subject A (trial 2) – Rotating Cube	1	Wkl0	178.7	0.50	57.5	0.0000	0.6408
		Wkl4	179.6	0.68	45.8	0.0000	
	2	Wkl0	118.3	0.29	68.1	0.0000	0.0000
		Wkl4	195.0	0.15	74.6	0.0000	
	3	Wkl0	165.7	0.69	45.2	0.0000	0.0000
		Wkl4	156.4	0.71	43.6	0.0000	
	4	Wkl0	143.2	0.23	71.0	0.0000	0.0000
		Wkl4	169.4	0.49	57.9	0.0000	
	5	Wkl0	143.1	0.58	52.4	0.0000	0.0000
		Wkl4	168.5	0.65	48.0	0.0000	
	6	Wkl0	143.8	0.69	44.8	0.0000	0.0000
		Wkl4	161.2	0.70	44.3	0.0000	
	7	Wkl0	134.8	0.45	59.9	0.0000	0.0000
		Wkl4	153.6	0.81	35.4	0.0000	
	8	Wkl0	174.1	0.78	38.1	0.0000	0.0000
		Wkl4	167.4	0.76	39.7	0.0000	
Subject B –Rotating Cube	1	Wkl0	119.7	0.34	65.6	0.0000	0.0000
		Wkl4	88.4	0.51	56.5	0.0000	
	2	Wkl0	176.3	0.60	51.4	0.0000	0.0000
		Wkl4	143.8	0.65	47.6	0.0000	

	3	Wkl0	118.9	0.43	61.2	0.0000	0.0000
		Wkl4	135.6	0.59	51.7	0.0000	
	4	Wkl0	190.6	0.69	45.1	0.0000	0.0000
		Wkl4	172.8	0.67	46.5	0.0000	
	5	Wkl0	151.1	0.71	43.9	0.0000	0.0000
		Wkl4	139.7	0.80	36.2	0.0000	
	6	Wkl0	122.1	0.62	49.7	0.0000	0.0000
		Wkl4	82.1	0.52	56.1	0.0000	
	7	Wkl0	153.8	0.50	57.3	0.0000	0.0000
		Wkl4	137.8	0.45	60.0	0.0000	
	8	Wkl0	168.1	0.75	40.9	0.0000	0.0000
		Wkl4	159.4	0.63	49.4	0.0000	
Subject C –Rotating Cube	1	Wkl0	175.5	0.78	38.1	0.0000	0.0000
		Wkl3	170.9	0.83	33.2	0.0000	
	2	Wkl0	173.5	0.70	44.1	0.0000	0.0000
		Wkl3	181.4	0.61	50.7	0.0000	
	3	Wkl0	172.3	0.87	28.9	0.0000	0.6187
		Wkl3	172.0	0.78	38.2	0.0000	
	4	Wkl0	190.1	0.75	40.8	0.0000	0.0000
		Wkl3	184.0	0.82	34.7	0.0000	
	5	Wkl0	154.9	0.87	29.2	0.0000	0.0012
		Wkl3	153.1	0.84	32.2	0.0000	
	6	Wkl0	172.6	0.84	32.3	0.0000	0.0000
		Wkl3	167.5	0.87	29.8	0.0000	
	7	Wkl0	171.4	0.87	29.0	0.0000	0.0666
		Wkl3	170.5	0.90	25.3	0.0000	
	8	Wkl0	157.3	0.87	29.1	0.0000	0.0198
		Wkl3	158.7	0.83	33.3	0.0000	
Subject D (trial 1) – Rotating Cube	1	Wkl0	186.2	0.70	44.2	0.0000	0.0910
		Wkl4	183.5	0.74	41.0	0.0000	
	2	Wkl0	156.8	0.56	53.6	0.0000	0.0006
		Wkl4	163.0	0.76	39.7	0.0000	
	3	Wkl0	158.4	0.42	61.8	0.0000	0.0000
		Wkl4	174.8	0.52	55.9	0.0000	
	4	Wkl0	173.6	0.87	29.4	0.0000	0.0000
		Wkl4	186.5	0.70	44.1	0.0000	
	5	Wkl0	139.1	0.48	58.7	0.0000	0.0000
		Wkl4	156.3	0.70	44.5	0.0000	
	6	Wkl0	170.7	0.51	56.5	0.0000	0.0000
		Wkl4	179.8	0.69	45.4	0.0000	
	7	Wkl0	170.8	0.44	60.6	0.0000	0.0000
		Wkl4	191.9	0.47	58.7	0.0000	
	8	Wkl0	235.0	0.06	78.4	0.0011	0.0000
		Wkl4	161.4	0.39	63.1	0.0000	
Subject D (trial 2) – Rotating Cube	1	Wkl0	152.5	0.27	69.1	0.0000	0.0000
		Wkl4	223.6	0.47	59.1	0.0000	
	2	Wkl0	163.9	0.65	47.9	0.0000	0.0000
		Wkl4	198.7	0.67	46.2	0.0000	
	3	Wkl0	184.5	0.57	53.0	0.0000	0.0000

		Wkl4	203.4	0.64	48.6	0.0000	
	4	Wkl0	191.7	0.56	53.7	0.0000	0.0010
		Wkl4	185.1	0.65	48.2	0.0000	
	5	Wkl0	163.0	0.58	52.6	0.0000	0.0000
		Wkl4	173.8	0.50	57.3	0.0000	
	6	Wkl0	167.8	0.52	55.9	0.0000	0.0000
		Wkl4	186.1	0.73	42.4	0.0000	
	7	Wkl0	175.5	0.51	56.9	0.0000	0.2265
		Wkl4	178.1	0.63	49.6	0.0000	
	8	Wkl0	107.2	0.33	66.3	0.0000	0.0218
		Wkl4	99.2	0.23	70.9	0.0000	
Subject E –Rotating Cube	1	Wkl0	33.5	0.41	62.1	0.0000	0.0000
		Wkl4	53.9	0.60	51.4	0.0000	
	2	Wkl0	100.1	0.44	60.5	0.0000	0.0000
		Wkl4	116.2	0.64	48.7	0.0000	
	3	Wkl0	74.2	0.43	61.1	0.0000	0.0230
		Wkl4	69.1	0.69	45.2	0.0000	
	4	Wkl0	175.4	0.38	63.8	0.0000	0.0000
		Wkl4	143.8	0.60	50.9	0.0000	
	5	Wkl0	151.7	0.42	61.4	0.0000	0.1842
		Wkl4	154.9	0.62	50.1	0.0000	
	6	Wkl0	3.8	0.47	58.9	0.0000	0.0014
		Wkl4	355.0	0.38	64.0	0.0000	
	7	Wkl0	223.1	0.21	72.0	0.0000	0.0000
		Wkl4	87.5	0.29	68.3	0.0000	
	8	Wkl0	191.0	0.61	50.6	0.0000	0.0003
		Wkl4	183.4	0.55	54.4	0.0000	
Subject A (trial 1) – Finger Tapping	5	Rest	140.1	0.37	64.3	0.0000	0.0000
		Tapping	158.6	0.47	58.9	0.0000	
	7	Rest	181.4	0.47	59.2	0.0000	0.0000
		Tapping	169.5	0.34	65.9	0.0000	
	8	Rest	91.8	0.46	59.3	0.0000	0.0087
		Tapping	96.5	0.42	61.4	0.0000	
Subject A (trial 2) – Finger Tapping	5	Rest	186.7	0.18	73.3	0.0000	0.0000
		Tapping	218.3	0.19	73.1	0.0000	
	7	Rest	173.4	0.13	75.6	0.0000	0.0002
		Tapping	185.5	0.09	77.0	0.0000	
	8	Rest	37.3	0.22	71.5	0.0000	0.0000
		Tapping	22.4	0.25	70.2	0.0000	

Tab. 6.1. Table of phase distribution statistical results: for each workload on each experiment, average phase value, resultant mean vector length, standard deviation of phase distribution, and Rayleigh test and Watson-Williams test between workload 0 and workload 4 (or finger tapping). P-value in shadow means not to reject the null hypothesis; others reject and accept H_a

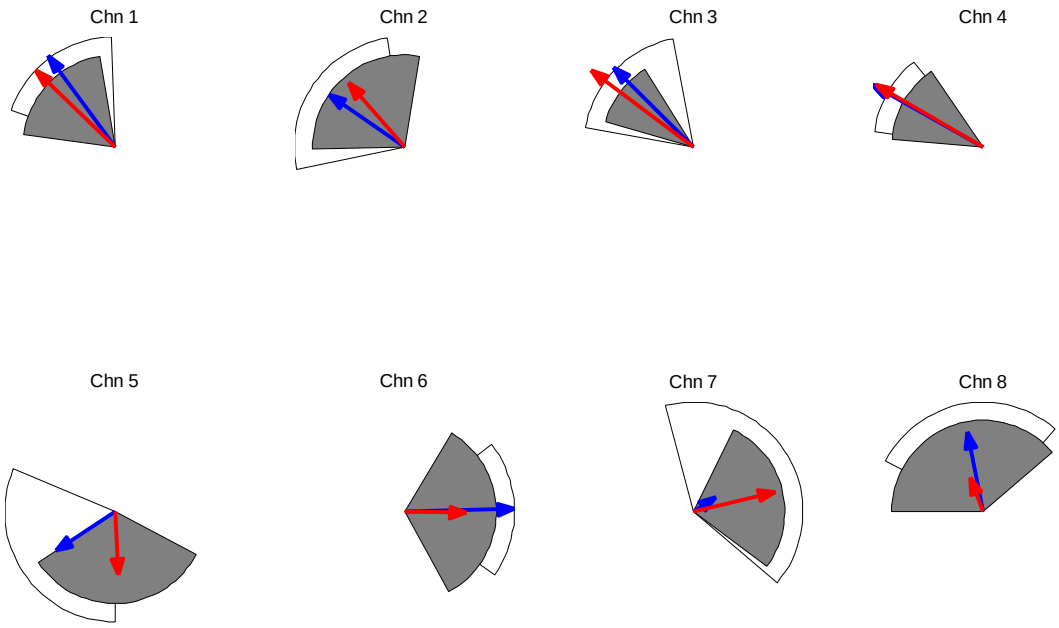

Fig. 6.22 (A). Phasor-sector on subject A (trial 1) calculated by **Phasor** method. Sector in white is Wkl 0 and gray is Wkl 4. Arrow in blue is resultant vector in Wkl 0 and red in Wkl 4

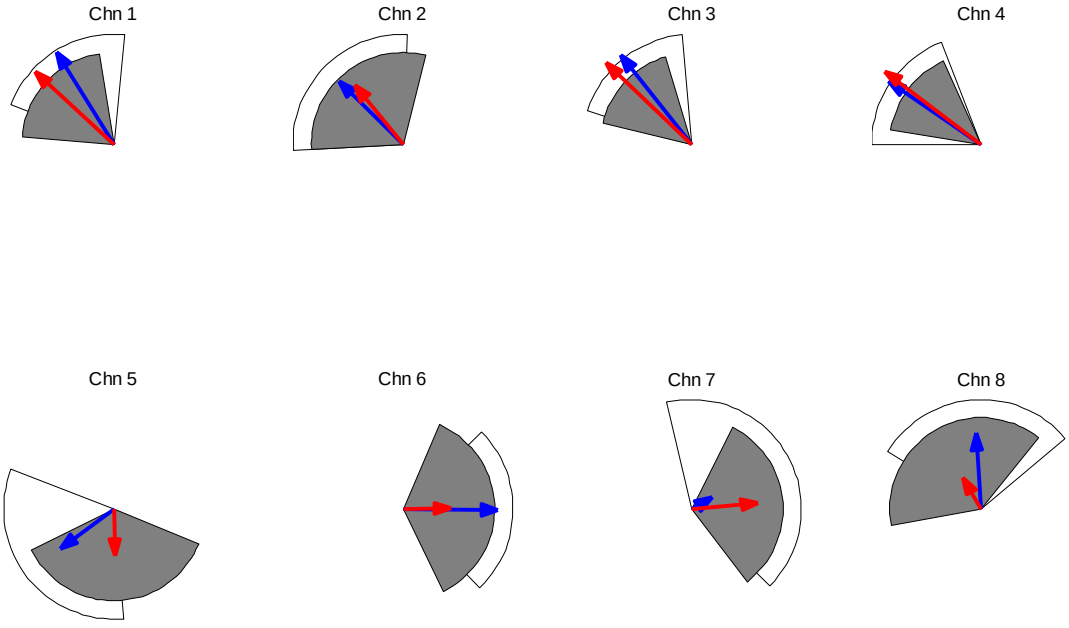

Fig. 6.22 (B). Phasor-sector on subject A (trial 1) calculated by **PSI** method. Sector in white is Wkl 0 and gray is Wkl 4. Arrow in blue is resultant vector in Wkl 0 and red in Wkl 4

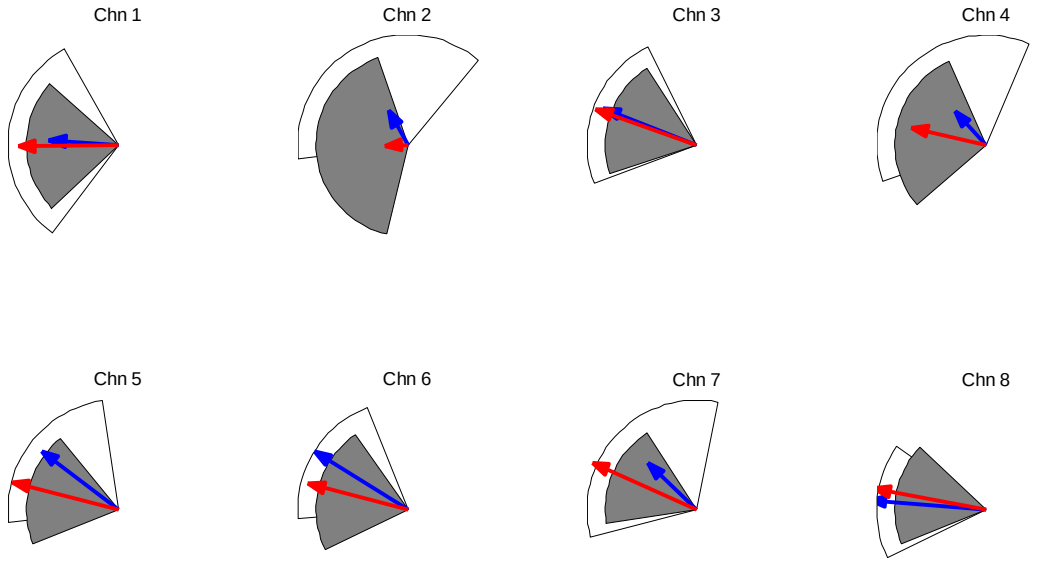

Fig. 6.23 (A). Phasor-sector on subject A (trial 2) calculated by **Phasor** method. Sector in white is Wkl 0 and gray is Wkl 4. Arrow in blue is resultant vector in Wkl 0 and red in Wkl 4

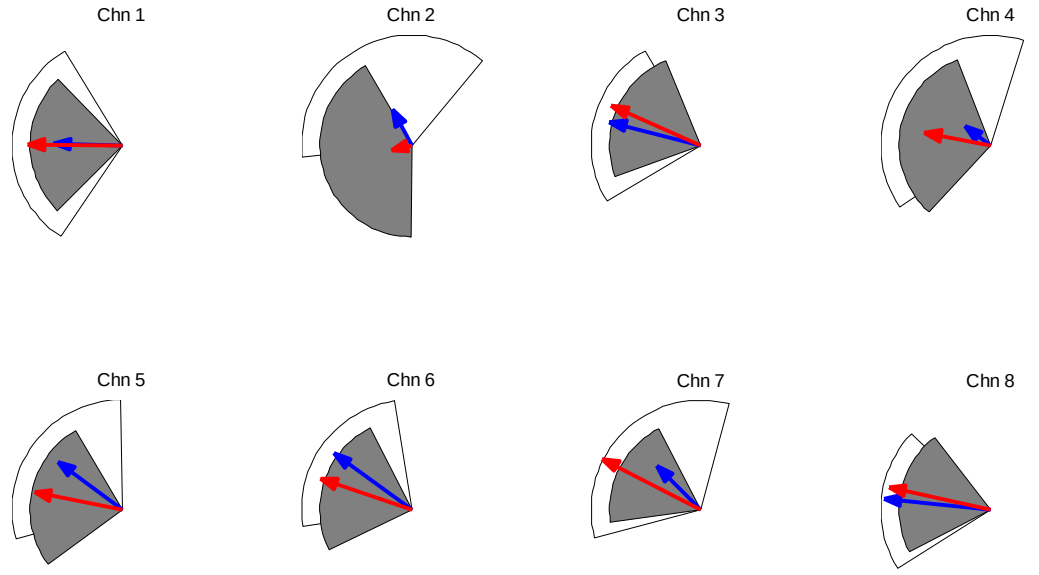

Fig. 6.23 (B). Phasor-sector on subject A (trial 2) calculated by **PSI** method. Sector in white is Wkl 0 and gray is Wkl 4. Arrow in blue is resultant vector in Wkl 0 and red in Wkl 4

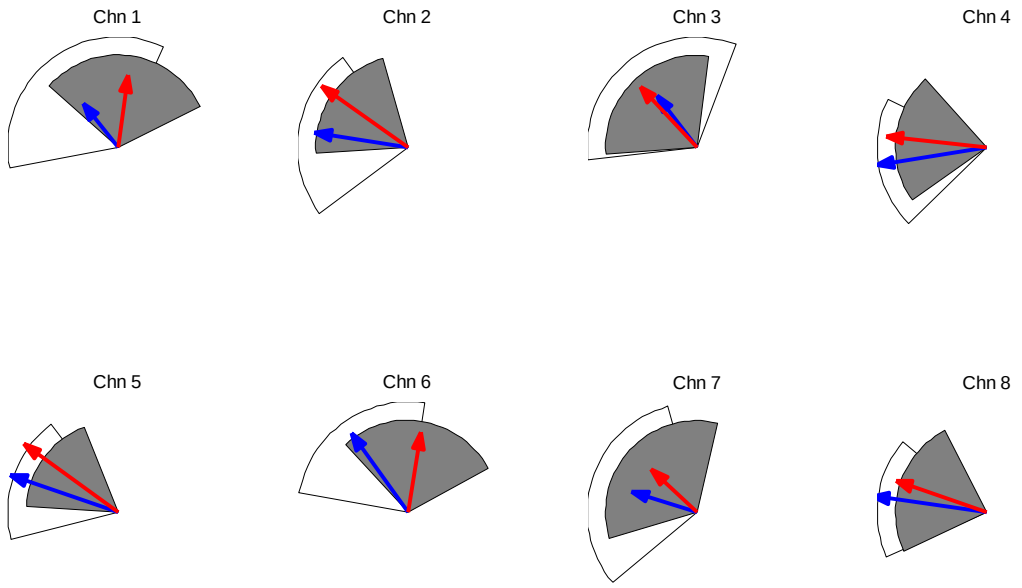

Fig. 6.24 (A). Phasor-sector on subject B calculated by **Phasor** method. Sector in white is Wkl 0 and gray is Wkl 4. Arrow in blue is resultant vector in Wkl 0 and red in Wkl 4

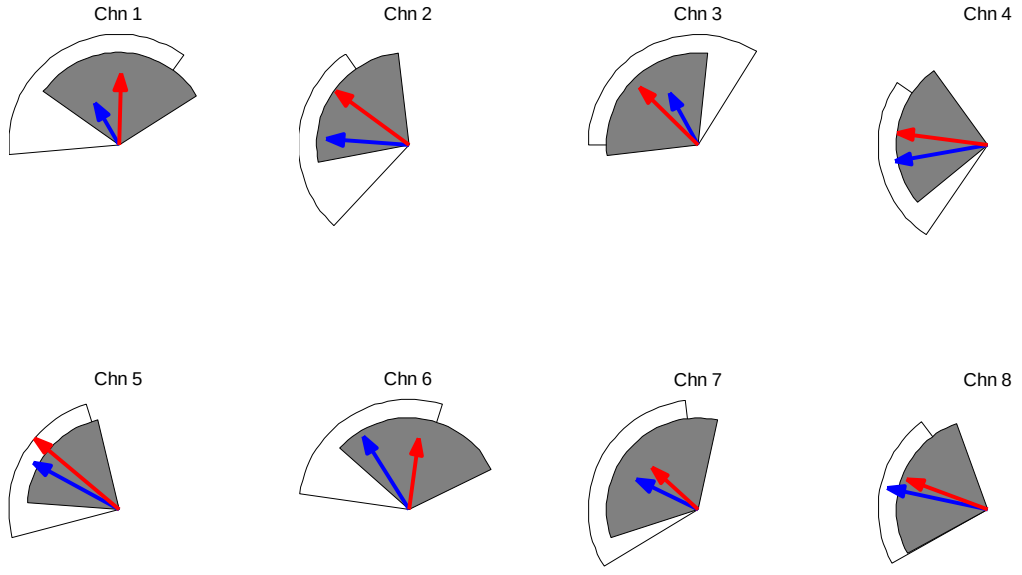

Fig. 6.24 (B). Phasor-sector on subject B calculated by **PSI** method. Sector in white is Wkl 0 and gray is Wkl 4. Arrow in blue is resultant vector in Wkl 0 and red in Wkl 4

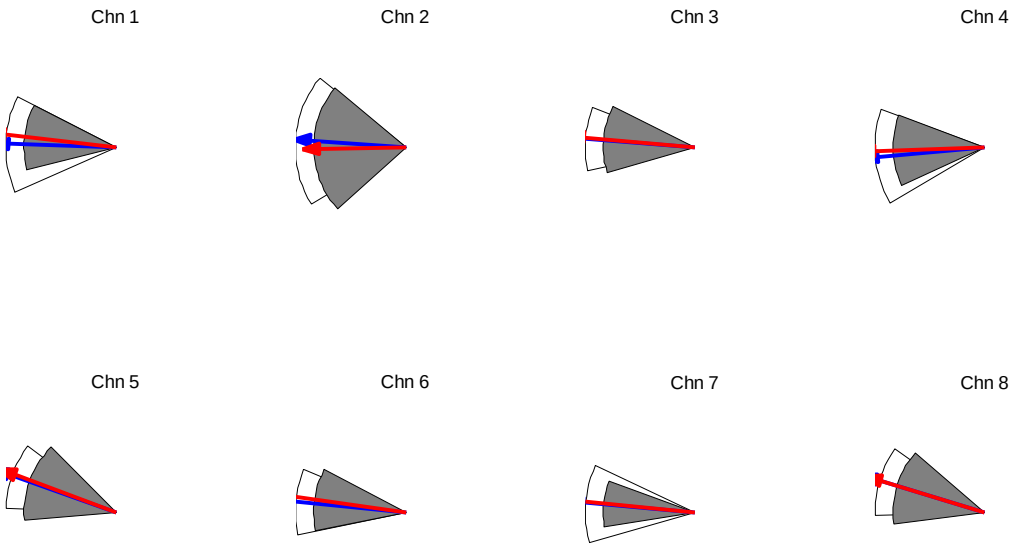

Fig. 6.25 (A). Phasor-sector on subject C calculated by **Phasor** method. Sector in white is Wkl 0 and gray is Wkl 3. Arrow in blue is resultant vector in Wkl 0 and red in Wkl 3

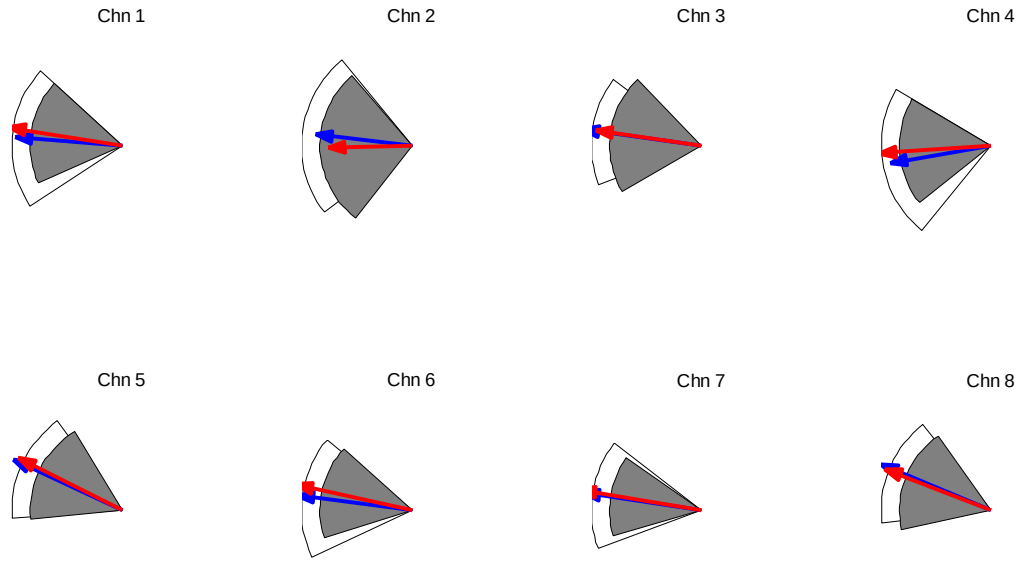

Fig. 6.25 (B). Phasor-sector on subject C calculated by **PSI** method. Sector in white is Wkl 0 and gray is Wkl 3. Arrow in blue is resultant vector in Wkl 0 and red in Wkl 3

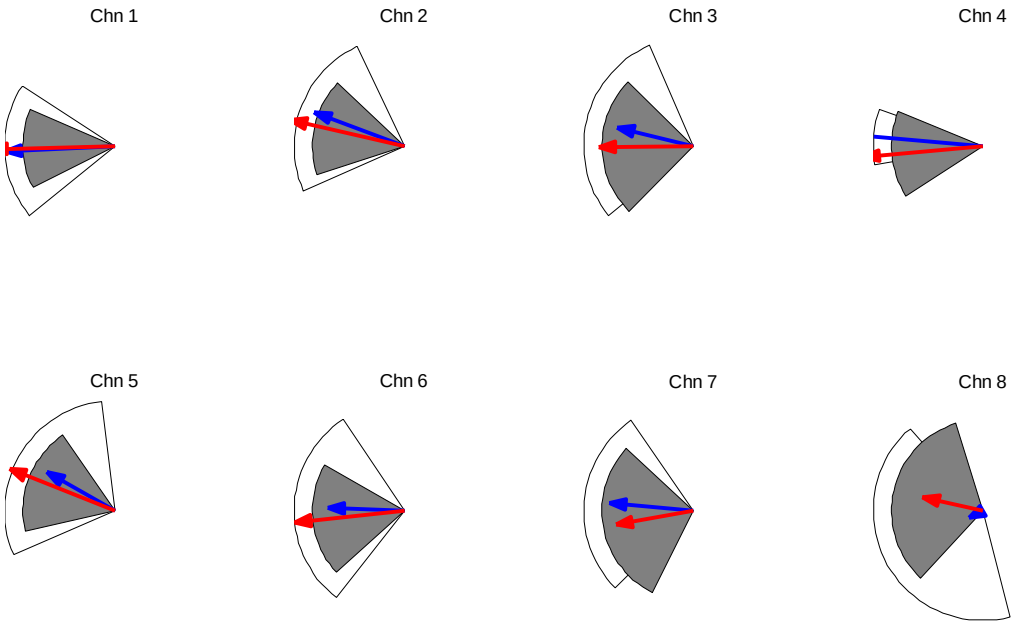

Fig. 6.26 (A). Phasor-sector on subject D (trial 1) calculated by **Phasor** method. Sector in white is Wkl 0 and gray is Wkl 4. Arrow in blue is resultant vector in Wkl 0 and red in Wkl 4

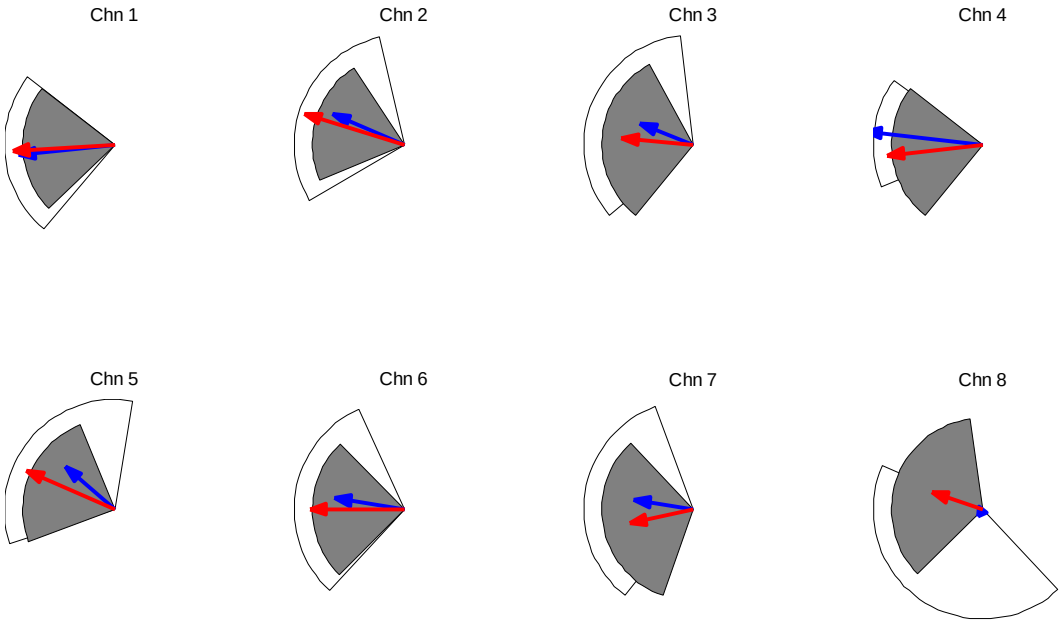

Fig. 6.26 (B). Phasor-sector on subject D (trial 1) calculated by **PSI** method. Sector in white is Wkl 0 and gray is Wkl 4. Arrow in blue is resultant vector in Wkl 0 and red in Wkl 4

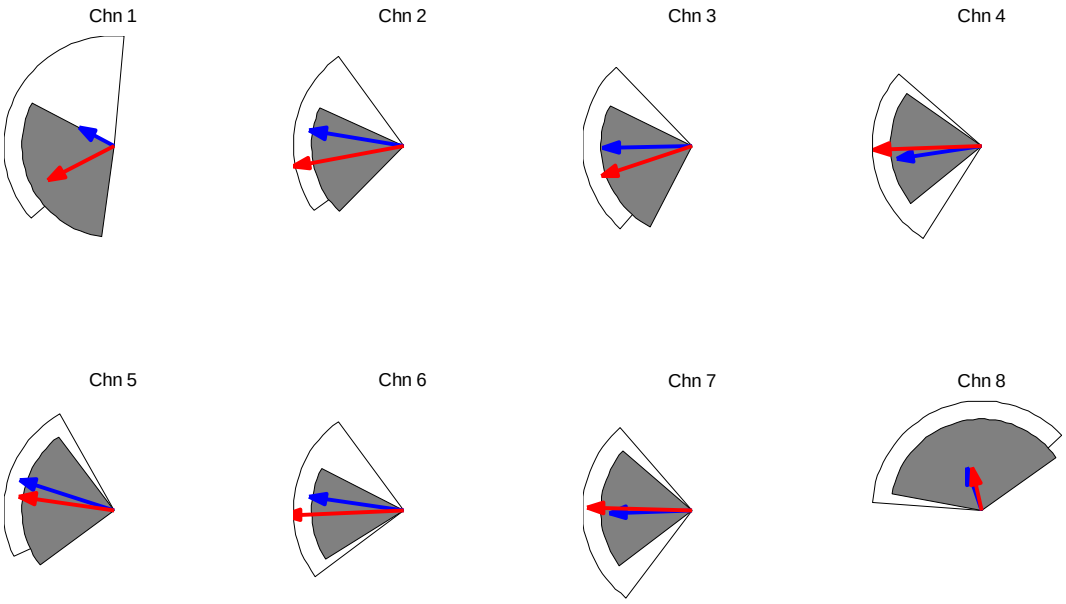

Fig. 6.27 (A). Phasor-sector on subject D (trial 2) calculated by **Phasor** method. Sector in white is Wkl 0 and gray is Wkl 4. Arrow in blue is resultant vector in Wkl 0 and red in Wkl 4

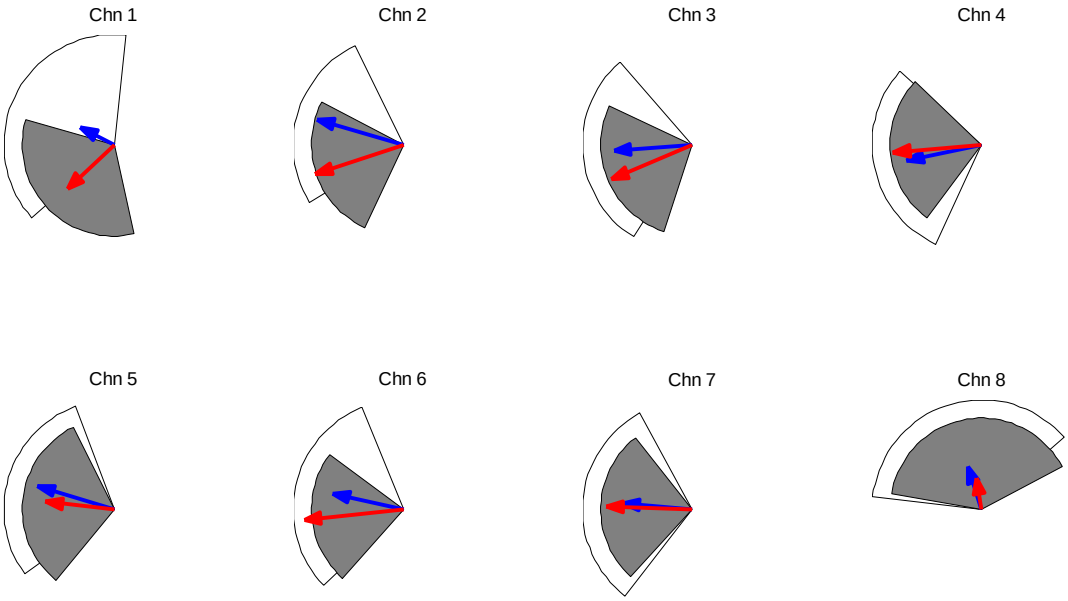

Fig. 6.27 (B). Phasor-sector on subject D (trial 2) calculated by **PSI** method. Sector in white is Wkl 0 and gray is Wkl 4. Arrow in blue is resultant vector in Wkl 0 and red in Wkl 4

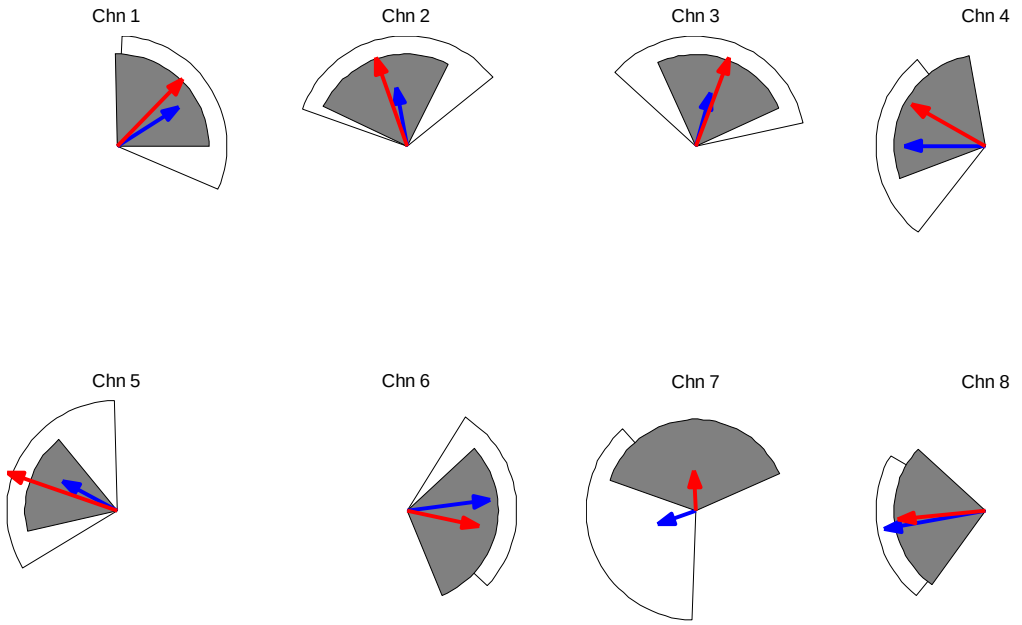

Fig. 6.28 (A). Phasor-sector on subject E calculated by **Phasor** method. Sector in white is Wkl 0 and gray is Wkl 4. Arrow in blue is resultant vector in Wkl 0 and red in Wkl 4

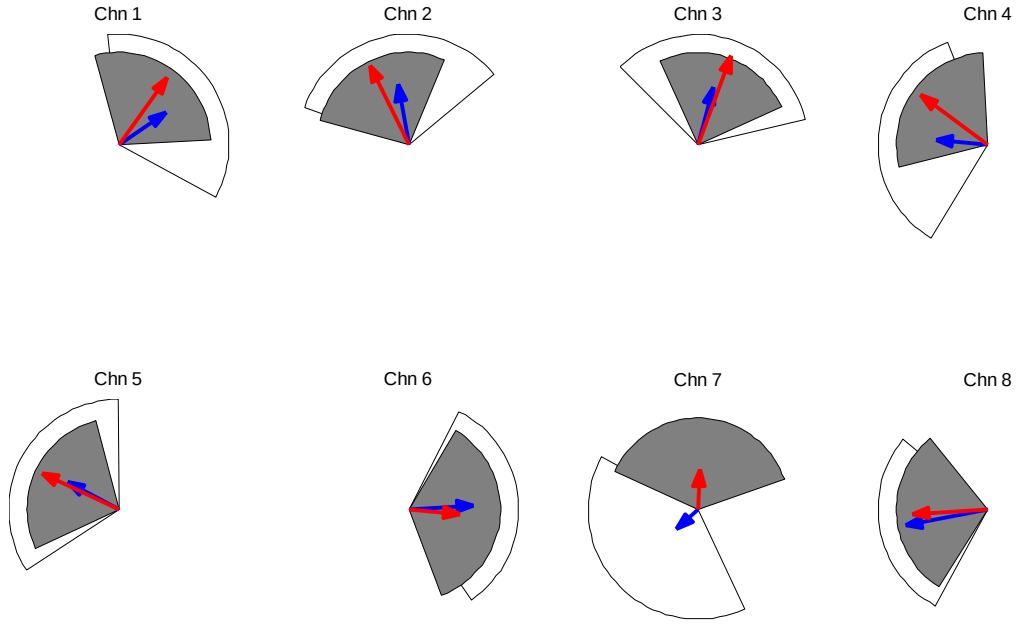

Fig. 6.28 (B). Phasor-sector on subject E calculated by **PSI** method. Sector in white is Wkl 0 and gray is Wkl 4. Arrow in blue is resultant vector in Wkl 0 and red in Wkl 4

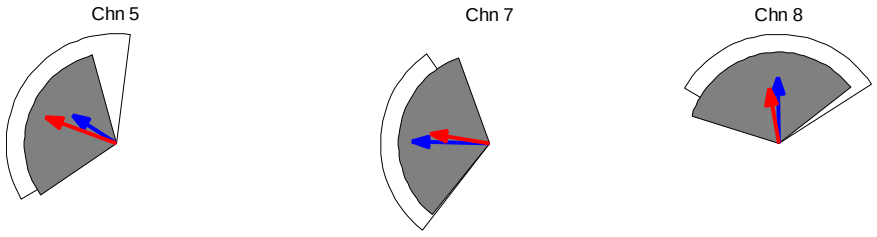

Fig. 6.29 (A). Phasor-sector on subject A (trial 1) calculated by **Phasor** method. Sector in white is Rest and gray is Finger Tapping. Arrow in blue is resultant vector in Rest and red in Finger Tapping

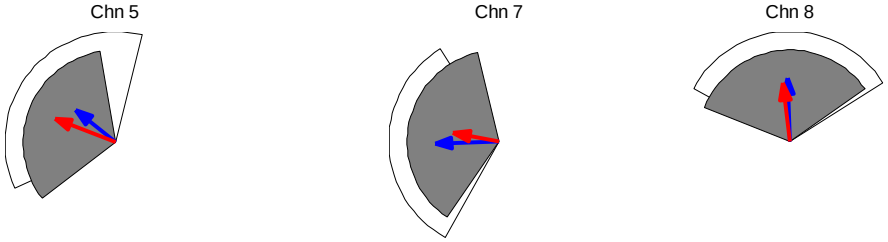

Fig. 6.29 (B). Phasor-sector on subject A (trial 1) calculated by **PSI** method. Sector in white is Rest and gray is Finger Tapping. Arrow in blue is resultant vector in Rest and red in Finger Tapping

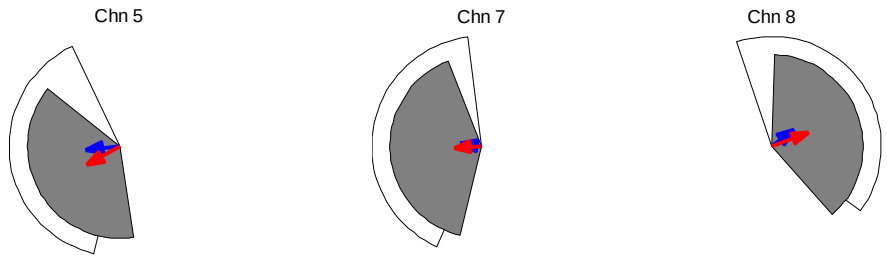

Fig. 6.30 (A). Phasor-sector on subject A (trial 2) calculated by **Phasor** method. Sector in white is Rest and gray is Finger Tapping. Arrow in blue is resultant vector in Rest and red in Finger Tapping

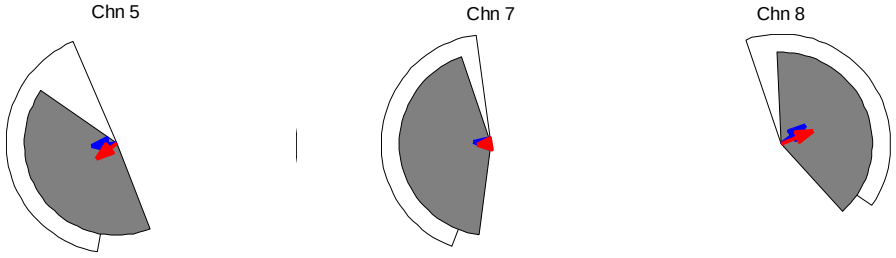

Fig. 6.30 (B). Phasor-sector on subject A (trial 2) calculated by **PSI** method. Sector in white is Rest and gray is Finger Tapping. Arrow in blue is resultant vector in Rest and red in Finger Tapping

The previous results are statistical in nature, but we don't know the dynamic of the phase temporal evolution during the experiment. Knowing the phase evolution is important because we can understand how the physiological processes change from one stage to another stage by the stimulus. We have developed a TARGET representation to demonstrate how the phase changes as a function of time. Fig. 6.31 shows the TARGET of subject D (trial 2) in rotating cube experiment.

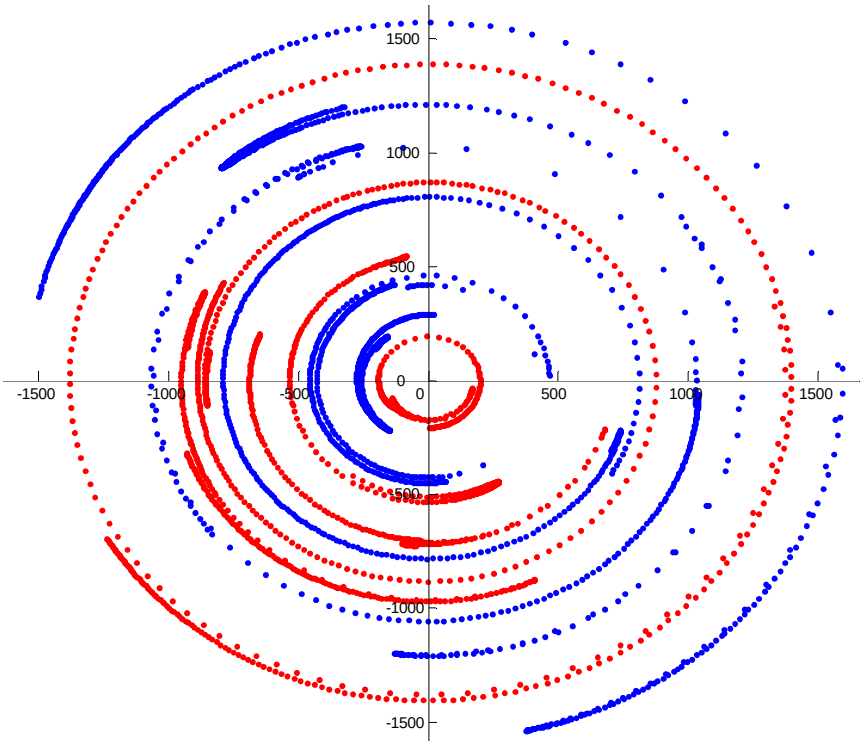

workload 0
workload 4

Channel 1 (Subject D trial 2)

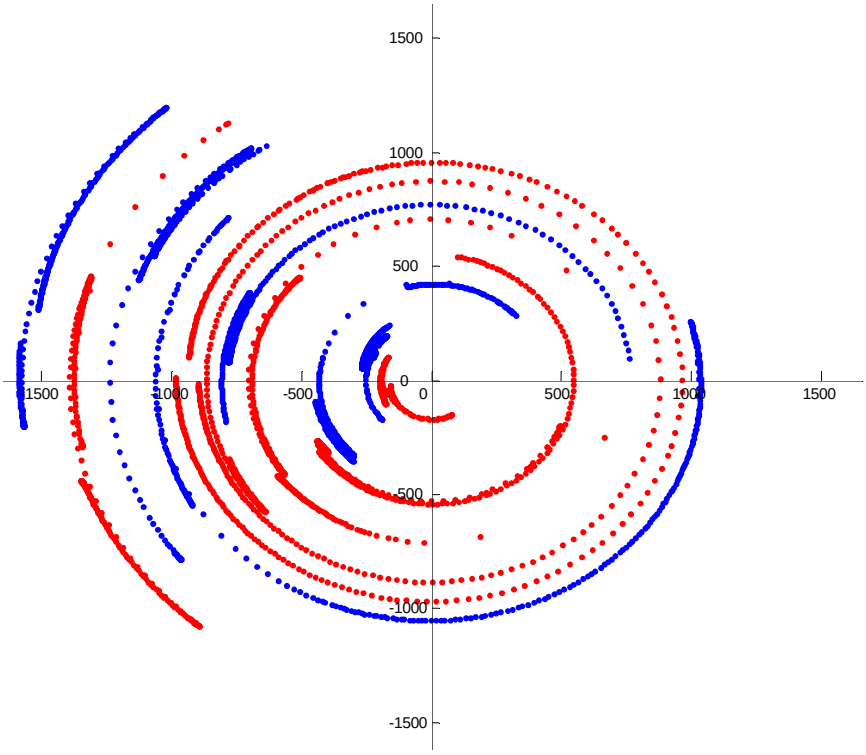

workload 0
workload 4

Channel 2 (Subject D trial 2)

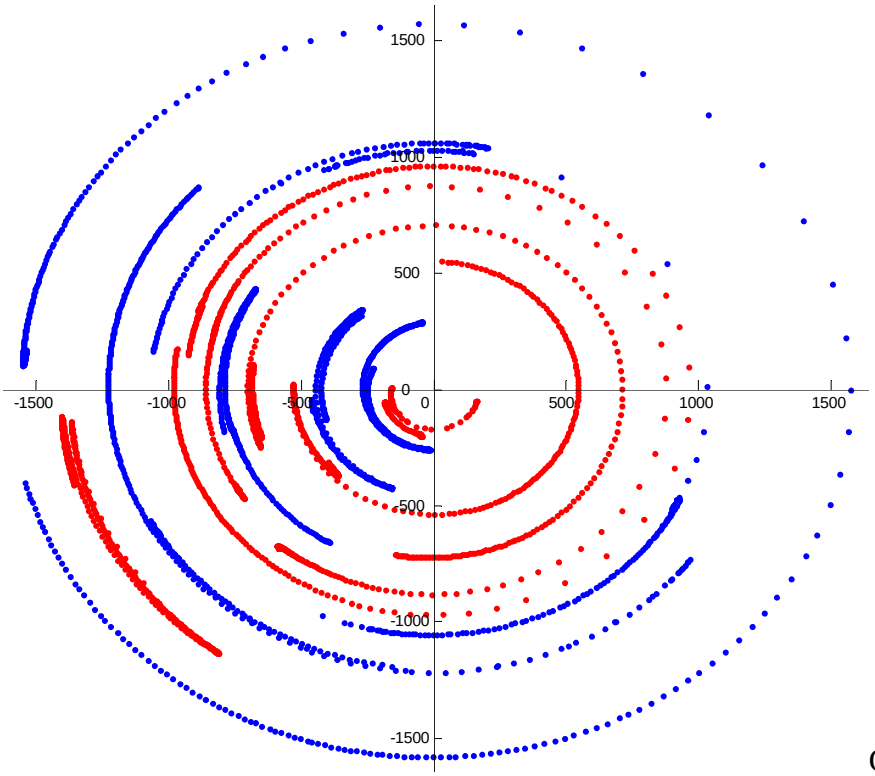

... workload 0
... workload 4

Channel 3 (Subject D trial 2)

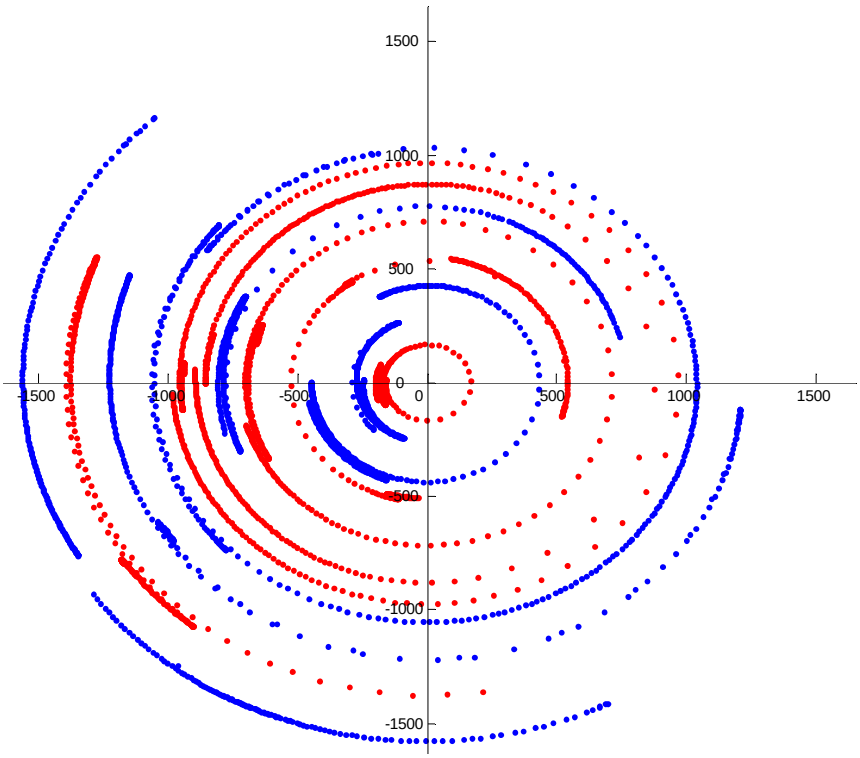

... workload 0
... workload 4

Channel 4 (Subject D trial 2)

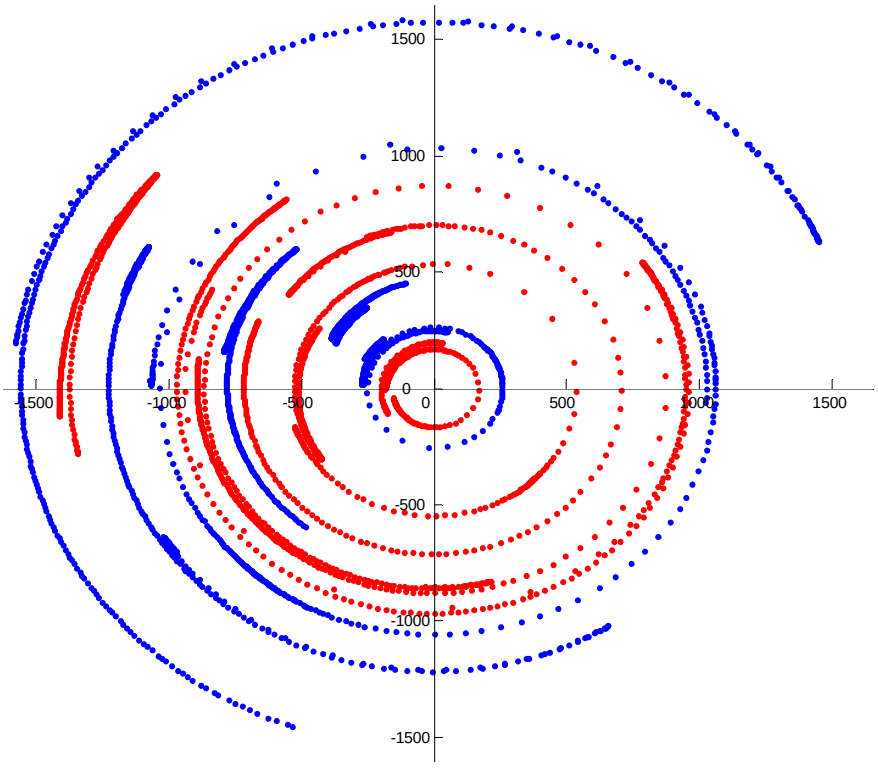

… workload 0
… workload 4

Channel 5 (Subject D trial 2)

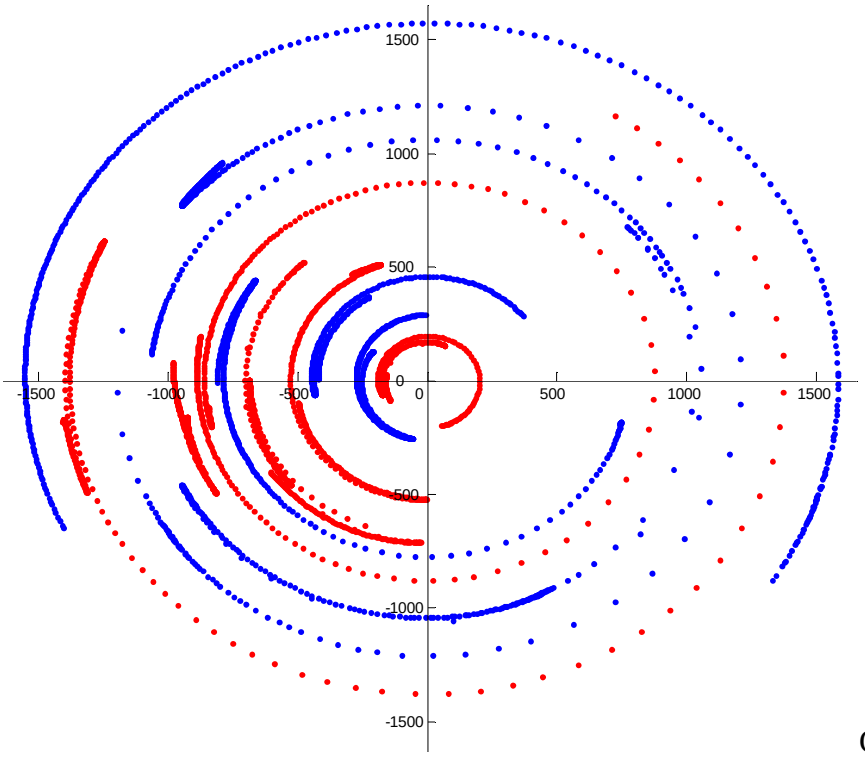

… workload 0
… workload 4

Channel 6 (Subject D trial 2)

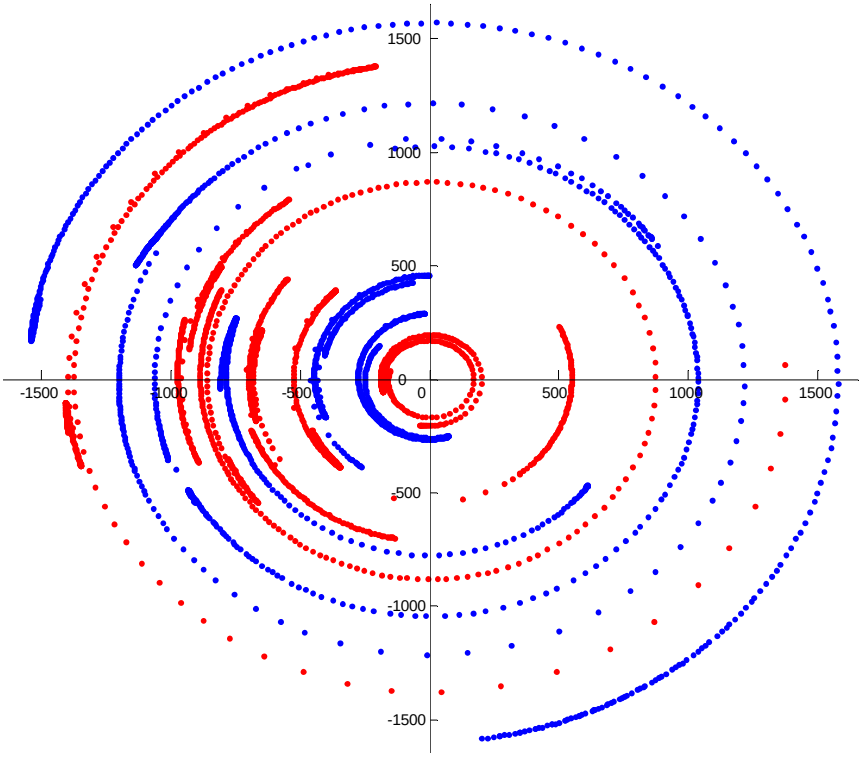

… workload 0
… workload 4

Channel 7 (Subject D trial 2)

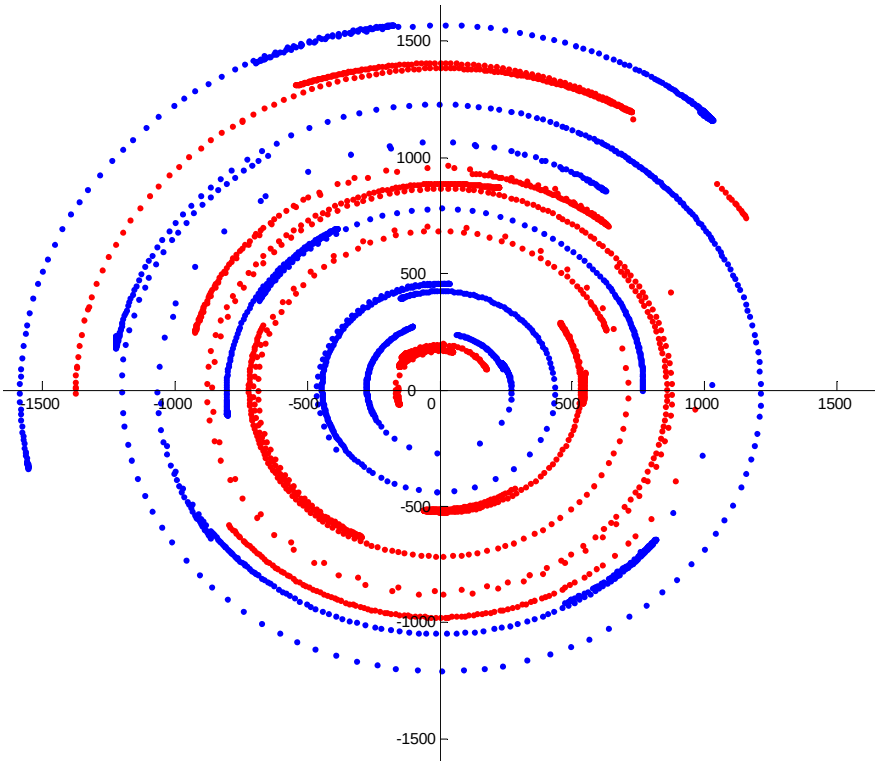

… workload 0
… workload 4

Channel 8 (Subject D trial 2)

Fig. 6.31. TARGET phase representation on rotating cube Subject D (trial 2).

In Fig. 6.31, we showed TARGET phase representation on rotating cube Subject D (trial 2) for all eight channels. Each phase point on the TARGET map relates to a time point data. The direction of the phase point equals to the phase value of the time point, and the radius of the phase point from the origin equals to the corresponding time value. Therefore x and y axis lower and upper limit are equal to the maximum time of experiment in seconds. The colors of the phase points represent the workloads: the blue and the red are workload 0 and workload 4 respectively.

The cloud or the cluster of the phase points may become one of the indicators of the physiological or metabolic states in human brain.

7. Discussion

From folding average results of Fig. 6.1 to Fig. 6.7, one can see that the rotating cube task did induce changes in the oscillations of $\Delta[Hb]$ and $\Delta[HbO]$ comparing with the workload 0 when subjects were at rest. The folding-average points that are significantly different from the initial baseline, according to the Dubey/Armitage-Parmar algorithm, are indicated by red color. In workload 0, all subjects, except subject C, show little significant difference from the baseline. Although $\Delta[Hb]$ and $\Delta[HbO]$ are not exactly flat in workload 0, the standard deviation are generally bigger than workload 4 and the trends are uncertain all over the channel. On the contrary, in workload 4, subject A, B, D (trial 1), and E show statistically significant concentration changes with an increase in $\Delta[HbO]$ and a decrease in $\Delta[Hb]$. Subject C performed workload 3 instead of workload 4, and the results show statistically significant changes in an opposite way: decrease in $\Delta[HbO]$ and increase in $\Delta[Hb]$. The possible reasons of this behavior were argued in a previous publication (Angelo et al, 2008). It is also interesting that subject C shows positive BOLD signal in rest but negative in rotating cube task, and the changes in rest and task are somehow inversed to each other. It suggests that subject C also had brain activity during the rest but acted as an opposite way during the task. Subject D (trial 2) didn't show clear significant difference in workload 4, however the increase in $\Delta[HbO]$ and the decrease in $\Delta[Hb]$ are much evident. On the other hand, in workload 0, subject D (trial 2) showed slight decrease in $\Delta[HbO]$ and increase in $\Delta[Hb]$ which are similar to subject C but opposite to himself in workload 4. For all the subjects, the $\Delta[HbO]$ and $\Delta[Hb]$ patterns are different from one channel to another channel suggest that these changes are due to localized cortex activities instead of global systematic changes. In finger tapping experiments, subject A showed the increase in $\Delta[HbO]$ and the decrease in $\Delta[Hb]$ with statistical significant difference to the baseline during

finger tapping task. Channel 5, 7, and 8 are located on the left motor cortex, so that they successfully detected significant deoxy- and oxy-hemoglobin changes stimulated by the right hand finger tapping. For those channels which didn't detect signals or were covered by hairs, the folding averages showed large standard deviation without statistical significant points. Based on folding average, we can say that we detected significant changes in deoxy- and oxy-hemoglobin, but if we want to know the physiological processes behind these changes and why there are changes and how they developed time after time, we have to rely on other data analysis methods, such as phase analysis.

Although cross-correlation phasor method and phase synchronization analysis method are two different methods, the results shown from Fig. 6.13 to Fig. 6.21 demonstrate that they yield similar results in phase calculation: not only the mean phase value but also the phase distributions are almost equivalent to each other. The circular histograms from Fig. 6.13 to Fig. 6.21 have big advantages over traditional histogram especially for those having angles around 180 degree or 0 degree. For convenience and validity in relatively broad bandpass filter, we discarded those points from phase distributions, of which frequency ratio in $\Delta[Hb]$ and $\Delta[HbO]$ are smaller than 2/3 or larger than 3/2. In the future, we might use more sophisticated way to deal with the frequency changes such as adaptive phase synchronization method which changes formula according to the n:m ratio as well as using very narrow bandpass filter to avoid dramatic frequency changes.

The numeric results of Fig. 6.13 to Fig. 6.21 are listed in Tab. 6.1. We can see that, for all the channels on the subjects in rotating cube and channel 5, 7 and 8 on subjects in finger tapping, the phase distributions in workload 0 and workload 4 are non-uniform based on the p-value of Rayleigh test ($p < 0.05$), which means that the phase values in our experiments are not random

noises which are uniform in the range of 0 to 2π in distribution. One point needs to be addressed is that the small resultant vector length doesn't necessarily suggest that the distribution is uniform. Taken workload 0 in channel 8 on Subject D (trial 1) for example, the resultant vector length is only 0.06, but in corresponding Fig. 6.17 (C) we can see that channel 8 still has two major phase bars around 225 degree and 315 degree but they are cancelled out by each other. And the whole distribution in channel 8 is not uniform around the circle.

The Watson-Williams circular statistical test is used to accept or reject the null hypothesis that each of the samples is drawn from a von Mises distribution, a circular analog to the normal distribution of linear data having the same mean value. The p-values of Watson-Williams test between workload 0 and workload 4 (workload 3 in Subject C) suggested that 55 out of 62 channels or 88.7% channels have significantly different average phase values between workload 0 and workload 4/3. The phase changes from workload 0 to workload 4 have been frequently observed in our experiments. During experiments, there are two different cerebral statuses from workload 0 to workload 4, which involve multiple physiological changes because of challenging task stimulus, such as blood volume increases, blood flow velocity increases and oxygen saturation increases etc. The changes of these physiological processes can be interplayed within a specific tissue region like the increase of blood flow induces the increase of blood volume or can be due to redistributed background hemoglobin concentration and/or saturation and in turn resulted in a change of the relative weights in the linear combinations of tissue phasors (see stimulated example). As a result, the phase difference from workload 0 to workload 4 would be observed.

In Fig. 6.16, Subject C shows similar phase distribution patterns between workload 0 and workload 3. Also in Tab 6.1, although p-values obtained when we applied the Watson-Williams

test are less than 0.05 in 6 channels, the average phase values between workload 0 and workload 3 are pretty close. This may be because the workload 3 rotating cube test is relative easy to Subject C. In fact, Subject C gave all correct answers. If the experiment is too easy for the subject, there won't be significant changes in physiological processes in subject's cognitive cortex. Although in folding average, we observed statistical changes in hemoglobin in workload 3 in subject C, we can't separate the workload 0 and workload 3 in phase difference of deoxy- and oxy- hemoglobin.

Except for Subject C and those channels with $p>0.05$ for the Watson Williams test, 5/7 or 71.4% of Subject A (trial 2), 6/7 or 85.7% of Subject D (trial 1) and 5/7 or 71.4% of Subject D (trial 2) have counter-clockwise mean phase value shift from workload 4 to workload 0 (or larger mean phase value in workload 4 than workload 0 in the range of 0 to 2π). On the contrary, 7/8 or 87.5% of Subject B and 5/7 or 71.4% of Subject E have clockwise mean phase value shift from workload 0 to workload 4. For Subject A (trial 1); these two possible outcomes are almost equiporbable. These results suggest that the change direction of average phase value or the phasor from workload 0 to workload 4 depends on subjects. This global phase shift may be resulted from characteristic physiological processes from different subjects. The reason why sometimes phase shifts are clockwise while sometimes counter-clockwise remains unknown so far. It is required further investigation. In finger tapping experiments, the average phase values are difficult to compare due to the relatively small resultant vector length.

The standard deviation of phase distribution describes the phase spread on the phase circle. It is inversely changed to the resultant vector length. In our experiments, Subject A (trial 2), Subject D (trial 1 and 2) and Subject E respectively showed 6/8, 7/8, 6/8, and 6/8 of channels having smaller phase standard deviation in workload 4 than in workload 0. These subjects have a

concentrated mental efforts and in turn relatively narrower phase oscillation range in workload 4 than in workload 0 which suggested that the rotating cube task might force the physiological processes in cognitive cortex more regular than those in the rest. Subject A (trial 1), Subject B and Subject C showed 3/8, 4/8 and 4/8 of channels having smaller standard deviation in workload 4 than in workload 0. These suggested that during these experiments the subjects might have more complicated physiological processes than others whose standard deviations of most channels in workload 4 are smaller than in workload 0. The more complicated the processes may cause the phase shifts spread in a wider angular range.

One point needed to be addressed is that Watson-Williams test is parametric while a non-parametric test should be more suitable to our experiments. Comparing p-value of Watson-Williams test and the figures of phase-distribution in Fig. 6.13 to Fig. 6.21, in those cases where we can't separate average phase values of workload 0 and workload 4 by naked eyes, Watson-Williams returns $p < 0.05$, which means we might reject the null-hypothesis when it should not have been rejected - type I error by using Watson-Williams test. In the future, we should further develop a modified circular statistical test analog to ANOVA test to avoid possible type I errors.

The Fig. 6.31 is a novel way to present the phase changes time by time during the experiment. Using phase points in different colors to represent different mental workloads, we can clearly see if the phase shift shows preferential directions in specific mental workloads. The cloud or the cluster of phase points may suggest a possible physiological status in the cerebral cortex. In Fig. 6.31, the phase points are much denser in second and third quadrants instead of the first and fourth quadrants, which matched our phase circular histograms in Fig. 6.18. With an animation we can show how those phase points moving on the coordinates in TARGET map, and this may provide a way to understand how human cerebral cortex responds to the different mental

workloads and how the physiological processes shift from one stage to another stage. The Matlab code for generating such animated maps is written in appendix. Nevertheless, the shortcoming of the TARGET map is that for long time experiment, the far phase points look like much sparser even though they have similar distribution as near phase points.

8. Conclusion and Future Direction

In this thesis, we reported phase analysis methods used in near-infrared spectroscopy. We suggested that the phase analysis has the potential in understanding the cerebral autoregulation, functional connectivity and underlying physiological processes in human brains. Two approaches were adopted to get the phase difference between deoxy- and oxy-hemoglobin. One is the cross-correlation phasor method; another is phase synchronization analysis method. Both methods produced similar results during two brain challenges: a) the rotating cube and b) the finger tapping tests. Instead of traditional statistical method, we used circular statistical test and methods to analyze phase distribution such as mean phase value, resultant vector length, circular standard deviation, Rayleigh test for uniformity and Watson-Williams test analog to ANOVA test. We developed circular histogram and novel phase-sector maps to represent the phase distribution in different mental workloads. Based on Watson-Williams test, for most subjects, there are phase shifts from workload 0 to workload 4, either counter-clockwise or clockwise, which may be resulted from the physiological processes change in cerebral cortex stimulated by the mental task. In most cases (Tab. 6.1), the standard deviation of phases in workload 4 is lower than those in workload 0 which may suggest that the mental tasks are going to regulate the physiological activities and in turn narrow the phase oscillations during workload 4 with respect to rest. The TARGET map was first introduced here to shed light on the future research to use it as a method to monitor the physiological evolution in a movie format.

For future studies we need to: first, improve instruments. In order to investigate the LFO on brain-autoregulation or functional connectivity, we have to perform the experiments on the subjects in a long time rest or sleeping status to rule out the effects of outcome stimulus. Also it

is needed a much higher resolution whole head helmet with large number of source-detector pairs for functional connectivity studies. Second, we need to try different filters bandwidths. For this study we used relatively broad filter with a band of 0.05 to 0.10 Hz. The filtered signals show matched oscillations around LFO in original signals. However, both the phasor and PSI methods require the frequencies of both filtered signals cannot be too big. In current studies, we used a 20 sec window that includes a few oscillations of hemodynamic signals and assume that within this 20 sec window the frequency between deoxy- and oxy- hemoglobin oscillations is comparable ($2/3 < f_1/f_2 < 3/2$). In the future, there are two possible ways to solve this problem: one is to use many narrow filters which pass band are 0.01 Hz or less. The summation of all these narrow filters is equivalent to the frequency band of LFO; another approach is to use adaptive algorithms to calculate PSI phase based on the specific n:m ratio, while for phasor method we need a cross-correlation calculation to adapt signals in different frequencies. Third is the experimental protocol, in our studies, we have already observed that for some subjects like subject C the mental tasks were easier. In this case, the task that induces big hemodynamic changes in subject A might affect little on subject C. We need to develop new adaptive mental workloads to adjust the difficulty of workload based on the feedback of the subject, such as increase counted colors or decrease of cube static time to make the task more difficult.

All in all, the analysis methods reported in the thesis could lead to a better characterization of cerebral hemodynamics, to provide opportunities for understanding the physiological origin of near-infrared signals and to a more sophisticated approach to the optical study of neurovascular coupling effects.

References

Aaslid, R., Lindegaard, K.F., Sorteberg, W., Nornes, H., 1989, Cerebral autoregulation dynamics in humans, 20: 45-52

Biswal B B, Hudetz A G. 1995. Synchronous oscillations in cerebrocortical capillary red blood cell velocity after nitric oxide synthase inhibition. Microvasc Res, 52: 1－12

Biswal, B., Yetkin, F.Z., Haughton, V.M., Hyde, J.S., 1995. Functional connectivity in the motor cortex of resting human brain using echo-planar MRI., Magnetic Resonance in Medicine, 34 (4): 537-541

Boashash, B. 1992. Estimating and Interpreting the Instantaneous Frequency of a Signal-part 1: fundamentals, Proceedings of the IEEE, 80(4), 520-538

Brady, K.M., Lee, J.K., Kibler K.K., Easley, R.B., Koehler, R.C., Shaffner, D.H., 2008, continuous measurement of autoregulation by spontaneous fluctuations in cerebral perfusion pressure: comparison of 3 methods, Stroke, 39(9): 2531-2537

Bressler, S.L. 2001, Cortical coordination dynamics and cognition. Trends in Cognitive Sciences, 5, 26-36

Chance, B., Zhuang, Z., UnAh, C., Alter, C., Lipton, L., 1993. Cognitionactiveated low-frequency modulation of light absorption in human brain. Proc. Natl. Acad. Sci. U.S.A. 90 (8), 3770-3774

Colantuoni A, Bertuglia S, Intaglietta M. 1994. Microvascular vasomotion: Origin of laser Doppler flux motion. Int J Microcirc, 14: 151－ 158

Cooley R L, Montano N, Cogliati C, et al. 1998. Evidence for a central origin of the low-frequency oscillation in RR-interval variability. Circulation, 98: 556－561

Corders, D., Haughton, V.M., Arfanakis, K., Carew, J.D., Turski, P.A., Mortz, C.H., Quigley, M.A., Meyerand, M.E., 2001. Frequencies contributing to functional connectivity in the cerebral cortex in “resting-state” data. Am. J. Neuroradiol. 22 (7), 1326-1333.

Dawson, S.L., Panerai, R.B., 2000, Dynamic but not static cerebral autoregulation is impaired in acute ischemic stroke, Cerebravasc. Dis. 10: 126-132

Diehl R R, Linden D, Lucke D, et al. 1995. Phase relationship between cerebral blood flow velocity and blood pressure. Stroke, 26: 1801－1804

Diehl, R.R., Diehl, B., Sitzer, M., Hennerici, M., 1991. Spontaneous oscillations in cerebral blood flow velocity in normal humans and in patients with carotid artery disease. Neurosci. Lett. 127 (1), 5-8

Diehl, R.R., Linden, D., Lucke, D., Berlit, P., 1998. Spontaneous blood pressure oscillations and cerebral autoregulation. Clin Auton. Res. 8(1), 7-12

Elwell C E, Springett R, Hillman E, et al. 1999. Oscillations in cerebral haemodynamics, implications for functional activation studies. Adv Exp Med Biol, 471: 57－65

Fagrell B, Intaglietta M, Ostergren J. 1980. Relative hematocrit in human skin capillaries and its relation to capillary blood flow velocity. Microvasc Res, 20: 327－335

Fantini, S. 2002. A haemodynamic model for the physiological interpretation of in vivo measurements of the concentration and oxygen saturation of haemoglobin. Phys. Med. Biol. 47. N249-N257

Fantini, S. and Franceschini, M.A. 2002. Frequency-Domain Techniques for Tissue Spectroscopy and Imaging. In Handbook of Optical Biomedical Diagnostics, V.V. Tuchin, Ed., (SPIE Press, Bellingham, WA), Chapter 7, pp, 405-453

Feng, S., Zeng, F.A., Chance, B., 1995, Photon migration in the presence of a single defect: a perturbation analysis, Applied Optics, 34 (19) 3826-3837

Finnerty, F.A.Jr., Witkin, L., Fazekas, J.F., 1954. Cerebral hemodynamics during cerebral ischemia induced by acute hypotension. J. Clin. Invest. 33: 1227-1231

Fisher, N.I. 1995. Statistical Analysis of Circular Data. Cambridge University Press.

Fog, M. 1937. Cerebral circulation: the reaction of the pial arteries to a fall in blood pressure. Arch Neurol Psych. 37: 351-364

Fox, M.D., Snyder, A.Z., Zacks, J.M. and Raichle, M.E., 2006, Coherent spontaneous activity accounts for trial-to-trial variability in human evoked brain responses., Nature Neuroscience, 9(1): 23-25

Franceschini, M.A., Joseph, D.K., Huppert, T.J., Diamond, S.G., Boas, D., 2006, Diffuse optical imaging of the whole head, J. Biomed. Opt. 11(5), 054007

Friston, K.J., 1993, Functional connectivity: the principal-component analysis of large (PET) data sets. Journal of Cerebral Blood Flow and Metabolism, 13, 5-14.

Friston, K.J., 1994, Functional and effective connectivity in neuroimaging: A synthesis. Human Brain Mapping, 2, 56-78

Golanov, E.V., Yamamoto, S., Reis, D.J., 1994. Spontaneous waves of cerebral blood flow associated with a pattern of electrocortical activity. Am. J. Physiol. 226 (1 Pt. 2), R204-R214.

Greicius M D, Srivastava G, Reiss A L, et al. Default-mode network activity distinguishes Alzheimer's disease from healthy aging: Evidence from functional MRI. Proc Natl Acad Sci USA, 2004, 101: 4637－4642

Guyton, A.C., Hall, J.E., 2000. The Textbook of Medical Physiology, 10th ed. W. B. Sunders Company, Philadelphia (Chapter 61)

Hudetz AG, Biswal BB, Shen H, Lauer KK, Kampine JP 1998 Spontaneous fluctuations in cerebral oxygen supply. In: Oxygen transport to tissue XX (Hudetz AG, Bruley DF, eds), New York: Plenum Press, 551–9

Katura, T., Tanaka, N., Obata, A., Sato, H., and Maki, A., 2006. Quantitative evaluation of interrelations between spontaneous low-frequency oscillations in cerebral hemodynamics and systemic cardiovascular dynamics. NeuroImage. 31. 1592-1600

Kety, S.S., Schmidt, C.F. 1948. The effects of altered arterial tensions of carbon dioxide and oxygen on cerebral blood flow and cerebral oxygen consumption of normal young men. J. Clin. Invest. 27: 484-492

Kuo, T.B., Chern, C.M., Yang, C.C., Hsu, H.Y., Wong, W.J., Sheng, W.Y., 2003, Mechanisms underlying phase lag between systemic arterial blood pressure and cerebral blood flow velocity, Cerebrovasc. Dis. 16 (4), 402-409

Lassen, N.A., 1974. Control of cerebral circulation in health and disease. 6: 749-760

Laufs H, Krakow K, Sterzer P, et al. 2003. Electroencephalographic signatures of attentional and cognitive default modes in spontaneous brain activity fluctuations at rest. Proc Natl Acad Sci USA, 100: 11053－11058

Livera, L.N., Wickramasinghe, Y.A., Spencer, S.A., Rolfe, P., Thorniley, M.S., 1992. Cyclical fluctuations in cerebral blood volume, Arch. Dis. Child 67 (Spec. No. 1), 62-63

Mayer, S., 1876. Studien zur physiologie des herzens und blutgeflaesse V. Ueber spontane blutdruckschwankungen. Akad. Wis. Wien. Math. Nat. Kl. 74, 281-307

Mayhew, J.E., Askew, S., Zheng, Y., Porrill, J., Westby, G.W., Redgrave, P., Rector, D.M., Harper, R.M., 1996. Cerebral vasomotion: a 0.1 Hz oscillation in reflected light imaging of neural activity

Obrig, H., Neufang, M., Wenzel, R., Kohl, M., Steinbrink, J., Einhaupl, K., Villringer, A., 2000. Spontaneous low frequency oscillations of cerebral hemodynamics and metabolism in human adults. NeuroImage 12 (6), 623-639.

Ogawa, S., Lee, T.M., Nayak, A.S., and Glynn, P., 1990. Oxygenation-sensitive contrast in magnetic resonance image of rodent brain at high magnetic fields, Magnetic Resonance in Medicine, 14: 68-78

Paulson, O.B., Strandgaard, S., Edvinson, L., 1990. Cerebral autoregulation. Cerebrovasc. Brain.

Metab. Rev. 2: 161-191

Rangel-Castilla, L. Gasco, J., Nauta H.J., Okonkwo, D.O., Robertson, C.S., 2008, Cerebral pressure autoregulation in traumatic brain injury, Neur. Focus., 25(4): E7

Reinhard, M., Wehrle-Wieland, E., Grabiak, D., Roth, M., Guschlbauer, B., Timmer, J., Weiller, C., Hetzel, A. 2006. Oscillatory cerebral hemodynamics-the macro- vs. microvascular level. J. Neurological. Sci. 250, 103-109

Sassaroli, A., Zheng, F., Hirshfield, L.M., Girouard, A., Solovey, E.T., Jacob, R. and Fantini, S., 2008, Discrimination of mental workload levels in human subjects with functional near-infrared spectroscopy, 1(2), 1-11

Sato, H., Kiguchi, M., Kawaguchi, F., Maki, A., 2004. Practicality of wavelength selection to improve signal-to-noise ratio in near-infrared spectroscopy. NeuroImage 21 (4), 1554-1562

Siebenthal, K., Beran, J., Wolf, M., Keel, M., Dietz, V., Kundu, S., Bucher, H.U., 1999. Cyclical Fluctuations in Blood Pressure, Heart Rate and Cerebral Blood Volume in Preterm Infants. Brain Dev. 21 (8), 529-534

Singer, W., and Gray, C.M., 1995, Visual feature integration and temporal correlation hypothesis, Annual Reviews of Neuroscience 18, 555-586

Spitzer M W, Calford M B, Clarey J C, et al. 2001. Spontaneous and stimulus-evoked intrinsic optical signals in primary auditory cortex of the cat. J Neurophysiol, 85: 1283－1298

Steiner, L.A., Pfister, D., Strebel, S.P., Radolovich, D., Smielewski, P.,Czosnyka, M., 2008, Near-infrared spectroscopy can monitor dynamic cerebral autoregulation in adults, Neurocrit Care, 10(1): 122-128

Taga, G., Konishi, Y., Maki, A., Tachibana, T., Fujiwara, M., Koizumi, H., 2000, Spontaneous oscillation of oxy- and deoxy- hemoglobin changes with a phase difference throughout the occipital cortex of newborn infants observed using non-invasive optical topography, Neuroscience Letters, 282, 101-104

Tass, P., Rosenblum, M.G., Weule, J., Kurths, J., Pikovsky, A., Volkmann, J., Schnitzler, A., and Freund, H.J., 1998, Detetion of n:m Phase Locking from Noisy Data: Application to Magnetoencephalography, Phys.Rev.Lett. 81(15), 3291-3294

Tiecks, F.P., Lam, A.M., Aaslid R., et al, 1995, Comparison of static and dynamic cerebral autoregulatory measurements, Strokes, 26: 1014-1019

Tomita M, Gotoh F, Sato T, et al. 1981. 4-6 cycle per minute fluctuation in cerebral blood volume of feline cortical tissue in situ. J Cereb Blood Flow Metab, 1: 443－444

Tononi, G., and Edelman, G.M., 1998, Consciousness and complexity, Science, 282, 1846-1851

Toronov, V., Franceschini, M.A., Filiaci, M., Fantini, S., Wolf, M., Michalos, A., and Gratton, E., 2000, Near-infrared study of fluctuations in cerebral hemodynamics during rest and motor stimulation: Temporal analysis and spatial mapping, Med.Phys. 27(4), 801-815

Urbano, F., Roux, F., Schindler, J., Mohsenin, V., 2008, Impaired cerebral autoregulation in obstructive sleep apnea, J. Appl. Physiol. 105(6): 1852-1857

Wise R G, Ide K, Poulin M J, et al. 2004. Resting fluctuations in arterial carbon dioxide induce significant low frequency variations in BOLD signal. NeuroImage, 21: 1652－1664

Wolf, M., U. Wolf, V. Toronov, A. Michalos, L. A. Paunescu, J. H. Choi, and E. Gratton, 2002, "Different time evolution of oxyhemoglobin and deoxyhemoglobin concentration changes in the visual and motor cortices during functional stimulation: A near-infrared spectroscopy study," Neuroimage 16, 704-712.

Zeff, B.W., White, B.R., Dehghani, H., Schlaggar, B.L., Culver, J.P., 2007, Retinotopic mapping of adult human visual cortex with high-density diffuse optical tomography, PNAS, 104(29), 12169-12174

Zheng, F, Sassaroli, A., Fantini, S. 2010. Phasor representation of oxy- and deoxyhemoglobin conecntrations: what is the meaning of out-of-phase oscillations as measured by near-infrared spectroscopy. J. Biomed. Opt. Lett. 040512

Zilles K, Wree A. 1985. Cortex: Areal and laminar structure. The Rat Nervous System, vol 1: Forebrain and Midbrain. Sydney: Academic Press. 375－415

Appendix

Main Function ==========

```
clear all;
close all;
clc;

% === copyright @ Feng Zheng Tufts 2010 ===
% this the main function for data processing including phasors
% generate figures of phasors and traditional histograms
% contact via Feng.Zheng@tuft.edu
% first version Nov 4, 2010
%
[FileName,PathName] = uigetfile('*.txt','Please select the .txt file...');
[data, physio] = fz_preprocessData(FileName, PathName);
fs = 6.25;
fid=fopen(strcat(PathName, FileName, '.set'),'rb', 'ieee-be');
r = str2num(fgetl(fid));
dc690 = data(:,str2num(fgetl(fid)));
dc830 = data(:,str2num(fgetl(fid)));
setting_physio = str2num(fgetl(fid));
disp('* SETTING DATA LOADED *');
fclose(fid);
% default physiology sequence is: Heart Rate, Respiration, Pulse
if setting_physio(1) == 0
   rate = [];    resp = [];    pulse = [];
else
   rate = physio(:,setting_physio(1)) ;
   resp = physio(:,setting_physio(2)) ;
   pulse = physio(:,setting_physio(3));
end
timemat = data(:,1);
[M, N] = size(dc690);
aux0 = data(:,3);
aux0 = fz_auxstatus(aux0, PathName);
list0 = find(aux0 ~= 0);
list1 = find(aux0 == 1);    % workload 0
list2 = find(aux0 == 2);    % workload 2, light challenge
list3 = find(aux0 == 3);    % workload 3, middle challenge
list4 = find(aux0 == 4);    % workload 4, intense challenge
list5 = find(aux0 == 5);    % workload 5, physical challenge
list6 = find(aux0 == 6);    % rest
mi = max(list0(1)-600, 1); ma = list0(1);
mean1 = mean(dc690(mi:ma,:),1);
mean2 = mean(dc830(mi:ma,:),1);
dpf1=6.51; % 690 nm
dpf2=5.86; % 830 nm
mua1 = log((ones(M,1)*mean1)./dc690);      % intensity change in 690nm
mua2 = log((ones(M,1)*mean2)./dc830);      % intensity change in 830nm
k_mat = repmat(r,M,1);
abs690=mua1./(dpf1*k_mat);         % absorption change in 690nm
```

```
abs830=mua2./(dpf2*k_mat);          % absorption change in 830nm
% calculation oxy & deoxy
value1 = input('Calculate HbO&Hb (y) or NOT (n)  ','s');
if strcmp(value1,'y');
   eo1=0.956; % extinction coefficient of HbO mM^-1xcm^-1 (690 nm)
   eo2=2.333; % extinction coefficient of HbO mM^-1xcm^-1 (830 nm)
   ed1=4.854; % extinction coefficient of Hb mM^-1xcm^-1 (690 nm)
   ed2=1.791; % extinction coefficient of Hb mM^-1xcm^-1 (830 nm)
   den=eo1*ed2-eo2*ed1;
   HbO = (abs690*ed2-abs830*ed1)/den*1000; % concentration change (micromolar)
   Hb = (abs830*eo1-abs690*eo2)/den*1000;  % concentration change (micromolar)
else
   HbO = abs690;
   Hb = abs830;
end
HbOp = polydetrend(HbO, timemat, 3);        % polynomial detrend for HbO
Hbp = polydetrend(Hb, timemat, 3);                    % polynomial detrend for Hb
value11 = input('Show folding average (y) or NOT (n)  ', 's');
if strcmp(value11, 'y');
   foldingAverage(HbOp, Hbp, list0, list4);
end
lf = input('Please input the lower bound of frequency:   ');
hf = input('Please input the higher bound of frequency:   ');
value2 = input('Which filter do you prefer (1) ellip or (2) cheby1 (protocol freq):  ');
value3 = input('Phasor final (1) or graphsPhasor sequence (2):   ');
if value2 == 1
   str = 'ellip';
elseif value2 == 2
   str = 'cheby1';
else
   error('NO SUCH OPTION');
end
figure(111) % draw the frequency response
psifilter([], str, lf, hf); % show the frequency response of the filter
HbOf = psifilter(HbOp, str, lf, hf);   % filter the HbO
Hbf = psifilter(Hbp, str, lf, hf);                  % filter the Hb
psiangle = angle(hilbert(Hbf)./hilbert(HbOf));
period_HbO = sponperiod(HbOf); % calculate the instantaneous period on HbO
period_Hb = sponperiod(Hbf);   % calculate the instantaneous period on Hb
clear data HbOp Hbp mua1 mua2 abs690 abs830 k_mat str;
%% protocol frequency
if value3 == 2
       % draw the phasor movie if user asked for
       drawPhasorSequence(HbO,Hb,HbOf,Hbf,psiangle,period_HbO,period_Hb,list0,timemat);
else
   %% LFO frequency
wlen = input('Please input the time window length (in sec)   ');
phase_mat = zeros(M, N);    % phase calculated by psi method
psi_mat = zeros(M, N);      % corresponding psi value
phase_corr = zeros(M, N);   % phase calculated by phasor method
corr_mat = zeros(M, N);     % corresponding crosscorrelation value
for i = 1: M
   [winlow, winhigh] = windowcut(i, wlen, M);
   for ch = 1: N
      [psi_mat(i,ch), phase_mat(i,ch)] = fpsi_mov(psiangle(winlow:winhigh,ch),(lf+hf)/2,1,0);
```

```
        [corr_mat(i,ch),phase_corr(i,ch)] =
phasor_calc(HbOf(winlow:winhigh,ch),Hbf(winlow:winhigh,ch),period_Hb(i,ch),1);
    end
end
phase_corr = 180*phase_corr/pi; % phase_mat and phase_corr are in range of 0 to 360 degree
% ========================================================================
% ================  END OF PHASE CALCULATION ============================
% ========================================================================
baseline_pt = dividetrace(list0, [], M);
wkl4_pt = dividetrace(list0, list4, M);  % extract the points of workload4
wkl0_pt = dividetrace(list0, list1, M);  % extract the points of workload0
if N > 8
    q = 5;
else
    q = 4;
end
p = ceil(N/q);
for ch = 1: N
% draw phase distribution histgram (psi method)
    figure(11)
    subplot(p,q,ch)
    drawhistsingle_periodJudge(wkl0_pt,ch,phase_mat,period_Hb,period_HbO);
    figure(12)
    subplot(p,q,ch)
    drawhistsingle_periodJudge(wkl4_pt,ch,phase_mat,period_Hb,period_HbO);
% draw pie chart (psi method)
    figure(13)
    subplot(p,q,ch)
    phasor_periodJudge(wkl0_pt,wkl4_pt,ch,phase_mat,period_Hb,period_HbO);
% draw phase distribution histgram (phasor method)
    figure(21)
    subplot(p,q,ch)
    drawhistsingle_periodJudge(wkl0_pt,ch,phase_corr,period_Hb,period_HbO);
    figure(22)
    subplot(p,q,ch)
    drawhistsingle_periodJudge(wkl4_pt,ch,phase_corr,period_Hb,period_HbO);
% draw pie chart (phasor method)
    figure(23)
    subplot(p,q,ch)
    phasor_periodJudge(wkl0_pt,wkl4_pt,ch,phase_corr,period_Hb,period_HbO);
end

end
```

Data Preprocess Function ==========

```
function [data, aux] = fz_preprocessData(FileName,PathName)
%FZ_PREPROCESSDATA is used to pre-process the experimental data and fetch the auxiliary data as well as
markers files.
% === copyright (c) Feng Zheng === 2011
% preprocess the iss data to remove header, process markers
% return pure data and auxillary channels, if any;
% first column of aux: heart rate
% second column of aux: respiration
% third column of aux: pulse
%
% fs = 6.25Hz
%
NirsFile = strcat(PathName, FileName);
fid=fopen(NirsFile,'rb', 'ieee-be'); % expects big-endian
% Remove the header
target= '#';
tline = fgetl(fid);
if strcmp(tline(1:4),'BOXY')    % ISS data
   data = [];
   ii = 0;
   while (~strcmp(tline, '#DATA BEGINS'))% remove the header of ISS file
      tline = fgetl(fid);
   end
   tline = fgetl(fid);
   tline = fgetl(fid);
   tline = fgetl(fid);
   while not (isequal(tline(1,1),target))
      data = [data;str2num(tline)];
      ii = ii + 1;
      clc;
      fprintf('NIRS DATA READ LINE %d',ii);
      tline = fgetl(fid);
   end
   fprintf('\n');
   fclose(fid);
   disp('* NIRS DATA HAS BEEN READ *');
   M = size(data,1);
   data(:,1) = 0:0.16:0.16*(M-1);
else
   fclose(fid);
   data = load(NirsFile);
end
if (data(1,3) == 1)
   data(:,3) = [];
end
if (data(1,end) == 255)
   data(:,end) = [];
end
aux = data(:,end-3:end);
```

Markers Process Function ==========

```
function aux_out = fz_auxstatus(aux_in, PathName )
%       FZ_AUXSTATUS function is used to transfer incremental markers into meaningful markers depends on
insequence.txt file
% input variables:
%                   aux_in: the markers ready for redefined
%                   PathName: the directory stored the insequence.txt file
% output variables:
%                   aux_out: the redefined markers, numbers are defined as wkl level
% Feng Zheng @ Tufts 2011
%
markersFile = strcat(PathName, 'insequence.txt');
markers = load(markersFile);
allindx = find(aux_in~=0);
nAux = length(allindx);
nMarkers = length(markers);
if nAux == 2*nMarkers+1
   nAux = nAux - 1;
   aux_in(allindx(end)) = 0;
   allindx(end) = [];
elseif nAux == 2*nMarkers
   1;
else
   error('<< INCORRECT INSEQUENCE.TXT >> ');
end
aux_out = zeros(size(aux_in));
if isempty(find(markers==4, 1))
   markers(markers==3) = 4;
end
if isempty(find(markers==1, 1))
   flag = true;
else
   flag = false;
end
i = 1;
j = 1;
while (i <= nAux)
   aux_out(allindx(i)) = markers(j);
   i = i + 1;
   if flag
      aux_out(allindx(i)) = 1;
   else
      aux_out(allindx(i)) = 6;
   end
   i = i + 1;
   j = j + 1;
end
```

Filter Function ==========

```
function y = psifilter(x, str, lf, hf)
%          psifilter function is used to pack different filters into one single function file for future usage
% Feng Zheng @ Tufts 2011
if nargin == 1
   str = 'fircls';
   disp('FIR-CLS bandpass filter has been used');
elseif nargin > 4 || nargin < 1
   error('No more than 4 input arguments needed');
else
end

if strcmp(str,'fircls') == 1
   Fs = 6.25;                  % Sampling Frequency
   N      = 50;      % Order
   Fc1    = lf;      % First Cutoff Frequency
   Fc2    = hf;      % Second Cutoff Frequency
   Dstop1U = 3;               % Upper Stopband Attenuation
   Dstop1L = 3;               % Lower Stopband Attenuation
   DpassU  = 30;              % Upper Passband Ripple
   DpassL  = 30;  % Lower Passband Ripple
   Dstop2U = 3;               % Upper Stopband Attenuation
   Dstop2L = 3;               % Lower Stopband Attenuation
   % Calculate the coefficients using the FIRCLS function.
   b  = fircls(N, [0 Fc1 Fc2 Fs/2]/(Fs/2), [0 1 0], [Dstop1U 1+DpassU ...
      Dstop2U], [-Dstop1L 1-DpassL -Dstop2L]);
   if isempty(x)
      freqz(b,1,512,Fs);
   else
      y = filter(b,1,x);
   end
elseif strcmp(str, 'movingaverage') == 1
   flp = hf;
   fs = 6.25;
   rate= fs;
   wwid = floor(rate / flp);
   b = ones(wwid,1)/wwid;
   a = 1;
   ma1L = filtfilt(b, a, x);
   %
   %lower frequency
   fhp = lf;
   a_wwid = floor(fs / fhp);
   a_b = ones(a_wwid,1)/a_wwid;
   a_a = 1;
   ma1H = filtfilt(a_b, a_a, x);
   y = ma1L - ma1H; % filtered absorption changes
elseif strcmp(str, 'ellip') == 1
   fs = 6.25;
   fhp = hf; flp = lf;
   wp = [flp fhp]/(fs/2);
   if lf == 0.05
      ws(1) = lf-0.01; ws(2) = hf+0.01;
```

```
        rp = 1; rs = 30;
    else
        ws(1) = lf-0.001; ws(2) = hf+0.001;
        rp = 1; rs = 40;
    end
    ws = ws/(fs/2);
    [nn,wn] = ellipord(wp,ws,rp,rs);
    [bbb,aaa] = ellip(nn,rp,rs,wn);
    if isempty(x)
        freqz(bbb,aaa,512,fs);
    else
        y = filtfilt(bbb,aaa,x);
    end
elseif strcmp(str, 'cheby1') == 1
    fs = 6.25;
    %CHEBY FILTER:
    %How to make a cheby pass band:
    Wp = 0.01/(fs/2); Ws = 0.02/(fs/2);
    Rp = 1; Rs = 40;
    [n,Wp] = cheb1ord(Wp,Ws,Rp,Rs);
    [e,f] = cheby1(n,Rp,Wp);
    if isempty(x)
        freqz(e,f,512,fs);
    else
        y = filtfilt(e,f,x);
    end
else
    error('wrong input string');
end
```

Polynomial Detrend Function ==========

```
function out = polydetrend( in, t, n )
%POLYDETREND function is used to detrend the input data by polynomial fitting
% Feng Zheng @ Tufts 2011
out = zeros(size(in));
col = size(in, 2);
for i = 1: col
   p = polyfit(t, in(:,i), n);
   out(:,i) = in(:,i) - polyval(p, t);
end
```

Instantaneous Period Function ==========

```
function period = sponperiod (signal)
% This function is used to calculate the instantaneous period
[M, N] = size(signal);
yh = hilbert(signal);  period = zeros(size(signal));
for j = 1: N
   for i = 1: M-1
      anglediff = angle(yh(i+1,j))-angle(yh(i,j));
      while anglediff > 2*pi
         anglediff = anglediff - 2*pi;
      end
      while anglediff < 0
         anglediff = anglediff + 2*pi;
      end
      period(i,j) = 1/((1/(2*pi))*(anglediff/0.16));
   end
   period(i+1,j) = period(i,j);
   clear i;
end
```

Extracting Workload Trial Function ==========

```
function x = dividetrace(list0, list, datalength)
% extract specified workload (list) points in the whole data trace
% list0 is the whole markers
% list is the specified workload markers
% datalength is size(data,1) in MAIN function
% Feng.Zheng @ Tufts. edu
if isempty(list)
   x = 1:(list0(1)-1);
else
   x = [];
   for i = 1: length(list)
      k = find(list0 == list(i));
      if k == length(list0)
         k1 = min(datalength, list0(k)+list0(k-1)-list0(k-2)+1);
         x = [x list0(k):k1];
      else
         x = [x list0(k):list0(k+1)-1];
      end
   end
end
```

Arrow Plot Function ==========

```
function handles = plot_arrow( x1,y1,x2,y2,varargin )
% plot_arrow - plots an arrow to the current plot
%
% format:   handles = plot_arrow( x1,y1,x2,y2 [,options...] )
%
% input:    x1,y1   - starting point
%           x2,y2   - end point
%           options - come as pairs of "property","value" as defined for
%                     "line" and "patch"
% additional options are:
%  'headwidth':  relative to complete arrow size, default value is 0.07
%  'headheight': relative to complete arrow size, default value is 0.15
% output:   handles - handles of the graphical elements building the arrow
%
% Example:  plot_arrow( -1,-1,15,12,'linewidth',2,'color',[0.5 0.5 0.5],'facecolor',[0.5 0.5 0.5] );
%           plot_arrow( 0,0,5,4,'linewidth',2,'headwidth',0.25,'headheight',0.33 );
%           plot_arrow;   % will launch demo
if (nargin==0)
   figure;
   axis;
   set( gca,'nextplot','add' );
   for x = 0:0.3:2*pi
      color = [rand rand rand];
      h = plot_arrow( 1,1,50*rand*cos(x),50*rand*sin(x),...
         'color',color,'facecolor',color,'edgecolor',color );
      set( h,'linewidth',2 );
   end
   hold off;
   return
end
alpha      = 0.15;   % head length
beta       = 0.07;   % head width
max_length  = 22;
max_width   = 10;
if ~isempty( varargin )
   for c = 1:floor(length(varargin)/2)
      try
         switch lower(varargin{c*2-1})
            % head properties - do nothing, since handled above already
         case 'headheight',alpha = max( min( varargin{c*2},1 ),0.01 );
         case 'headwidth', beta = max( min( varargin{c*2},1 ),0.01 );
         end
      catch
         fprintf( 'unrecognized property or value for: %s\n',varargin{c*2-1} );
      end
   end
end
% calculate the arrow head coordinates
den        = x2 - x1 + eps;                        % make sure no devision by zero occurs
teta       = atan( (y2-y1)/den ) + pi*(x2<x1) - pi/2;      % angle of arrow
cs         = cos(teta);                            % rotation matrix
ss         = sin(teta);
R          = [cs -ss;ss cs];
```

```
line_length = sqrt( (y2-y1)^2 + (x2-x1)^2 );               % sizes
head_length = min( line_length*alpha,max_length );
head_width  = min( line_length*beta,max_length );
x0          = x2*cs + y2*ss;                          % build head coordinats
y0          = -x2*ss + y2*cs;
coords      = R*[x0 x0+head_width/2 x0-head_width/2; y0 y0-head_length y0-head_length];
% plot arrow  (= line + patch of a triangle)
h1          = plot( [x1,x2],[y1,y2],'k' );
h2          = patch( coords(1,:),coords(2,:),[0 0 0] );
% return handles
handles = [h1 h2];
% check if styling is required
% if no styling, this section can be removed!
if ~isempty( varargin )
   for c = 1:floor(length(varargin)/2)
      try
         switch lower(varargin{c*2-1})
          % only patch properties
         case 'edgecolor',   set( h2,'EdgeColor',varargin{c*2} );
         case 'facecolor',   set( h2,'FaceColor',varargin{c*2} );
         case 'facelighting',set( h2,'FaceLighting',varargin{c*2} );
         case 'edgelighting',set( h2,'EdgeLighting',varargin{c*2} );
         % only line properties
         case 'color'     , set( h1,'Color',varargin{c*2} );
         % shared properties
         case 'linestyle', set( handles,'LineStyle',varargin{c*2} );
         case 'linewidth', set( handles,'LineWidth',varargin{c*2} );
         case 'parent',    set( handles,'parent',varargin{c*2} );
         % head properties - do nothing, since handled above already
         case 'headwidth',;
         case 'headheight',;
         end
      catch
         fprintf( 'unrecognized property or value for: %s\n',varargin{c*2-1} );
      end
   end
end
```

Phasor Calculation Function ==========

```
function phasor_periodJudge(wkl0,wkl4,ch,phase,periodHb,periodHbO)
% flag = it's workload or rest
% ch = chnum
% phase = whole phase matrix
% value = whole psi/xcorr value
% thres = the threshold set
flagmat1 = (periodHb < 1.5*periodHbO);
flagmat2 = (periodHbO < 1.5*periodHb);
flagmat = and(flagmat1, flagmat2);
%warning('no period threshold set, refer to drawpiechartsingle_periodJudge.m for details');
flagmat = ones(size(flagmat));
%%
y1 = [];
for i = 1: length(wkl0)
   if flagmat(wkl0(i),ch)
      y1 = [y1; phase(wkl0(i),ch)];
   end
end
%%
y4 = [];
for i = 1: length(wkl4)
   if flagmat(wkl4(i),ch)
      y4 = [y4; phase(wkl4(i),ch)];
   end
end
%%
y1 = y1*pi/180;
y4 = y4*pi/180;
p = circ_wwtest(y1,y4);
[p1,z1] = circ_rtest(y1);
[p4,z4] = circ_rtest(y4);
%L = 10;
[meany1,Ly1,Vary1,Disy1] = circularMean(y1);
plot_arrow(0, 0, Ly1*cos(meany1), Ly1*sin(meany1), 'linewidth', 2, 'color', 'b', 'edgecolor', 'b', 'facecolor', 'b');
axis(gca,'equal','off',[-1 1 -1 1]);
hold on;
[meany4,Ly4,Vary4,Disy4] = circularMean(y4);
plot_arrow(0, 0, Ly4*cos(meany4), Ly4*sin(meany4), 'linewidth', 2, 'color', 'r', 'edgecolor', 'r', 'facecolor', 'r');
axis(gca,'equal','off',[-1 1 -1 1]);
hold on;
plot([-1,1],[0,0],':k');
hold on;
plot([0,0],[-1,1],':k');
hold on;
circle([0,0],1,1000,':k');
title({['Dsp0=',num2str(Disy1,'%10.2f')];['Dsp4=',num2str(Disy4,'%10.2f')];['p=',num2str(p,'%5.3f')];['p1=',num2str(
p1,'%5.3f'),' p4=',num2str(p4,'%5.3f')];['z1=',num2str(z1,'%5.3f'),' z4=',num2str(z4,'%5.3f')]});
end
```

Single Phasor Drawing Function ==========

```
function phasorsingle_periodJudge(wkl,flag,ch,phase,periodHb,periodHbO)
```

```
% flag = 1 workload, 0 rest
% ch = chnum
% phase = whole phase matrix
% value = whole psi/xcorr value
% thres = the threshold set
flagmat1 = (periodHb < 1.5*periodHbO);
flagmat2 = (periodHbO < 1.5*periodHb);
flagmat = and(flagmat1, flagmat2);
%warning('no period threshold set, refer to drawpiechartsingle_periodJudge.m for details');
flagmat = ones(size(flagmat));
%%
y = [];
for i = 1: length(wkl)
   if flagmat(wkl(i),ch)
      y = [y; phase(wkl(i),ch)];
   end
end
y = y*pi/180;
[meany,Ly,Vary,Disy] = circularMean(y);
if flag
   plot_arrow(0, 0, Ly*cos(meany), Ly*sin(meany), 'linewidth', 2, 'color', 'r', 'edgecolor', 'r', 'facecolor', 'r');
else
   plot_arrow(0, 0, Ly*cos(meany), Ly*sin(meany), 'linewidth', 2, 'color', 'b', 'edgecolor', 'b', 'facecolor', 'b');
end
axis(gca,'equal','off',[-1 1 -1 1]);
hold on;
plot([-1,1],[0,0],':k');
hold on;
plot([0,0],[-1,1],':k');
hold on;
circle([0,0],1,1000,':k');
title({['Dsp=',num2str(Disy,'%10.2f')]});
end
```

Phasor Sector Drawing Function ==========

```
function drawpiechart_periodJudge(wkl0,wkl4,ch,phase,periodHb,periodHbO)
% flag = it's workload or rest
% ch = chnum
% phase = whole phase matrix
% value = whole psi/xcorr value
% thres = the threshold set
flagmat1 = (periodHb < 1.6*periodHbO);
flagmat2 = (periodHbO < 1.6*periodHb);
flagmat = and(flagmat1, flagmat2);
%warning('no period threshold set, refer to drawpiechartsingle_periodJudge.m for details');
flagmat = ones(size(flagmat));
%%
y1 = [];
for i = 1: length(wkl0)
   if flagmat(wkl0(i),ch)
      y1 = [y1; phase(wkl0(i),ch)];
   end
end
if 2*std(y1) > 180
   for i = 1: length(y1)
      while y1(i) > 180
         y1(i) = y1(i) - 360;
      end
   end
end
%%
y4 = [];
for i = 1: length(wkl4)
   if flagmat(wkl4(i),ch)
      y4 = [y4; phase(wkl4(i),ch)];
   end
end
if 2*std(y4) > 180
   for i = 1: length(y4)
      while y4(i) > 180
         y4(i) = y4(i) - 360;
      end
   end
end
%%
drawpie(mean(y1),std(y1),1.2);
hold on;
drawpie(mean(y4),std(y4),1);
end
```

Circular Histogram Drawing Function ==========

```
function hpol=circhist(v,varargin)
% does a phase histogram between -180 and 180
% first unwrap the data
% function circhist(v,option1,option2,...)
% includes a number of variable options
% 'numcat',x,         : set number of bins, (default 36)
% 'balls'             : Default: draws circles
% 'polar'             : Standard polar plot
% 'line'              :  Line plot
% 'fill'              :  Filled line plot
% 'smooth'            : Oversamples the histogram,
%                       to make the places where it's zero to lie on the circumference
%                       kernel-smoothing still has to be programmd
% COMMENT: The Polygon is not defined well enough, so there is a problem importing to AI and
%          one connecting line is visible.
% 'arrow',kind        1:arrow of constantlength
%                     2:arrow of variable length, reflecting the 1-variance
%                     0:no arrow
% 'color',c           : color of arrow and plot
% 'scale',p           : maximal percentage on the radial axis
%                       if not given it scales the max category to max=80%
% Written December 2001, joern Diedrichsen jdiedri@socrates.berkeley.edu
% Rewritten January 2011, Feng Zheng Feng.Zheng@tufts.edu

% define the default constants
plotlength=1;
num_circ=20;
circ_size=plotlength/num_circ;

% defaults
line_style = 'auto';
style='balls';
arrow=1;color='k';percent=-1;
i=1;numcat=36;
while (i<=length(varargin))
   switch varargin{i}
   case 'numcat'
      numcat=varargin{i+1};
      i=i+2;
   case {'balls','polar','line','fill','smooth'}
      style=varargin{i};
      i=i+1;
   case 'arrow'
      arrow=varargin{i+1};
      i=i+2;
   case 'color'
      color=varargin{i+1};
      i=i+2;
   case 'scale'
      percent=varargin{i+1};
      i=i+2;
   otherwise
```

```
        fprintf('Unknown Option: %s\n',varargin{i});
        return;
    end;
end;

over=find(v>360);
under=find(v<0);
v(over)=v(over)-360;
v(under)=v(under)+360;
binwidth=360/numcat;
Edges=[0-(binwidth/2):binwidth:360-(binwidth/2)];
BinMid=[0:binwidth:360-binwidth]';

% count the occuances in the bins
N=histc(v,Edges);
rho=N(1:end-1);
rho(1)=rho(1)+N(end); % leftovers
theta=BinMid./180*pi;

% transform data to Cartesian coordinates.
% collect the number of circles
% theta=-theta+pi/2;
tot_count=sum(rho);
if percent==-1;
   percent=max(rho./tot_count*130);
end;
rhoScale=tot_count/100*percent;
one_circ=rhoScale/num_circ;
barh=round(rho./one_circ);

if(strcmp(style,'polar'));
    polar(theta,rho);
    return;
end;

% now calculate the arrow in length and angle

cmean=circ_mean(v./180*pi);
% cmean=-cmean+pi/2; % align with general zero-up +clockwise
if (arrow==1)
    arrowlength=0.6;
end;
if (arrow==2)
%   arrowlength=(1-circvar(v/180*pi))*.8;
    arrowlength = circ_r(v/180*pi);
end;
arrowhead=arrowlength*.83;

% get hold state
cax = newplot;
next = lower(get(cax,'NextPlot'));
hold_state = ishold;

% get x-axis text color so grid is in same color
```

```
tc = get(cax,'xcolor');
ls = get(cax,'gridlinestyle');
% Hold on to current Text defaults, reset them to the
% Axes' font attributes so tick marks use them.
fAngle  = get(cax, 'DefaultTextFontAngle');
fName   = get(cax, 'DefaultTextFontName');
fSize   = get(cax, 'DefaultTextFontSize');
fWeight = get(cax, 'DefaultTextFontWeight');
fUnits  = get(cax, 'DefaultTextUnits');
set(cax, 'DefaultTextFontAngle',  get(cax, 'FontAngle'), ...
   'DefaultTextFontName',   get(cax, 'FontName'), ...
   'DefaultTextFontSize',   get(cax, 'FontSize'), ...
   'DefaultTextFontWeight', get(cax, 'FontWeight'), ...
   'DefaultTextUnits','data')

% only do grids if hold is off
if ~hold_state
% make a radial grid
   hold on;
   maxrho = 1+plotlength;

   hhh=plot([-maxrho -maxrho maxrho maxrho],[-maxrho maxrho maxrho -maxrho]);
   set(gca,'dataaspectratio',[1 1 1],'plotboxaspectratiomode','auto')
   v1 = [get(cax,'xlim') get(cax,'ylim')];
   ticks = sum(get(cax,'ytick')>=0);
   delete(hhh);
% check radial limits and ticks
   rmin = 0; rmax = v1(4); rticks = max(ticks-1,2);
   if rticks > 5   % see if we can reduce the number
      if rem(rticks,2) == 0
         rticks = rticks/2;
      elseif rem(rticks,3) == 0
         rticks = rticks/3;
      end
   end
% define a circle
   th = 0:pi/50:2*pi;
   th =-th+pi/2;
   xunit = cos(th);
   yunit = sin(th);
% now really force points on x/y axes to lie on them exactly
   inds = 1:(length(th)-1)/4:length(th);
   yunit(inds(2:2:4)) = zeros(2,1);
   xunit(inds(1:2:5)) = zeros(3,1);
% plot background if necessary
   if ~isstr(get(cax,'color')),
     patch('xdata',xunit*rmax,'ydata',yunit*rmax, ...
         'edgecolor',tc,'facecolor',get(gca,'color'),...
         'handlevisibility','off');
   end
% draw radial circles
   c82 = cos(82*pi/180);
   s82 = sin(82*pi/180);
   for (i=1:plotlength:1+plotlength)
      hhh = plot(xunit*i,yunit*i,ls,'color',tc,'linewidth',1,...
```

```
                'handlevisibility','off');

        set(hhh,'linestyle','-') % Make outer circle solid
    end;
% plot spokes
%     th_sp = [4*pi/12:-2*pi/12:-pi/2]; % start up and go around
    th_sp = [pi/4:pi/4:pi];
    cst = cos(th_sp); snt = sin(th_sp);
    cs = [-cst; cst];
    sn = [-snt; snt];
    %plot(rmax*cs,rmax*sn,ls,'color',tc,'linewidth',1,...
    %     'handlevisibility','off')

% annotate spokes in degrees
    rt = 0.85;%1.1*rmax;
    for i = 1:length(th_sp)
        text(rt*cst(i),rt*snt(i),int2str(i*45),...
             'horizontalalignment','center',...
             'handlevisibility','off','FontSize',10);
        if i == length(th_sp)
            loc = int2str(0);
        else
            loc = int2str(i*45+180);
        end
        text(-rt*cst(i),-rt*snt(i),loc,'horizontalalignment','center',...
             'handlevisibility','off','FontSize',10)
    end

% set view to 2-D
    view(2);
% set axis limits
    axis(rmax*[-1 1 -1.15 1.15]);
end

% Reset defaults.
set(cax, 'DefaultTextFontAngle', fAngle , ...
    'DefaultTextFontName',   fName , ...
    'DefaultTextFontSize',   fSize, ...
    'DefaultTextFontWeight', fWeight, ...
    'DefaultTextUnits',fUnits );

% calculate circles
if(strcmp(style,'balls'))
    xx=[];
    yy=[];
    for (bar=1:length(theta))
        if(barh(bar)>0)
            for(circ=1:barh(bar))
                radi=1+circ_size*circ-circ_size/2;
                xx(end+1)=radi*cos(theta(bar));
                yy(end+1)=radi*sin(theta(bar));
            end;
        end;
    end;
    % draw the circles
```

```
    q=[];
    for (circ=1:length(xx))
        posi=[xx(circ)-circ_size/2 yy(circ)-circ_size/2 circ_size circ_size];
        q(end+1)=rectangle('Position',posi,'Curvature',[1 1],'EdgeColor',color,'FaceColor',color);
    end;
end;

rho(end+1)=rho(1);
theta(end+1)=-pi/2;
% draw line
% plot data on top of grid
if (strcmp(style,'smooth'))
    rho=interp1(theta,rho,th','linear');
    theta=th';
end;
if(strcmp(style,'line') || strcmp(style,'fill') || strcmp(style,'smooth'))
    xx = (1+rho/rhoScale).*cos(theta);
    yy = (1+rho/rhoScale).*sin(theta);
    q = plot(xx,yy,color);
end;
if(strcmp(style,'fill')|| strcmp(style,'smooth'))
    patch([xx;xunit'],[yy;yunit'],color);
end;

% draw the mean vector
pvalue = circ_rtest(wrapToPi(v*pi/180));
if pvalue < 0.05
    color2 = 'r';
else
    color2 = 'b';
end
if arrow>0
    arrow=line([0 arrowlength*cos(cmean)],[0 arrowlength*sin(cmean)],'LineWidth',2);
    set(arrow,'Color',color2);
    % arrowhead
    p=patch([arrowlength*cos(cmean) arrowhead*cos(cmean-0.1)
arrowhead*cos(cmean+0.1)],[arrowlength*sin(cmean) arrowhead*sin(cmean-0.1)
arrowhead*sin(cmean+0.1)],color2);
    set(p,'EdgeColor',color2);
end;

if nargout > 0
    hpol = q;
end
if ~hold_state
    set(gca,'dataaspectratio',[1 1 1]), axis off; set(cax,'NextPlot',next);
end
set(get(gca,'xlabel'),'visible','on')
set(get(gca,'ylabel'),'visible','on')
```

Circular Mean Function ==========

```
function [meantheta, vectorlength, CI, dispersion] = circularMean(phi)
%CIRCULARMEAN function is used to calculate the mean phase and statistical parameters
% reference: N.I.Fisher, Statistical analysis of circular data, 1995
% Feng Zheng @ Tufts University, 2010
if length(size(phi)) > 2
   error('No more than 2 dimensions');
end
[M,N] = size(phi);
if M == 1
   phi = phi';
   M = N;
end
if max(max(abs(phi))) > 2*pi
   warning('Function circularMean"s input argument should be in radian angle');
end
cosPhi = cos(phi);
sinPhi = sin(phi);
% calculate the mean phase
meantheta = atan2(mean(sinPhi),mean(cosPhi));
% calculate the resultant vector length
vectorlength = sqrt((sum(cosPhi)).^2 + (sum(sinPhi)).^2)/M;
% calculate the confidential level
CI = acos(sqrt((2*M*(2*M*M*vectorlength*vectorlength-M*3.841))/(4*M-3.841))/(vectorlength*M));
m2 = mean(cos(2*(phi-repmat(meantheta,M,1))));
% calculate the dispersion
dispersion = (1-m2)./(2*vectorlength.*vectorlength);
end
```

TARGET Map Movie Function ==========

```
function drawPhaseDisk_mov(timemat, phase, aux0)
% function drawPhaseDisk_mov is used to generate the TARGET Map movie
% input variables:
%                       timemat – time sequence
%                       phase – corresponding phase values
%                       aux0 – markers
% created by Feng Zheng @ Tufts Univ 2011
if nargin < 2                   % read the input
   error('At Least Two Input Arguments Required');
elseif nargin < 3
   aux0 = [];
end
Ntime = length(timemat);
[M,N] = size(phase);
if M < N
   phase = phase';
   [M,N] = size(phase);
end
if Ntime ~= M
   error('Time and phase dimension unmatched');
end
if max(max(abs(phase))) > 2*pi      % adjust the phase range
   warning('Phase value changed to rad');
   phase = phase*pi/180;
end
figureid = input('which channel you want to watch movie?  ');
step = input('step length?   ');                    % adjust the fps for the movie
x = timemat.*cos(phase(:,figureid));
y = timemat.*sin(phase(:,figureid));
list0 = find(aux0~=0);
figure(110+figureid)
pause;
for i = 1: step: Ntime
   scatter(x(1:i), y(1:i), '.k', 'SizeData',30); % build the TARGET
   if ~isempty(aux0)
      for ti = 1: length(list0)
         if mod(ti,2) == 1
            hold on;                    % draw the markers circles
            circle([0 0], timemat(list0(ti)), 10000, '--r');
         else
            hold on;
            circle([0 0], timemat(list0(ti)), 10000, '--b');
         end
      end
   end
   axescenter;
   set(gca,'pos',[.25 .1 .5 .8]);
   ymax = max(timemat);
   xlim([-ymax ymax]);
   ylim([-ymax ymax]);
   F(i) = getframe;                             % catch the current frame
end
movie2avi(F,'TARGET.avi');                      % output as avi file
```

Folding Average Function ==========

```
function foldingAverage(HbO, Hb, list2, list)
%FOLDINGAVERAGE function is used to calculate folding average function, compatible to MAIN.m
% original written by Angelo Sassaroli and Yunjie Tong
% rewritten by Feng Zheng @ Nov 2010 by packing it as a function for convenience

fs = 6.25;
t2 = list;
t=[0:size(HbO,1)-1]'./fs;

% Do the block average
prePoints = 0;
postPoints = ceil(mean([list2(3)-list2(1)+1, list2(5)-list2(3)+1, list2(7)-list2(5)+1]));
aa = postPoints/fs;
tavg = [-prePoints:postPoints]' / fs;
nr=length(tavg);
ch_av = 'y';
nBlocks = 0;
%
clear blocks
%block average HbO
for idx=1:length(t2)
    if (t2(idx)-prePoints)>=1 && (t2(idx)+postPoints)<=size(HbO,1)
       nBlocks = nBlocks + 1;
       Tonset( nBlocks ) = t2(idx);
       if ch_av=='y'
          blocks_hbo(:,:,nBlocks) = HbO((t2(idx)-prePoints):(t2(idx)+postPoints),:)-ones(postPoints-
prePoints+1,1)*HbO((t2(idx)-prePoints),:);
       else
         blocks_hbo(:,:,nBlocks) = HbO((t2(idx)-prePoints):(t2(idx)+postPoints),:);
       end
       lastOnset = t2(idx);
   end
end
blockAvgHbO = mean(blocks_hbo,3);
errHbO=std(blocks_hbo,0,3);
blockStdErrorHbO = std(blocks_hbo,0,3) / sqrt(nBlocks);
nBlocks = 0;
clear blocks

%block average Hb
for idx=[1:length(t2)]
   if (t2(idx)-prePoints)>=1 && (t2(idx)+postPoints)<=size(Hb,1)
       nBlocks = nBlocks + 1;
       Tonset( nBlocks ) = t2(idx);
       if ch_av=='y'
          blocks_hb(:,:,nBlocks) = Hb((t2(idx)-prePoints):(t2(idx)+postPoints),:)-ones(postPoints-
prePoints+1,1)*Hb((t2(idx)-prePoints),:);
       else
          blocks_hb(:,:,nBlocks) = Hb((t2(idx)-prePoints):(t2(idx)+postPoints),:);
       end
       lastOnset = t2(idx);
   end
```

```
end
blockAvgHb = mean(blocks_hb,3);
errHb=std(blocks_hb,0,3);
blockStdErrorHb = std(blocks_hb,0,3) / sqrt(nBlocks);
%
nBlocks = 0;
clear blocks
% %
ch10='tt';
ch11='an';
p_t= .05;
ch12= 'mb';
nDet = size(blockAvgHbO,2);
for idx=1:nDet
      if strcmp(ch_av,'y')
         mat_HbO=squeeze(blocks_hbo(2:end,idx,:))';
         corrHbO=corrcoef(mat_HbO);
         avg_corrHbO(idx)=(sum(sum(corrHbO))-nr+1)/((nr-1)*(nr-2));
         xx1_hbo=(sum(corrHbO,2)-ones(nr-1,1))/(nr-2);
         if strcmp(ch12,'mb')
            mk_hbo=(nr-1).^(ones(nr-1,1)-xx1_hbo);
         else
            mk_hbo=(nr-1)*ones(nr-1,1);
         end
      else
         mat_HbO=squeeze(blocks_hbo(:,idx,:))';
         corrHbO=corrcoef(mat_HbO);
         avg_corrHbO(idx)=(sum(sum(corrHbO))-nr)/((nr)*(nr-1));
         xx1_hbo=(sum(corrHbO,2)-ones(nr,1))/(nr-1);
         if strcmp(ch12,'mb')
            mk_hbo=(nr).^(ones(nr,1)-xx1_hbo);
         else
            mk_hbo=(nr)*ones(nr,1);
         end
      end
   pnum_hbo=0;
   cc_hbo=0;
   pnum_new_hbo=0;
   cc_new_hbo=0;
   c_hbo=0;
   c_new_hbo=0;
   %_____________________________________
   if strcmp(ch_av,'y')
      if strcmp(ch10,'tt')
         zz=(squeeze(blocks_hbo(2,idx,:)));
         [h,p,ci] = ttest(zz,0);
      elseif strcmp(ch10,'st')
         zz=(squeeze(blocks_hbo(2,idx,:)));
         [p,h] = signtest(zz,0);
      else
         zz=(squeeze(blocks_hbo(2,idx,:)));
         [p,h] = signrank(zz,0);
      end
      c_hbo=p;
       if strcmp(ch11,'an')
         [p1, anovatab] = anova1((squeeze(blocks_hbo(2:end,idx,:)))',[],'off');
```

```
    else
      [p1, anovatab] = kruskalwallis((squeeze(blocks_hbo(2:end,idx,:)))',[],'off');
    end
   p_anova_hbo(idx)=p1;
   p_new_hbo=1-(1-p)^mk_hbo(1,1);
   c_new_hbo=p_new_hbo;
   for i=3:length(tavg)
      if (p<p_t)
         pnum_hbo=[pnum_hbo i-1];
         cc_hbo=1;
      end
      if (p_new_hbo<p_t)
         pnum_new_hbo=[pnum_new_hbo i-1];
         cc_new_hbo=1;
      end
      if strcmp(ch10,'tt')
         zz=(squeeze(blocks_hbo(i,idx,:)));
         [h,p,ci] = ttest(zz,0);
      elseif strcmp(ch10,'st')
          zz=(squeeze(blocks_hbo(i,idx,:)));
         [p,h] = signtest(zz,0);
      else
         zz=(squeeze(blocks_hbo(i,idx,:)));
         [p,h] = signrank(zz,0);
      end
      p_new_hbo=1-(1-p)^mk_hbo(i-1,1);
      c_hbo=[c_hbo p];
      c_new_hbo=[c_new_hbo p_new_hbo];
   end
else
   if strcmp(ch10,'tt')
      zz=(squeeze(blocks_hbo(1,idx,:)));
       [h,p,ci] = ttest(zz,0);
   elseif strcmp(ch10,'st')
      zz=(squeeze(blocks_hbo(1,idx,:)));
      [p,h] = signtest(zz,0);
   else
      zz=(squeeze(blocks_hbo(1,idx,:)));
      [p,h] = signrank(zz);
   end
   c_hbo=p;
   if strcmp(ch11,'an')
      [p1, anovatab]=anova1((squeeze(blocks_hbo(1:end,idx,:)))',[],'off');
    else
      [p1, anovatab]=kruskalwallis((squeeze(blocks_hbo(1:end,idx,:)))',[],'off');
    end
   p_anova_hbo(idx)=p1;
   p_new_hbo=1-(1-p)^mk_hbo(1,1);
   c_new_hbo=p_new_hbo;
   for i=2:length(tavg)
      if (p<p_t)
         pnum_hbo=[pnum_hbo i-1];
         cc_hbo=1;
      end
      if (p_new_hbo<p_t)
         pnum_new_hbo=[pnum_new_hbo i-1];
```

```
            cc_new_hbo=1;
        end
        if strcmp(ch10,'tt')
            zz=(squeeze(blocks_hbo(i,idx,:)));
            [h,p,ci] = ttest(zz,0);
        elseif strcmp(ch10,'st')
             zz=(squeeze(blocks_hbo(i,idx,:)));
            [p,h] = signtest(zz,0);
        else
            zz=(squeeze(blocks_hbo(i,idx,:)));
            [p,h] = signrank(zz,0);
        end
        p_new_hbo=1-(1-p)^mk_hbo(i,1);
        c_hbo=[c_hbo p];
        c_new_hbo=[c_new_hbo p_new_hbo];
      end
   end
end
for idx = 1: nDet
   a_up = max(max(abs(blockAvgHbO))) + max(max(abs(blockStdErrorHbO)));
   a_low = -a_up;
   figure(1984)
   if nDet > 8
      subplot(nDet/5,5,idx);
   else
      subplot(nDet/4,4,idx);
   end
   set(gca,'FontSize',13);
   errorbar(tavg,blockAvgHbO(:,idx),blockStdErrorHbO(:,idx),'Color','b')

   if (cc_new_hbo==1)
      [f_new_hbo,g_new_hbo]=size(pnum_new_hbo);
      count_new_hbo(idx)=g_new_hbo-1;
      pnum_new_hbo=pnum_new_hbo(2:g_new_hbo);
      hold on;

errorbar(tavg(pnum_new_hbo),blockAvgHbO(pnum_new_hbo,idx),blockStdErrorHbO(pnum_new_hbo,idx),'Color',
'r');
   end
   hold off
   if idx==1
      title('\Delta[HbO] (\mu M)')
   end
   xlim([-prePoints/fs postPoints/fs])
   grid on
   ylim([a_low a_up])
   xlabel(['Chn ',num2str(idx)]);
end
%
nDet = size(blockAvgHb,2);
for idx=1:nDet
      if ch_av=='y'
         mat_Hb=squeeze(blocks_hb(2:end,idx,:))';
         corrHb=corrcoef((squeeze(blocks_hb(2:end,idx,:)))');
         avg_corrHb(idx)=(sum(sum(corrHb))-nr+1)/((nr-1)*(nr-2));
         xx1_hb=(sum(corrHb,2)-ones(nr-1,1))/(nr-2);
```

```
        if strcmp(ch12,'mb')
            mk_hb=(nr-1).^(ones(nr-1,1)-xx1_hb);
        else
            mk_hb=(nr-1)*ones(nr-1,1);
        end
    else
        mat_Hb=squeeze(blocks_hb(:,idx,:))';
        corrHb=corrcoef((squeeze(blocks_hb(:,idx,:)))');
        avg_corrHb(idx)=(sum(sum(corrHb))-nr)/((nr)*(nr-1));
        xx1_hb=(sum(corrHb,2)-ones(nr,1))/(nr-1);
        if strcmp(ch12,'mb')
            mk_hb=(nr).^(ones(nr,1)-xx1_hb);
        else
            mk_hb=(nr)*ones(nr,1);
        end
    end
pnum_hb=0;
cc_hb=0;
pnum_new_hb=0;
cc_new_hb=0;
c_hb=0;
c_new_hb=0;
%_____________________________________
if strcmp(ch_av,'y')
    if strcmp(ch10,'tt')
        zz=(squeeze(blocks_hb(2,idx,:)));
         [h,p,ci] = ttest(zz,0);
    elseif strcmp(ch10,'st')
        zz=(squeeze(blocks_hb(2,idx,:)));
        [p,h] = signtest(zz,0);
    else
        zz=(squeeze(blocks_hb(2,idx,:)));
        [p,h] = signrank(zz,0);
    end
    c_hb=p;
    if strcmp(ch11,'an')
        [p2, anovatab]=anova1((squeeze(blocks_hb(2:end,idx,:)))',[],'off');
     else
        [p2, anovatab]=kruskalwallis((squeeze(blocks_hb(2:end,idx,:)))',[],'off');
     end
    p_anova_hb(idx)=p2;
    p_new_hb=1-(1-p)^mk_hb(1,1);
    c_new_hb=p_new_hb;
    for i=3:length(tavg)
        if (p<p_t)
            pnum_hb=[pnum_hb i-1];
            cc_hb=1;
        end
        if (p_new_hb<p_t)
            pnum_new_hb=[pnum_new_hb i-1];
            cc_new_hb=1;
        end
        if strcmp(ch10,'tt')
            [h,p,ci] = ttest(blocks_hb(i,idx,:),0);
        elseif strcmp(ch10,'st')
             zz=(squeeze(blocks_hb(i,idx,:)));
```

```
            [p,h] = signtest(zz,0);
        else
            zz=(squeeze(blocks_hb(i,idx,:)));
            [p,h] = signrank(zz,0);
        end
        p_new_hb=1-(1-p)^mk_hb(i-1,1);
        c_hb=[c_hb p];
        c_new_hb=[c_new_hb p_new_hb];
    end
  else
    if strcmp(ch10,'tt')
        [h,p,ci] = ttest(blocks_hb(1,idx,:),0);
    elseif strcmp(ch10,'st')
        zz=(squeeze(blocks_hb(1,idx,:)));
        [p,h] = signtest(zz,0);
    else
        zz=(squeeze(blocks_hb(1,idx,:)));
        [p,h] = signrank(zz,0);
    end
    c_hb=p;
   if strcmp(ch11,'an')
        [p2, anovatab]=anova1((squeeze(blocks_hb(1:end,idx,:)))',[],'off');
    else
        [p2, anovatab]=kruskalwallis((squeeze(blocks_hb(1:end,idx,:)))',[],'off');
    end
    p_anova_hb(idx)=p2;
    p_new_hb=1-(1-p)^mk_hb(1,1);
    c_new_hb=p_new_hb;
    for i=2:length(tavg)
        if (p<p_t)
            pnum_hb=[pnum_hb i-1];
            cc_hb=1;
        end
        if (p_new_hb<p_t)
            pnum_new_hb=[pnum_new_hb i-1];
            cc_new_hb=1;
        end
        if strcmp(ch10,'tt')
            [h,p,ci] = ttest(blocks_hb(i,idx,:),0);
        elseif strcmp(ch10,'st')
            zz=(squeeze(blocks_hb(i,idx,:)));
            [p,h] = signtest(zz,0);
        else
            zz=(squeeze(blocks_hb(i,idx,:)));
            [p,h] = signrank(zz,0);
        end
        p_new_hb=1-(1-p)^mk_hb(i,1);
        c_hb=[c_hb p];
        c_new_hb=[c_new_hb p_new_hb];
    end
  end
end
for idx = 1: nDet
  a_up = max(max(abs(blockAvgHb))) + max(max(abs(blockStdErrorHb)));
  a_low = -a_up;
  figure(1986)
```

```
    if nDet > 8
        subplot(nDet/5,5,idx);
    else
        subplot(nDet/4,4,idx);
    end
    set(gca,'FontSize',13);
    errorbar(tavg,blockAvgHb(:,idx),blockStdErrorHb(:,idx),'Color','b')
    if (cc_new_hb==1)
        [f_new_hb,g_new_hb]=size(pnum_new_hb);
        count_new_hb(idx)=g_new_hb-1;
        pnum_new_hb=pnum_new_hb(2:g_new_hb);
        hold on;
errorbar(tavg(pnum_new_hb),blockAvgHb(pnum_new_hb,idx),blockStdErrorHb(pnum_new_hb,idx),'Color','r');
    end
    hold off
    if idx==1
        title('\Delta[Hb] (\mu M)')
    end
    xlim([-prePoints/fs postPoints/fs])
    grid on
    ylim([a_low a_up])
    xlabel(['Chn ',num2str(idx)]);
end
```